Turbulence Decay of a Shear-Thinning Fluid in Pipe Flow

A DNS Study

Anunay Prasanna

Master of Science Thesis

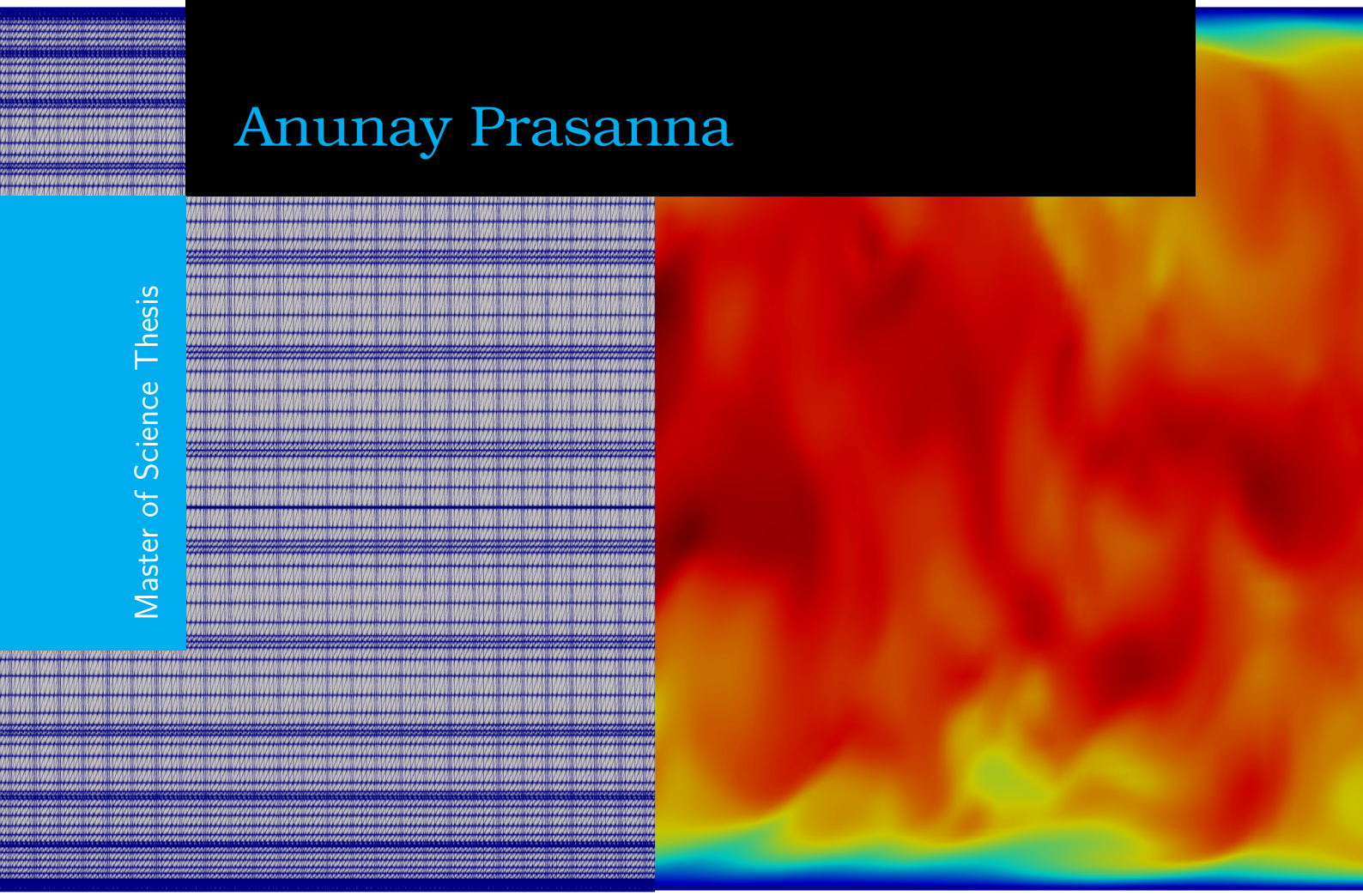

TU Delft Delft University of Technology

Process & Energy Department

Turbulence Decay of a Shear-Thinning Fluid in Pipe Flow

A DNS Study

Master of Science Thesis

Anunay Prasanna

P&E report number 3046
submitted on September 28, 2021

Committee Members:

Prof. dr. ir. C. Poelma,	TU Delft, Supervisor, Chair
Dr. ir. M. Pourquie,	TU Delft, Supervisor
Dr. ir. R. Pecnik,	TU Delft, Committee Member
Dr. ir. S. J. Hulshoff	TU Delft, Committee Member

Faculty of Mechanical, Maritime and Materials Engineering (3mE) · Delft University of Technology

Abstract

The human body is the subject of several interesting phenomena and blood flow comes under that category. The main motivator for this thesis is the flow of blood in aneurysms. An aneurysm is a sudden expansion of an artery, with large expansion angles causing an adverse pressure gradient and leading to flow separation. Several studies have shown the transitional nature of the flow in aneurysms, and it has been seen that the variation of the wall shear stress from cycle-to-cycle is one of the major reasons for the growth of aneurysms, and possibly leading to their rupture at a later stage. It has also been noticed that the turbulent kinetic energy (TKE) does not decay with the mean flow kinetic energy and the periodic kinetic energy of the cardiac cycle. Therefore, it is intersting to research the turbulent decay to see how the flow in an aneurysm can be affected. However, the number of variables in an aneurysm are too high to effectively characterise this, and therefore, a simplified geometry was chosen. Pipe flow is a good choice to start with, as it can mimic the wall-bounded nature of an aneurysm. It also has a well-defined statistically steady turbulent state from where the decay of turbulence can be studied. Additionally, blood being a non-Newtonian fluid, makes it interesting to study the effects of shear-thinning.

To this extent, a Direct Numerical Simulation (DNS) study has been carried out using a higher-order spectral element method code. First, statistics for fully-developed pipe flow are compared with existing results. To a fully-developed turbulent state, a deceleration is applied to bring the flow to a steady, laminar state. The decay of the turbulent quantities is monitored during this process. Comparison studies are undertaken to study the influence of the ramp rate, the dependence of the decay on the initial Reynolds number, and the variation of the results between Newtonian and generalized Newtonian fluids. A modelling approach using RANS has also been undertaken to see if only studying the mean flow is sufficient to characterize the decay.

It is seen that two regimes of decay exist – a power-law decay based on turbulent scaling, and an exponential viscous decay. The power-law decay is further divided into two stages – one before the saturation of the integral length scale, and one after the saturation of the length scale – with the maximum length scale being set by the diameter of the pipe. The exponential model has been validated using the hypothesis of Skrbek 2008. The point of divergence from the power-law to the exponential decay has been hypothesized here. It is seen that for all the

cases studied, the point of divergence occurred at $Re_\tau = 60$. It is noticed that the decay is independent of the ramp rates when they are applied at times on the order of magnitude of 1 Eddy Turnover Time (ETT). The decay does show a dependence on the initial Reynolds number and the reasons for this are hypothesized. The RANS modelling used was found to be insufficient due to the inability of the RANS model to gauge the size of the domain. For generalized Newtonian fluids, it is noticed that the decay rate increases with shear-thinning. The results obtained are discussed in the context of an aneurysm. Based on the diameter, length and flow rate of the aneurysm, it can be hypothesized at which stage of decay the flow is, and based on this, it has been discussed whether using a non-Newtonian modelling approach is more beneficial than using a Newtonian approach for the decay.

Table of Contents

Acknowledgements

In what has essentially been a tough few months for the world, I am grateful to have undertaken this work and to have come out on top. With this regard, I would like to thank my supervisors Prof. dr. ir. Christian Poelma and Dr. ir. Mathieu Pourquie, for their assistance during this thesis. It was quite challenging to motivate myself every day while working from home, but the ideas provided by them would always pique my interest as well. I also want to thank the other committee members for taking the time to read and attend my defense.

I would like to thank my parents who continuously supported me during the Masters'. Their thoughts were always with me. To all those friends who pushed me to think, enjoy and improve myself, while we were playing tennis, badminton or basketball, brewing and drinking beer, and spending time at the city center or travelling, I want to let all of you know that I have a lot of fond memories, which I'll cherish for life. I hope the feeling is mutual.

Thank you and success!

Delft, University of Technology
September 28, 2021

Anunay Prasanna

"There is a physical problem that is common to many fields, that is very old, and that has not been solved. It is not the problem of finding new fundamental particles, but something left over from a long time ago – over a hundred years. Nobody in physics has really been able to analyze it mathematically satisfactorily in spite of its importance to the sister sciences. It is the analysis of circulating or turbulent fluids."

— *Richard P. Feynman*, The Feynman Lectures on Physics Vol 1

Chapter 1

Introduction

Turbulence is observable everywhere in our day-to-day life. From natural flows, such as smoke rising from a chimney, to moving objects, like airplanes and cars, to important technological applications, such as, heat exchangers and nozzles, the prevalence of turbulence is evident. It plays an important role in geophysical flows arising in the atmosphere and the ocean, while also being crucial to transport phenomena. Nearly every outdoor sport in the world is somehow or the other affected by turbulence, both advantageously and disadvantageously (Pope 2000).

Interest in turbulent flows has been omnipresent. It remains an unsolved problem from a physical as well as a mathematical point of view, and it is seen that insufficient turbulence modelling is the most obstructive factor in determining solutions for practical problems (Nieuwstadt et al. 2016). Drawing a comparison between turbulent flows and its' counterpart, laminar flows, it is seen that the main contrast between the two is the state of order. Laminar flow is ordered, smooth and regular, while turbulence is disordered, characterised by fluctuations and outright chaotic (Nieuwstadt et al. 2016). These characteristics make turbulence a very interesting subject to research.

Blood flow in arteries is a high motivator for the current study. It is a pulsating flow, dominated by unsteady phenomena (Ku 1997). During diastole, the flow can be zero or even reversed in certain arteries. Hemodynamic parameters play a crucial role in determining treatment options for atherosclerosis, arterial stenoses, and aneurysms (Steinman 2012). In particular, this work is focused on understanding the blood flow in an aneurysm. An aneurysm is a sudden expansion of the artery, with large expansions leading to blood flow separation on entry. In their Computational Fluid Dynamics (CFD) simulation, Rawat et al. 2019 show that the computational model for the aneurysms are subject to the formation of vortex rings, with the setting in of azimuthal instabilities causing the ring to destabilize and break down. The whole mechanism is privy to turbulent fluctuations, and this has also been noticed in other studies of aneurysms, even when the flow is predominantly laminar for the majority of the cardiac cycle (Biasetti et al. 2011). The pulsatile nature of blood flow can lead to cyclic transition to turbulence in aneurysms (Yip et al. 2001). This transitional nature leads to significant variation in wall shear stress distributions in the artery, even in consecutive

cardiac cycles (Poelma et al. 2015). Additionally, it is also seen that the turbulent kinetic energy (TKE) peaks at a diferent time in a cycle, as compared to the mean flow and periodic kinetic energies (see Figure 1.1) (Poelma et al. 2015). These variations in flow quantities are shown to be of major importance in analysing the origin, progression and possibly, the rupture of the aneurysm, and thus, are crucial in providing proper care for the artery.

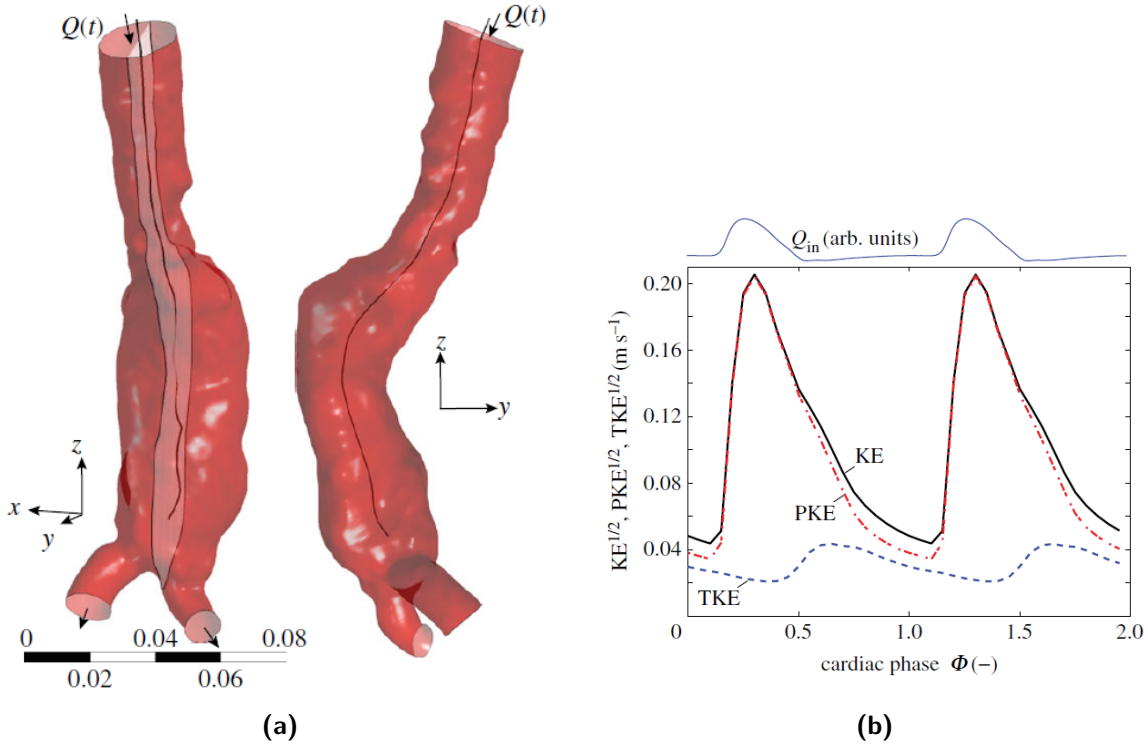

Figure 1.1: (a) An abdominal aortic aneurysm with an expansion on flow entry (b) Variation of the different kinetic energies per cycle (Images from Poelma et al. 2015)

An interesting aspect of blood flow is the non-Newtonian nature of blood (viscosity varying with shear rate, strain rate or other factors). The range of applicability of the non-Newtonian nature of blood in aneurysms is subject to considerable debate (Steinman 2012). Blood is considered to be a shear-thinning fluid (Steinman 2012), where shear-thinning is defined as a decrease in viscosity as shear rate increases (Macosko 1994). Yip et al. 2001 state that blood can be treated as a Newtonian fluid for small internal diameters of arteries (upto 1 mm), and at high strain rates (80 s^{-1} and above). Other studies such as, Biasetti et al. 2011 find variations of up to 10% while predicting the wall shear stress in aneurysms, by using a non-Newtonian, shear-thinning model for blood, as compared to the Newtonian model. Arzani 2018 proposes including rouleaux formation in non-Newtonian models to account for variable shear-thinning behaviour based on the residence time of blood, and claims this to be highly accurate to determine exact locations of low and high shear rates, and therefore, determine the behaviour of the hemodynamic parameters more precisely.

It is clear from the literature on aneurysms, that the number of variable parameters governing the flow in an aneurysm are too many. This makes quantifying turbulence, and in particular, transition in aneurysms, very hard. Therefore, it becomes necessary to simplify things to

isolate the effects seen in aneurysm, and to obtain more clarity about them. The geometrical nature of an artery is similar to a pipe, and turbulent pipe flow is better understood. Expounding further on non-Newtonian applications in pipe flow, drag reducing dilute polymer solutions, and slurry transport in pipes can also be modelled as non-Newtonian fluids, and thus, it is of considerable interest to study the same. The subject of laminar-turbulent transition in pipe flow has been widely regarded for these specific fluids as well (Draad et al. 1998; Peixinho et al. 2005; Radhakrishnan et al. 2020). The non-Newtonian nature coupled with the linear stability of pipe flows provides great complexities in understanding this topic.

In several aneurysms, it is noticed that the turbulence decays within a cardiac cycle itself. The cycle-to-cycle variations are then absent, since the initial conditions are the same. For larger aneurysms, the turbulence remains within an aneurysm and does not decay completely (see Figure 1.1 again), which gives rise to the cycle-to-cycle variations. Since it is interesting to discuss the breakdown of turbulence in an aneurysm, this study is focused on the decay of turbulent pipe flow. Studying decay of turbulence in pipe flow can serve as a good building block. It can also be useful in quantifying transitional flow, and also provide some detail on how transition can be predicted. The physics behind turbulence decay in pipes is a highly debated topic, enabling discussion on the very nature of turbulence itself.

As mentioned above, the important property of these processes is that they are nonlinear and highly chaotic, which makes analyzing them theoretically a tough task (Sekimoto et al. 2016). Direct Numerical Simulation (DNS) is a powerful tool that provides rich data sets, and has been recently moving into the same range of Reynolds numbers as most experiments. It has been at the forefront of understanding turbulence, with studies ranging from pulsatile flow (Varghese et al. 2007) and vortex rings (Archer et al. 2008), to realizing pipe flows (Eggels et al. 1994; Toonder et al. 1997a) and grid turbulence (Touil et al. 2002; Biferale et al. 2003). Therefore, to study the decay, DNS using a high-order spectral element code will be carried out. Higher-order methods are more accurate and thus, it is sensible to employ this to study transition, which is a sensitive phenomenon by nature.

This report entails a description of the important physical and technological aspects related to this project. It starts with a brief introduction of wall-bounded turbulence and turbulent pipe flow, for both Newtonian and non-Newtonian fluids, in Chapter 2. Chapter 3 provides insight on previous studies related to decay of turbulence, and tries to connect existing ideas with the problem at hand. Chapter Chapter 4 gives a description of the spectral element method, and the code which will be used to evaluate this problem. The methodology used is validated and the results for this are shown in Chapter 5. Finally, the results of the study are presented in Chapter 6, and some discussion is presented on the validity and quality of the results obtained.

Chapter 2

Pipe Flow

To quantify the problem described in Chapter 1, the idea of turbulence will be developed from basic concepts. This chapter will elucidate some of the basic ideas applicable to all kinds of turbulence, followed by an explanation of wall-bounded turbulence and pipe flows specifically. It is then followed by a description on non-Newtonian modelling of viscosity and its applicability to turbulent pipe flows.

2-1 General Characteristics of Turbulence

As mentioned previously, turbulence is characterised by chaos. It is the general belief, that turbulence exists in vortical structures, called eddies. Turbulence can be thought of to occur at two scales – the macrostructure, involving the largest length scales, and the microstructure, having the smallest dimensions (Nieuwstadt et al. 2016). The macrostructure is characterized by a length scale, $\mathcal{L}$, and a velocity scale, $\mathcal{U}$. These are generally properties of the flow geometry. Every flow can be characterised by a Reynolds number, defined as the ratio of the inertial forces to the viscous forces.

$$\mathrm{Re} = \frac{\mathcal{U}\mathcal{L}}{\nu} \tag{2-1}$$

For a fully turbulent flow, $Re >> 1$, which implies that the flow is dominated by inertia and nonlinear processes, as compared to viscous effects. The large-scale structure is thus, independent of the only property determined by the fluid, the viscosity (Nieuwstadt et al. 2016).

Turbulence is highly dissipative. Proceeding in a similar fashion as before, if the kinetic energy scales as $e \sim \mathcal{U}^2$, and the characteristic time scale as $\tau \sim \mathcal{L}/\mathcal{U}$, then the rate of dissipation is given by

$$\epsilon \propto \frac{\mathcal{U}^3}{\mathcal{L}} \tag{2-2}$$

Eq. 2-2 can be inferred as the loss of energy of the macrostructure through instability processes, which has to be dispelled at a lower scale as heat or friction. The only available

mechanism for the dissipation to occur is through viscosity, and this brings up the concept of the microstructure. The gradient of the velocity can be large at small scales and that means the viscosity can no longer be neglected (Nieuwstadt et al. 2016). Kolmogorov 1941 provided one of the first ideas for the microstructure. The dissipation takes place through a cascade process, wherein the input of energy occurs at the larger scales ($\mathcal{L}$), which is transferred onto smaller, intermediate scales (r), in the form of eddies, and then dissipated through even smaller scales (η). The intermediate scales are large compared to the smallest scales, but small with respect to the largest scales ($\eta << r << L$). They do not dissipate energy and only transfer it. This intermediate range is called the inertial subrange. The overall energy cascade now translates to the presence of large eddies in the macrostructure, which break-up into smaller eddies and therefore, transfer energy to the microstructure. To appropriately scale the microstructure, the important parameters to be considered are the viscosity, ν, and the dissipation rate, ϵ. From a dimensional analysis, the following scales can be defined (Kolmogorov 1941)

$$\eta = \left(\frac{\nu^3}{\epsilon}\right)^{1/4}, \quad \tau = \left(\frac{\nu}{\epsilon}\right)^{1/2}, \quad v = (\nu\epsilon)^{1/4} \tag{2-3}$$

These are collectively called the Kolomogorov scales. It can also be noticed that $\mathrm{Re}_\eta = v\eta/\nu = 1$, which implies that friction is predominant in the microstructure as compared to the macrostructure.

2-2 Turbulent Pipe Flow and its Structure

This section is dedicated to providing some insight on the structure and statistics of fully developed pipe flow. It is important to quantify pipe flows, as this study will begin from a realization of fully developed pipe flow, after which the decay of this turbulent state will be researched. Above, the role of turbulence in pipe flows was elucidated. Therefore, it should be no surprise that this is a field that has been studied extensively. The incompressible Navier-Stokes equations, governing the temporal and spatial variation of the flow, can be written as (Khoury et al. 2013)

$$\begin{aligned} \boldsymbol{\nabla} \cdot \boldsymbol{u} &= 0 \\ \frac{\partial \boldsymbol{u}}{\partial t} + \boldsymbol{u} \cdot \boldsymbol{\nabla} \boldsymbol{u} &= -\boldsymbol{\nabla} p + \frac{1}{\mathrm{Re}_b} \boldsymbol{\nabla^2} \boldsymbol{u} \end{aligned} \tag{2-4}$$

where $\mathrm{Re}_b = \overline{u_b} D/\nu$ is the bulk Reynolds number dependent on the bulk mean velocity, $\overline{u}_b$, and the pipe diameter, D. Pipe flows are simple in the sense that the mean flow is axisymmetric, and the turbulent field is inhomogeneous in one direction only. Laufer 1954 performed experiments on turbulent pipe flows using hot wire anemometry. He explains a division of the turbulent structure into three regions - the wall region, the central region and the region in between connecting the two.

This concept has been further expanded by other authors. In fact, it has been generalised for wall-bounded flows, such as channel flows and turbulent boundary layers. First, it is useful

to introduce some quantities. Wall-bounded flows are characterized by existing friction from the walls. Therefore, a wall friction velocity, u_*, can be defined as

$$u_* = \sqrt{\frac{\tau_w}{\rho}} \tag{2-5}$$

where τ_w is the wall shear stress. A scaling can be provided for the three regions mentioned. For the outer region, which would be near the center of the pipe, the appropriate length scale would be the radius, R, and an equivalent velocity scale would be the friction velocity, u_* (Nieuwstadt et al. 2016). Then, a velocity defect law can be defined for the region as

$$\frac{u_0 - \overline{u}}{u_*} = F\left(\frac{y}{R}\right) \tag{2-6}$$

where u_0 is a reference velocity, which is usually the mean centerline velocity in a pipe, unless stated otherwise. Moving closer towards the wall, it is seen that the size of the eddies decrease because of the influence of the wall. Eq. 2-6 is not valid in this region, and a new scaling is required. Assuming that the flow is fully turbulent, a balance between the shear stress in the region and the wall shear stress gives

$$\frac{\overline{u}}{u_*} = \frac{1}{\kappa} \ln\left(\frac{y}{y_0}\right) \tag{2-7}$$

Here, y_0 is an integration constant, and $\kappa = 0.41$ is the Von Kármán constant, which arises from finding a closure relation for the turbulent stresses. This profile is logarithmic, and therefore, called the logarithmic layer (Nieuwstadt et al. 2016). Eq. 2-7 is not valid at $y = 0$. Thus, for the inner region, which is located near the wall, Prandtl's law of the wall is followed (Perry et al. 1986).

$$\frac{\overline{u}}{u_*} = F\left(\frac{y u_*}{\nu}\right) \tag{2-8}$$

This is called the viscous sublayer, as turbulent stresses are negligible here, and the fluctuations arising in this region are induced by the layers above. To write the equations in an appropriate manner, wall units are introduced – $u^+ = \overline{u}/u_*$ and $y^+ = y u_*/\nu$. From several mean velocity measurements, it is noticed that the profile for the viscous sublayer is valid for $y^+ < 5$, and the logarithmic profile for $y^+ > 30$. The region in between is called the buffer layer, where no simple solution exists. This is a region of the flow where both the turbulent and the viscous stresses are equally important (Nieuwstadt et al. 2016). It is also important to match the logarithmic layer with the core region of the flow. A direct matching condition for the velocity is not possible, and therefore, a matching condition is applied to the velocity gradients. This gives rise to the velocity profile for the core as (Perry et al. 1986; Nieuwstadt et al. 2016)

$$\frac{u_0 - \overline{u}}{u_*} = \frac{1}{\kappa} \ln\left(\frac{y}{R}\right) + A \tag{2-9}$$

Using all the relations given above, the velocity in wall-bounded flows can be empirically summarised as

$$u^+ = \begin{cases} y^+, & 0 < y^+ < 5 \\ 2.5 \ln y^+ + 5.5, & y^+ > 30 \end{cases} \tag{2-10}$$

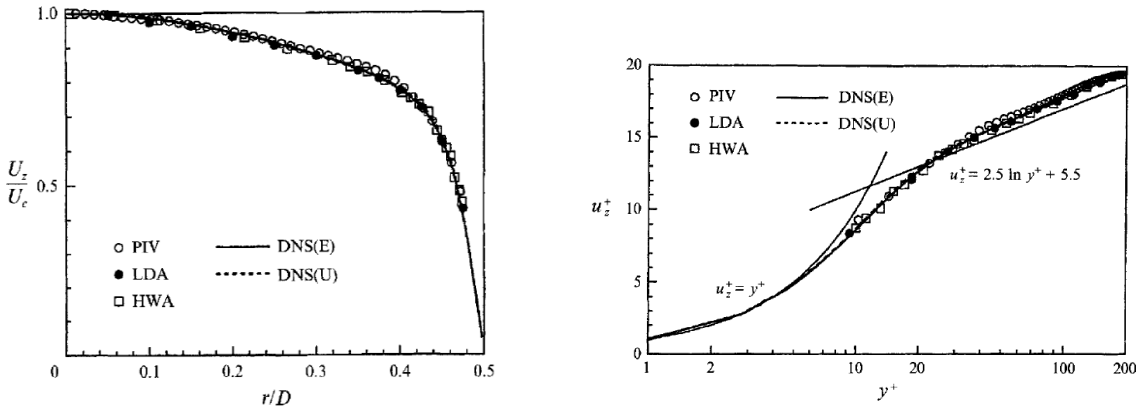

Figure 2.1: (a) Normalized axial mean velocity (b) Axial mean velocity scaled on inner variables (Images taken from Eggels et al. 1994)

Eggels et al. 1994 provide good estimates for the velocity profile. The results show good agreement with eq. 2-10. A plot depicting the profile, in both linear and logarithmic coordinates, is given in Figure 2.1.

A conveninet approach to model turbulence is that any instantaneous turbulent quantity can be split into two components - an average part, and a fluctuating part. This can be expressed as

$$f = \overline{f} + f' \tag{2-11}$$

where a bar denotes the average of a quantity, and a prime denotes a fluctuating part. This is referred to as the Reynolds decomposition. The average of fluctuating parts is zero ($\overline{f'} = 0$) (Nieuwstadt et al. 2016). Expanding eq. 2-4 in radial coordinates, (r, θ, z), introducing Reynolds decomposition, and applying the conditions for fully developed flow ($\overline{u_\theta} = \overline{u_r} = 0$ and $\overline{\partial/\partial\theta} = 0$),

$$\begin{aligned} \frac{\partial \overline{u_z}}{\partial z} &= 0 \\ \frac{1}{\rho}\frac{\partial \overline{p}}{\partial z} &= \frac{1}{r}\frac{\partial}{\partial r}\left(\nu\frac{\partial \overline{u_z}}{\partial r} - r\overline{u_z' u_r'}\right) \end{aligned} \tag{2-12}$$

It is easy to prove that $\partial\overline{p}/\partial z = d\overline{p}/dz$, by differentiating the radial momentum equation (not given here), with respect to z. This implies that $p = p(z)$. The quantity $\overline{u_z' u_r'}$ is the normalized turbulent shear stress, also called the Reynolds stress (Laufer 1954). A wall friction velocity can be defined as $u_* = \sqrt{-\nu(\partial\overline{u_z}/\partial r)_{r=R}}$, and the normalized viscous shear stress, $-\nu(\partial\overline{u_z}/\partial r)$, becomes u_*^2 at the wall. The total shear stress is given by

$$\frac{\tau_{rz}}{\rho} = \overline{u_r' u_z'} - \nu\frac{\partial \overline{u_z}}{\partial r} \tag{2-13}$$

For fully developed flow, the momentum balance yields the total shear stress as $\tau_{rz}/\rho u_*^2 = 2r/D$, which is a linear profile. Additionally, the Reynolds stress is zero at both the wall and the centerline. The variation of the shear stress is depicted in Figure 2.2.

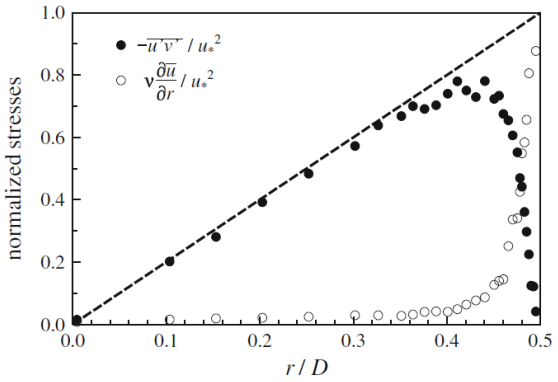

Figure 2.2: Total Shear Stress Normalized using ρu_*^2 at Re = 10,000 (Toonder et al. 1997a)

An interesting aspect of pipe flow is the dependence of statistics on the Reynolds number. Toonder et al. 1997a conducted high-resolution LDV measurements in a turbulent pipe flow, and found that the turbulence statistics scaled on inner-variables are Reynolds number dependent for a range of Re = 5000 − 25000. This implies that the constants to depict the logarithmic velocity profile are Reynolds number dependent as well, along with other higher-order statistics, such as the skewness and the flatness.

The discussion on the energy budgets will play a key role in interpreting the results obtained when the decay of turbulence is studied, and therefore, a short summary is provided here. The turbulent kinetic energy budget can be defined as (Khoury et al. 2013)

$$\frac{Dk}{Dt} = P^k + \epsilon + \Pi^k + \mathcal{D}^k + T^k \tag{2-14}$$

where $2k = \overline{u_r'^2} + \overline{u_\theta'^2} + \overline{u_z'^2}$. The other terms are described as follows (the Einstein summation convention is used here):

- $P^k = -\overline{u_i' u_j'}\frac{\partial \overline{u}_i}{\partial x_j}$: **Production** - Supply of energy by the mean flow, through interaction with the turbulent shear stress
- $\epsilon = -\nu\overline{\left(\frac{\partial u_i'}{\partial x_j}\right)^2}$: **Viscous Dissipation** - Always negative, acts as a sink for the turbulent kinetic energy
- $\Pi^k = -\frac{1}{\rho}\frac{\partial \overline{p' u_i'}}{\partial x_i}$: **Pressure-related Diffusion**: Turbulence transport by pressure fluctuations
- $\mathcal{D}^k = \frac{\nu}{2}\frac{\partial^2 \overline{u_i' u_j'}}{\partial x_j^2}$: **Viscous Diffusion**: Turbulence transport by viscosity
- $T^k = -\frac{1}{2}\frac{\partial \overline{u_i' u_i' u_j'}}{\partial x_j}$: **Turbulent Diffusion**: Turbulence transport by velocity fluctuations

Figure 2.3 shows the contribution of the various terms to the turbulent kinetic energy budget. From the definition of k, it is clear that the budget of k is obtained from the summation of the budgets of the three turbulence intensities (Eggels et al. 1994). The major component

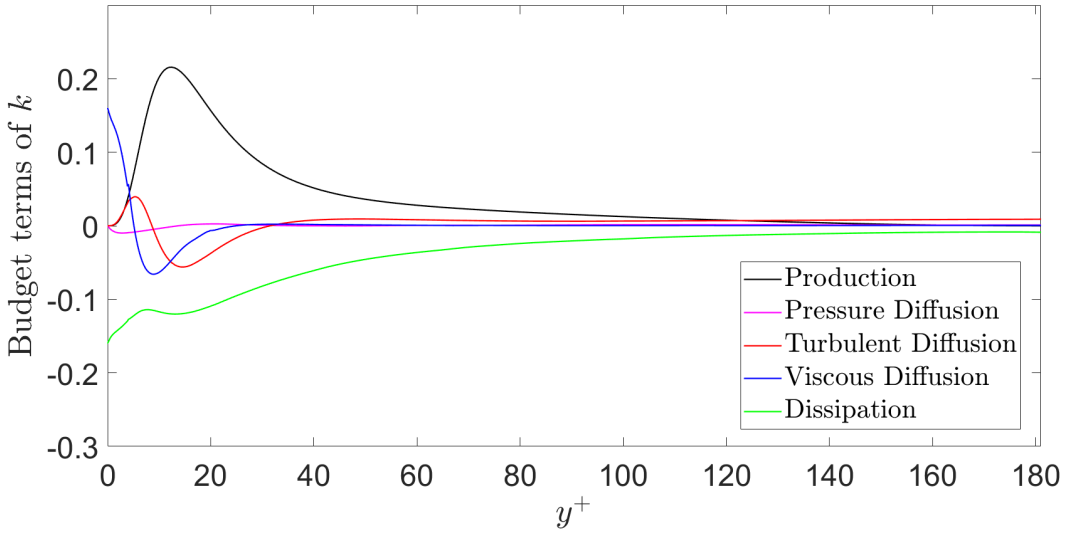

Figure 2.3: Budget Terms Normalized by ν/u_*^4

contributing to the TKE is the term $\overline{u_z'^2}$. From Figure 2.3, it is seen that near the wall, the dissipation is balanced by the viscous diffusion. Further away from the wall, in the buffer layer, the production of turbulence reaches a maximum. This is then redistributed throughout the flow by the different diffusion terms. Eggels et al. 1994 states that the viscous diffusion plays an important role in redistributing the energy towards the wall, while the turbulent diffusion is predominant in redistributing the energy in the buffer layer to the other regions of the flow. Pressure diffusion is nearly zero in the budget - the term is important only for the redistribution of energy from the axial component to the other two velocity components.

Several studies have also been dedicated to understanding the cascade process in pipe flow. This involves plotting the energy spectrum at different locations, and determining the regions of interest. Kolmogorov 1941 famously hypothesized that in the inertial subrange, the energy spectrum is universal and is of the form,

$$E(k) = C\epsilon^{2/3}\kappa^{-5/3} \tag{2-15}$$

where ϵ is the viscous dissipation and κ here refers to the wavenumber. This is easily proved for homogeneous, isotropic turbulence, but is slightly more difficult to verify for cases that are anisotropic. Laufer 1954 measured the various energy contributions and plotted the spectra. He fit a -1 power law for the spectrum, but was unable to fit Kolmogorov's universal -5/3 power law for higher Reynolds numbers, and thus, concluded that an inertial subrange doesn't exist in pipe flow. However, Lawn 1971 disputes this claim, and proved the existence of an inertial subrange, and thus, the presence of a -5/3 power law.

The cascade of energy in a turbulent flow takes place through vortex stretching. The larger eddies deform the smaller eddies, increasing the vorticity of the smaller eddies and transferring energy to them. Wall-bounded flows are characterized by bursting. This involves the presence of regions near the wall, where the velocity is small, and these are called low-speed streaks (Nieuwstadt et al. 2016). Perturbations on these streaks will grow, and cause these streaks roll up and form hairpin vortices. Hairpin vortices move low-speed fluid close to the wall

into a region having a higher mean velocity away from the wall. This is induced by the two counter-rotating vortices which form the base of the hairpin vortex, and are referred to as ejections ($u_z' < 0, u_r' > 0$) (Araya et al. 2018). The hairpin vortices are stretched by the mean deformation field, which leads to the growth of these local vortices, until they become unstable and disintegrate into smaller structures. This process is called a "turbulent burst" (Nieuwstadt et al. 2016). Most of the turbulent shear stress and kinetic energy is produced in these bursting events. After bursting, high-speed fluid moving towards the wall replaces the fluid close to the wall. This is called as a sweep event ($u_z' > 0, u_r' < 0$) (Araya et al. 2018).

The bursting process is crucial in trying to understand how the turbulence is produced and dissipated. Another interesting observation of the process is made by Lee et al. 1990, where the authors found the presence of streaks in homogeneous turbulence at high shear rates, that were similar to the ones found in wall-bounded turbulence. Their study shows that a solid boundary is not completely necessary for the production of streaks, and a high shear rate alone could be sufficient. This is intriguing, as it raises the question, as to how similar a wall-bounded flow is to homogeneous turbulence at high shear rates. This question becomes even more important to answer when considering decay of turbulence, because of the predictability of decay in homogeneous turbulence as compared to wall-bounded turbulence, and will be revisited in later sections.

2-3 Non-Newtonian Modelling and Application in Pipe Flow

Some part of research is now dedicated to turbulent, non-Newtonian, fully-developed pipe flow. This section is a means to understand the similarities and differences between Newtonian and non-Newtonian with respect to the turbulence statistics. It is useful to introduce a few concepts about non-Newtonian fluids here. Newtonian fluids are defined as those fluids for whom the shear stress is directly proportional to the strain rate. Non-Newtonian fluids do not adhere to this rule. First, the deformation gradient needs to be defined. The velocity gradient is defined as $\boldsymbol{\nabla u} = \partial u_i / \partial x_j$. Then, the deformation gradient is described as (Macosko 1994)

$$\boldsymbol{D} = [\boldsymbol{\nabla u} + (\boldsymbol{\nabla u})^T]/2 \tag{2-16}$$

The shear stress is a function of the deformation gradient. For the simplest case of non-Newtonian fluids, the viscosity varies with the shear rate only and these are called generalised Newtonian fluids. Using the deformation gradient, the stress tensor can be defined as (Bessonov et al. 2016)

$$\boldsymbol{\tau} = \mu(\dot{\gamma}) 2\boldsymbol{D} \tag{2-17}$$

with the shear rate, $\dot{\gamma}$, given by

$$\dot{\gamma} = \sqrt{2\mathrm{tr}(\boldsymbol{D}^2)} = \sqrt{-4II_D} \tag{2-18}$$

Here, II_D denotes the second principal invariant of the rate of deformation tensor, given as

$$II_D = \frac{1}{2}[(\mathrm{tr}\boldsymbol{D})^2 - \mathrm{tr}(\boldsymbol{D}^2)] \tag{2-19}$$

For incompressible flow, $\mathrm{tr}\boldsymbol{D} = 0$. The most widely used form of the constitutive relation to model the viscosity is the power law model.

$$\mu(\dot{\gamma}) = K\dot{\gamma}^{n-1} \tag{2-20}$$

where, K is called the consistency and n is the power-law index (Bessonov et al. 2016). The value of n dictates the type of fluid being modelled – $n < 1$, indicates a shear-thinning fluid, whose viscosity decreases as the shear rate increases; $n > 1$, indicates a shear-thickening fluid, whose viscosity increases as the shear rate increases. The case of $n = 1$ indicates a Newtonian fluid. The power-law has one defect however – for shear-thinning fluids, as the shear rate tends to zero, the model predicts infinite viscosity as opposed to a fixed value seen in experiments (Macosko 1994). This indicates the need for other models as well.

Applying a non-Newtonian model to pipe flow raises certain questions. The first question is on how to define a generalised Reynolds number, since the viscosity is not constant. Metzner et al. 1955 propose a Reynolds number, derived theoretically for laminar flow, such that the Fanning friction factor conditions are satisfied by this Reynolds number ($f = 16/Re_{MR}$). This is the Metzner-Reed Reynolds number and is given for a power-law fluid as

$$\mathrm{Re}_{MR} = \frac{8\rho U_b^{2-n} D^n}{K(6+2/n)^n} \tag{2-21}$$

Eq. 2-21 reduces to the standard Reynolds number for $n = 1$. The Metzner-Reed Reynolds number performs well in predicting the friction factor for laminar flow of generalised Newtonian fluids. However, its behaviour is not acceptable for transitional and turbulent flows. A good reason for this is the method in which the relation is derived analytically, on the basis of laminar flow considerations. Therefore, several authors (Pinho et al. 1990; Toonder et al. 1997b; Pinho 2003) propose another Reynolds number based on the wall viscosity, μ_w, as

$$\mathrm{Re}_w = \frac{\rho U_b D}{\mu_w} \tag{2-22}$$

The wall Reynolds number provides more physical significance for turbulent pipe flows. As mentioned previously, most of the turbulence is produced and dissipated near the wall in pipe flows, and the region near the wall has the highest shear rate (Rudman et al. 2004). Furthermore, this Reynolds number can be predetermined from experiments via the momentum balance (Toonder et al. 1997b), and can also be fixed numerically using an iterative procedure, if the viscosity model requires it (Ptasinski et al. 2001; Singh et al. 2017).

In the following paragraphs, description of changes to the structure and the statistics of pipe flow due to non-Newtonian fluids is summarized. The results presented are for generalized Newtonian fluids or for dilute polymer solutions behaving in the same fashion. For non-Newtonian fluids, Bewersdorff et al. 1993 explain the thickening of the buffer layer, as compared to Newtonian systems. Toonder et al. 1997b performed experiments and numerical simulations with dilute polymer solutions and notice similar results. This is represented in the form of an upward shift of the logarithmic profile of the mean velocity. Unlike the suggestions of Virk et al. 1970, the shift is not quite parallel to Newtonian flow, and in fact the slope for polymer solutions is quite larger than the Newtonian profile (see also Pinho et al. 1990).

Toonder et al. 1997b also provide compulsive evidence about the root mean square (RMS) statistics. In comparison with Newtonian values, the axial RMS has its maximum shifted slightly away from the wall, and also shows a higher magnitude. Additionally, they find a slight decrease of this quantity for $y^+ \leq 10$, and also at the centerline. A possible explanation for this is the creation of a shear-sheltering layer, with high turbulence above and lower turbulence below (Ptasinski et al. 2001). The radial and azimuthal RMS values decrease

almost across the entire cross-section, and the peak of the profile for both of the cases is shifted slightly away from the wall. The results are also consistent with the increase in size of the buffer layer (Bewersdorff et al. 1993). In their dilute polymer experiments, Pinho et al. 1990 find the radial and azimuthal fluctuations to be nearly five times less than the axial fluctuations, and they have comparable results to Toonder et al. 1997b. Similar results are also seen for purely shear-thinning fluids (Rudman et al. 2004; Rudman et al. 2006). This reduction suggests that the strength of the vortices is weaker for non-Newtonian fluids, and thus, a weaker bursting process must be observable (Rudman et al. 2006). The numerical study of Singh et al. 2017 on generalized Newtonian fluids also emphasizes the increase in the size of the structures as the degree of shear-thinning increases.

Taking a look at higher-order statistics for these flows provides a much deeper understanding of the interaction of the non-Newtonian nature of the fluid with the turbulence. A decrease in the magnitude of the Reynolds' stress is observed, as compared to the Newtonian fluid, at all regions except the center (Toonder et al. 1997b; Rudman et al. 2004), and similar to the RMS values and fluctuations, the peak is shifted away from the wall. Simulations on power-law fluids by Rudman et al. 2004 indicate that this distance from the wall decreases, as the power-law index (n) decreases, which they claim is a reflection of the increased viscosity away from the wall damping out the turbulent fluctuations. It is also interesting to note that the Reynolds stress deficit increases with a decrease in the power-law index.

These studies indicate a modification to the shear stress formulation when employing a dilute polymer solution or a non-Newtonian fluid. For generalised Newtonian fluids, Pinho 2003 provides an analytical view of the problem at hand. He derives transport equations for momentum, Reynolds stress, and other quantities, by applying a Reynolds' decomposition to the viscosity. Therefore, writing the viscosity as $\nu = \overline{\nu} + \nu'$, the unsteady Reynolds averaged momentum equation, using the Einstein convention, is given as

$$\frac{D\overline{u_i}}{Dt} = -\frac{1}{\rho}\frac{\partial \overline{p}}{\partial x_i} + \frac{\partial}{\partial x_j}(2\overline{\nu}D_{ij} + 2\overline{\nu' D'_{ij}} - \overline{u_i u_j}) \tag{2-23}$$

where D_{ij} are the components of the deformation gradient introduced in eq. 2-16, and $D'_{ij} = \partial u'_i/\partial x_j$, are the fluctuations of the deformation gradient. Eq. 2-23 introduces a new diffusive term, $2\overline{\nu' D'_{ij}}$, and the classical viscous stress is slightly modified. Looking back at eq. 2-13, which provides a stress balance for Newtonian flows, this can be modified as

$$\tau^+_{rz} = \tau^+_V + \tau^+_{fv} + \tau^+_R \tag{2-24}$$

where τ^+_R indicates the non-dimensionalized Reynolds stress, τ^+_V is the non-dimensionalized viscous stress, and τ^+_{fv} is the turbulent viscous stress. The total stress (τ^+_{rz}) remains constant for Newtonian and non-Newtonian fluids, which makes it clear from the relation above, that the turbulent stress deficit seen in these experiments and simulations, is manifested as a polymeric stress for dilute polymer solutions (Toonder et al. 1997b; Ptasinski et al. 2001), or a non-Newtonian viscous stress (Pinho 2003; Singh et al. 2017), which is represented by τ^+_{fv} in eq. 2-24. From the experiments and also from eq. 2-23, it can be noticed that the viscous stress is slightly modified for non-Newtonian systems. Comparing eqs. 2-23 and 2-24, it is clear that the turbulent viscous stress contains these deficit values, and is equivalent to the term $2\overline{\nu' D'_{ij}}$. This extra term can be evaluated in experiments from simple algebra using eq. 2-24 (Toonder et al. 1997b; Ptasinski et al. 2001), and also numerically, by using the

expression given above (Singh et al. 2017). The turbulent viscous stress does not vanish at the wall, as neither the fluctuations of the viscosity, nor the fluctuations of the shear rates vanish at the wall. The term can either be positive or negative, and is in fact dependent on the rheology of the fluid used (Singh et al. 2017). Proceeding in a similar fashion, Pinho et al. 1990 derive a transport equation for the turbulent kinetic energy as well, akin to eq. 2-14.

$$\frac{Dk}{Dt} = P^k + \epsilon + \Pi^k + \mathcal{D}^k + T^k + \xi_{nn} + \mathcal{D}_{nn} + \chi_{nn} + \epsilon_{nn} \tag{2-25}$$

Here, the subscript nn is used to indicate the fact that these terms arise due to the non-Newtonian analysis, and the viscous terms adopted from eq. 2-14, such as $\mathcal{D}^k$ and ϵ, now employ the mean viscosity ($\overline{\nu}$) in their formulation. The new terms are detailed as follows:

- $\xi_{nn} = \frac{\partial}{\partial x_j}(2\overline{\nu' u_i'} D_{ij})$: Turbulent viscous transport due to the mean shear
- $\mathcal{D}_{nn} = \frac{\partial}{\partial x_j}(2\overline{\nu' u_i' D_{ij}'})$: Turbulent viscous transport, similar to the mean viscous transport, $\mathcal{D}^k$
- $\chi_{nn} = -2\overline{\nu' D_{ij}'} D_{ij}$: Turbulent viscous dissipation due to the mean shear
- $\epsilon_{nn} = -2\overline{\nu' D_{ij}' D_{ij}'}$: Turbulent viscous dissipation, comparable with the mean viscous dissipation, ϵ

The turbulent viscous dissipation due to mean shear, χ_{nn} also appears in the mean flow kinetic energy equation, and can be either positive or negative, based on the shear rheology. A positive value implies that the kinetic energy dissipation is reduced. Additionally, the sign for this term is the same for both the mean flow and the turbulent kinetic energy budgets, which suggests that this term impacts both the budgets in a similar manner. ϵ_{nn}, unique to the TKE budget, can also be either a positive or negative value (Singh et al. 2017).

Similar to other quantities, the peak production of kinetic energy (P^k) is shifted away from the wall, with the general trend showing a decrease in production with increasing shear thinning. On deeper analysis, it is fairly obvious that this decrease in P^k coincides with the decrease in the Reynolds stress mentioned earlier, since the velocity gradient does not change much with shear thinning (Singh et al. 2017; Toonder et al. 1997b). The decrease is more prominent near the wall ($y^+ < 10$ as per Toonder et al. 1997b, $y^+ \leq 6$ as per Singh et al. 2017), as compared to the rest of the regions. Decreasing the power-law index also elevates the mean viscous transport, $\mathcal{D}^k$, and the mean dissipation, ϵ, close to the wall (Pinho 2003).

The two non-Newtonian dissipation terms, χ_{nn} and ϵ_{nn}, are found to be positive for shear-thinning and negative for shear-thickening fluids. These terms are to be interpreted for shear-thinning fluids as "quantities that reduce the mean flow dissipation (ϵ) over the entire pipe radius, but particularly for $y^+ < 40$" (Singh et al. 2017). The overall effect is to reduce the total dissipation for shear-thinning fluids for $y^+ \leq 30$, with the reduction balancing the net reduction in the transport and the production as well.

While eqs.2-24 and 2-25 provide a nice basis to approximate the results obtained for non-Newtonian fluids, these results are largely unverified experimentally. This is one of the main reasons, why several experiments related to drag reducing polymers are discussed, as they provide a good analogy to generalised Newtonian fluids (Toonder et al. 1997b; Ptasinski et al.

2001). There is some solace to be found in the fact that these studies find similar results as those provided by Rudman et al. 2004, Rudman et al. 2006 and Singh et al. 2017, and the equations for the momentum and the turbulent kinetic energy provided by Ptasinski et al. 2001 are analogous to the ones derived by Pinho 2003. Along with the equivalence of statistics between drag reducing polymers and generalised Newtonian fluids, this is particularly useful to show that the equations derived by Pinho 2003 can be employed for predicting turbulent quantities for non-Newtonian systems. Furthermore, Ptasinski et al. 2001 find the polymeric dissipation to be the largest loss term in the TKE budget, and thus, postulates that most of the energy is transferred directly to the polymers and not by the route of turbulence. It will be interesting to see if the viscosity fluctuations contribute in a similar fashion to the dissipation in generalised Newtonian fluids.

Toonder et al. 1997b also plot the one-dimensional power spectra at various locations in the form popularised by Perry et al. 1975. The wavenumber is non-dimensionalised using the quantity, u_*/ν, and the velocity is made non-dimensional using, u_*. Here, the viscosity used is the wall viscosity, and u_* is the wall-friction velocity. The axial component spectrum shows a shift towards smaller wavenumbers as compared to Newtonian results, which indicates a decrease of energy at the smaller scales, and an increase at the larger scales. The turbulent energy of the radial component is found to be suppressed over the entire range of wavenumbers, with a small shift in the peak towards smaller wavenumbers. The shift from small to large scales is more prominent at $y^+ = 30$.

To conclude this section, a discussion about the Reynolds number is undertaken. In the aforementioned description of turbulent pipe flows, the wall Reynolds number was chosen to contrast the results obtained. One of the reasons provided for using the wall viscosity to scale the Reynolds number is the location of maximum production of turbulent kinetic energy coinciding with the Newtonian fluid for the whole range of the flow index covered in various studies (Toonder et al. 1997b; Rudman et al. 2006). This result is not completely accurate though, with Singh et al. 2017, showing a slight shift in the production of TKE in non-Newtonian fluids away from the wall. However, the shift is not large enough to influence the results by a large margin, and this Reynolds number is still the most logical choice, since turbulence is mainly produced and dissipated near the wall. All the results mentioned here for turbulent flows employ the wall Reynolds number, and there is no anomaly noticed in the results by doing so. Therefore, this is the first choice of generalised Reynolds number that will be employed in this research.

Chapter 3

Decay of Turbulence

The mechanisms of how turbulence breaks down and decays in different flows has been observed for years. Of particular interest has been homogeneous, isotropic turbulence, which will be discussed here to see if any of the findings in this field can be applied to the current research. Isotropic turbulence is an ideal state wherein the turbulent fluctuations are statistically uniform in all directions. This can be visualised as a flow far away from boundaries, and is a simplification tool to research the underlying fundamental properties of turbulence. Isotropic turbulence does not have any production or transport, and therefore, the TKE budget only has dissipation. The most effective way to study isotropic turbulence experimentally is to look at flow behind grids (grid-generated turbulence), which is homogeneous in the frame of reference moving with the mean velocity of the flow (Pope 2000).

Unique solutions can be found, and it can be shown that the energy decays according to the law, $\overline{u'^2} \propto t^{-n}$. Various authors provide different values for the decay index. Kármán et al. 1938 gives an index of -1, while Batchelor et al. 1948 provides an index of -1 for the initial period of decay, and an index of -5/2 for the final period of decay. This gives an overall decay index of $n = -10/7$. Using a similar hypothesis, Saffman 1967 finds a decay exponent of -3/2.

Skrbek et al. 2000 studied decaying, homogeneous isotropic turbulence on a model based on the three-dimensional energy spectra. They performed experiments where they truncate the energy spectrum, by predefining the smallest and the largest wave number in the flow. The smallest wavenumber is determined by the domain size, while the largest wavenumber is effectively determined by the Kolmogorov length scale. They also study the effects of intermittency on the decay, and find that its' effect is to introduce a virtual origin for the decay law, rather than actually change the decay exponent. Due to the introduction of an energy containing length scale, special care was required in the study to distinguish between the final period of decay, and the change in the nature of decay due to the truncation of the length scale. Their theory provides good agreement with existing wind tunnel experiments on grid turbulence and a decay index of -2 is found for the TKE, once the length scale has reached saturation. A similar analysis of decay is also considered for a bounded domain without any mean flow by Touil et al. 2002. Here, the use of introducing a low wavenumber cut-off is to account for the effect of the geometry, and DNS is performed on this bounded geometry. The

results obtained are similar to those of Skrbek et al. 2000 for experiments involving Helium II in a finite channel, wherein the RMS vorticity decays as $\omega \sim t^{-3/2}$, and the TKE decays with an exponent of -2.

While it is tough to characterize the results of pipe flow with those of the studies mentioned here, it is quite useful to understand the general character of decay for isotropic as well as anisotropic, homogeneous flows. Towards the core of the pipe, far away from the wall, the flow can be considered to be sufficiently isotropic. However, this analysis fails as one moves closer to the wall. It has been noticed that turbulent boundary layers subject to favourable pressure gradients, and sub-critical pipe and channel flows undergo relaminarization, i.e., a process by which an initially turbulent flow is rendered effectively laminar (Sreenivasan 1982). The precursor to relaminarization is called laminarescence, where large departures occur from the initial fully turbulent stage. There is further suggestion that if the agency responsible for creating laminarescence is removed, the flow can possibly become retransitional again. A revision of the various studies on decay of turbulence related to pipe flows is provided in the next section, followed by an extension of the presented research for non-Newtonian fluids.

3-1 Transition and Decay in Pipe Flows

In this section, a discussion is first provided to understand how turbulence is generated from a laminar state. This will be helpful to set up fully-developed pipe flow simulations, while also providing insight into how authors have approached the issue of transition. This could also be helpful in analyzing the decay of turbulence and the reverse transition from a turbulent to a laminar state. In the previous sections, it was mentioned that pipe flows belong to the class of shear flows that are linearly stable. Providing perturbations of sufficient amplitude generates an intermittent transition to turbulence for sufficiently high Reynolds numbers. Using the idea of a nonlinear turbulence cycle for the regeneration of the vortices and the streaks, Faisst et al. 2003 conducted numerical studies to provide traveling wave solutions, i.e., "coherent structures that move with constant wave speed", akin to those found in Couette and Taylor-Couette flows.

Initiation of turbulence at low Reynolds numbers generates turbulent flow with distinct structures. Wygnanski et al. 1973 show a region of localized turbulence upto Re = 2250, with a length of approximately $20D$, and this region is called a puff. Puffs travel at a speed of $0.9U$ (U here referes to the mean velocity), and contain a block of disordered flow, with a decaying wave at the front and a sharp interface at the rear (Peixinho et al. 2006). Thus, a puff is considered as a "minimal flow unit" that can sustain turbulence, wherein the generation of turbulent motion is balanced by the viscous dissipation of kinetic energy (Nieuwstadt et al. 2016). As the flow rate increases, these puffs split and delocalize into smaller puffs. Further increase of Re, create rapidly expanding active regions of turbulence called slugs.

Several studies have been undertaken to characterize the pertubation amplitude required to cause this transition to turbulence. Darbyshire et al. 1995 conducted experiments where they introduce disturbances by injecting a constant fluid volume, at a certain distance downstream of the fully developed laminar flow at different Reynolds numbers. By assigning a time, T_0, a point was marked as "transition" or "decay", based on whether the perturbation still persists after the time or not. The required amplitude of perturbation was found to be proportional

to the injected fluid volume. Further experiments conducted by Hof et al. 2003 generalize this result and a scaling for the amplitude (A) with the Reynolds number, $A \sim \mathcal{O}(\mathrm{Re}^{-1})$, is given. As expected, the required amplitude of perturbation to cause transition decreases with increased Reynolds numbers (Peixinho et al. 2006).

The current study is not based on determining the onset of turbulence or on the point of transition itself. Puffs are not usually observed in the decay of turbulence by switching-off the forcing, as this is a gradual process. It is of interest however, to note that several different ideas of decaying turbulence exist.

The relaminarization of an initially turbulent flow was first noticed in accelerated boundary layers. The sudden acceleration imposed causes a reduction in the turbulent intensities, due to the pressure forces dominating over the Reynolds stresses (Narasimha et al. 1979). In pipe and channel flows, the reversion from turbulent to laminar flow is due to the action of the viscosity. Several experiments have been carried out where a slight divergence is created in the duct to reduce the pressure gradient. The divergence is such that there is no flow separation, and thus, the turbulent stresses are dissipated by viscosity (Sreenivasan 1982).

Relaminarization is a gradual process, with some notable changes to both the structure and the statistics, as compared to the fully developed turbulent flow state. The reduction in turbulent intensities and stresses is accompanied by a departure of the velocity profile from the "law of the wall" (Patel et al. 1968), and under suitable local conditions, will approach the laminar velocity profile (Sibulkin 1962; Narayanan 1968). The experiments conducted show a rapid adjustment near the wall, while the outer layer is manifested with slower processes. Since the energy input is reduced, it is clear that the turbulent energy production will also decrease, and this is accompanied by a reduction in the wall-layer bursting process (Sreenivasan 1982). It has also been noticed that the low-speed streaks are elongated in the streamwise direction, with longer survival of the hairpin vortices during relaminarization, as compared to full turbulent flow (Araya et al. 2018).

Sibulkin 1962 was one of the first authors to perform experiments on the relaminarization in pipe flow. A fully developed turbulent flow was initiated, which is then allowed to pass through a diverging section of angle 1°. He found that the rate of decay of the longitudinal fluctuations was Reynolds number dependent, and the fluctuations decayed more rapidly near the wall and at the center, rather than at an intermediate radius, during the initial period of relaminarization. Furthermore, he measured the energy spectrum of the fluctuations along the pipe centerline, and found these spectra at different axial locations to be similar to each other in the measured wavenumber range.

A similar experimental setup was used to study reverse transition in a two-dimensional channel flow by Narayanan 1968. He found that the longitudinal and vertical RMS values decrease exponentially with the streamwise distance, and the Reynolds stress $\overline{u'v'}$ tends to become zero. Here, u' represents the axial fluctuation, while v' represents the wall-normal fluctuation. Additionally, he comments that the streamwise velocity fluctuations persist for a longer period of time than the vertical fluctuations. A new quantity is introduced here, termed as the correlation coefficient (Narasimha et al. 1979), or the "loss of correlation", given as

$$C = \frac{\overline{u'v'}}{\sqrt{\overline{u'^2}}\sqrt{\overline{v'^2}}} \tag{3-1}$$

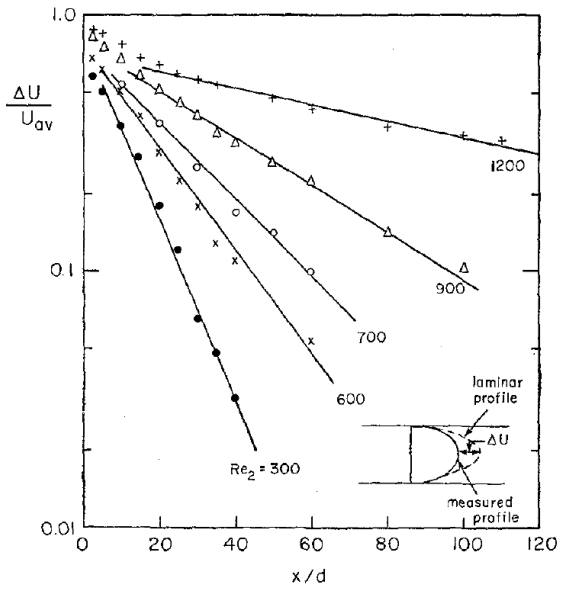

Figure 3.1: Departure of measured mean velocity from the expected Poiseuille value at the center (Narasimha et al. 1979)

Narayanan 1968 finds that this quantity decreases as the flow moves downstream. The decrease in the correlation coefficient indicates that there is a decorrelation mechanism at work as the flow relaminarizes. It is difficult to state when exactly relaminarization is complete. Narasimha et al. 1979 define relaminarization to be complete "when the effect of the Reynolds stresses on the mean flow development becomes negligible". This effectively translates to determining when the Reynolds stresses are approximately zero. Additionally, Narasimha et al. 1979 and Narayanan 1968 suggest monitoring the reduction in the correlation coefficient (given by eq. 3-1) as a suitable method to determine the process of relaminarization.

Narasimha et al. 1979 provide another method to determine the relaminarization effectively. They characterize the departure of the velocity at the center-line, from the case of fully developed laminar flow. If this quantity is given by ΔU, then it is seen that

$$\Delta U = \exp(-\alpha x/2R) \tag{3-2}$$

where α is a constant for a given Reynolds number. Furthermore, a dependence of α on the Reynolds number is provided as $\alpha \propto (\mathrm{Re}_{cr} - \mathrm{Re}_2)^{1.5}$. Here, Re_2 signifies the Reynolds number that the flow is supposed to attain downstream of the expansion. Re_{cr} is the critical Reynolds number, below which the flow is laminar. The relation provided shows that α increases as Re_2 decreases. Fig. 3.1 shows this departure for different values of Reynolds numbers. Assuming an isotropic flow, and using the precursor works of Owen 1969 on the flow in a trachea, Narasimha et al. 1979 provides an empirical relation for the TKE as

$$\overline{u'^2} = \exp\left(-B(Re_{cr} - Re)^3(x - x_0)/R\right) \tag{3-3}$$

It is interesting to note that a critical Reynolds number is tough to define for fully developed

turbulent pipe flow, which is expected due to the highly non-linear nature of turbulence. The experiments presented here for pipe and channel flows provide methods for the determination of a critical Reynolds number for the case of relaminarization. Narasimha et al. 1979 state that pipe and channel flows are unambiguously laminar for values of $\mathrm{Re}_{cr} < 1500 \pm 100$ and below. On the route to transition from a laminar to a turbulent state, the definition of a critical Reynolds number is difficult. It is noticed in several studies of pipe flows that triggering turbulence is highly dependent on the sensitivity of the initial conditions. The initial conditions do not play a role in how the quantities scale or are defined – fully-developed pipe flows are "memoryless". They play an important role in determining whether the realized state is fully turbulent or not. Additionally, between the laminar and the turbulent state, there exists no intermediate region with simple spatial or temporal characteristics, and therefore the definition of a critical Reynolds number is ambiguous while achieving a fully-developed turbulent flow. Provided sufficient observation time, even a statistically steady turbulent flow may decay (Eckhardt et al. 2007). The crucial point of interest would be to provide some comment on the point of complete relaminarization. Determining the decay of the TKE, the turbulent fluctuations and the correlation coefficient, along with the structures, should provide a picture of the relaminarization process.

3-2 Decay of Non-Newtonian Systems

With so many variables to factor in for the decay in a Newtonian system, introducing the non-Newtonian nature of the fluid makes the discussion intriguing. The results are again provided for generalized Newtonian fluids or for fluids modelled in a similar fashion. Chow et al. 1967 try to hypothesize on some of the effects this inclusion may have on the decay of isotropic turbulence. A viscoelastic fluid was studied using the Oldroyd constitutive equation. They found that having suspended particles in the fluid speeds up the rate of decay, but they also attributed most of the decay effects seen to the elasticity of the fluid, rather than its shear-thinning behaviour. The small-scale structure of grid turbulence was modified by adding a polymer additive, which is considered to show high shear-thinning behaviour, in the experiments of McComb et al. 1977. Similar to pipe flows and other non-Newtonian experiments mentioned, the polymer additive reduces the turbulence intensity behind the grid. This consequently leads to a reduction in the rate of decay of velocity fluctuations behind the grid, as compared to the Newtonian case. Besides, the concentration of the polymer additive made a difference as well, with lower concentrations having an energy spectrum similar to water (a Newtonian fluid), but higher concentrations showing considerable attenuation.

Doorn et al. 1999 measured the decay of turbulence in polymer and surfactant solutions behind a towed grid, using Particle Image Velocimetry (PIV). They find distinct anisotropy in these fluids as compared to water, and the differences are more persistent in the initial period of decay. The anisotropy observed is comparable to the wall-region in wall-bounded flows of Newtonian fluids. The surfactant case shows the existence of small-scale anisotropy even at later stages, while this is suppressed in the polymer case. The energy spectra do show a -5/3 power-law variation in a small range of wavenumbers, but it is not so conspicuous in the surfactant case. This is possibly because of the suppression of large-scale energy in the surfactant case, but the effect cannot be explained by the increased viscosity of the surfactant solution.

To understand the decay of a purely shear-thinning fluid, Rahgozar et al. 2017 performed experiments in a boundary-free, uniformly sheared flow at high Reynolds number. They employed a pulsatile flow similar to a heart beat to study the decay of TKE in a periodic cycle. They used xanthan gum, which is similar to blood in its' shear-thinning nature, and found that the turbulent kinetic energy and the dissipation rate are modified, along with significant alteration to the characteristics of the large-scale eddies. They find the decay rate of the TKE to be much larger at the initial period for the non-Newtonian case, as compared to the Newtonian case, and attribute this to the high viscosity at low shear rates.

It must be remembered from eq. 2-25 that the dissipation in a non-Newtonian fluid has two extra terms as compared to a Newtonian fluid, and therefore, mention of dissipation here is a summation of both the Newtonian and non-Newtonian terms. Rahgozar et al. 2017 find the dissipation rate decreases with respect to the Newtonian case at the initial part of towing, an then increases in the latter part. This is attributable to the fact that polymers probably absorb and store the turbulent energy at high shear rates and then release it at low shear rates. It can also be inferred that when the Reynolds stresses weaken towards the end of decay, polymers and shear-thinning fluids have more room to modify the structures. This combination of absorbing and releasing energy leads to a higher overall dissipation rate. Other studies on grid turbulence in polymer solutions also provide comparable results qualitatively, especially with respect to the modification of structures in the flow (Liberzon et al. 2006; Vonlathen et al. 2013).

The discussion now moves forward to the study of transition and decay in non-Newtonian pipe flows. Similar to Newtonian Poiseuille flow, pipe flow of non-Newtonian fluids is also linearly stable (López-Carranza et al. 2012). Indeed, it is shown that a non-Newtonian fluid is more stable than its' Newtonian counterpart (Peixinho et al. 2005; López-Carranza et al. 2012). G. Tripathi 1971 found that the presence of a non-Newtonian fluid in the system delays transition to turbulence, which is evident from the previous statement on linear stability. Draad et al. 1998 also find a delay in transition in their experiments, although they can only confirm this result for extended fresh polymers. An interesting point to note here is that the natural transition number (transition to turbulence with minimal perturbation) is increased for these dilute polymer solutions. The route to transition in non-Newtonian fluids is similar to that of Newtonian fluids, with the manifestation of puffs and turbulent spots, followed by slugs. The required amplitude of perturbation to cause turbulence is now slightly higher than that for Newtonian fluids (Rudman et al. 2006).

Research on turbulence decay in pipe flows of non-Newtonian fluids has been limited. Relaminarizing flows have not been comprehensively researched for non-Newtonian fluids. Certain details can be hypothesized - a higher critical Reynolds number can be obtained as compared to the Newtonian flow, with possibly faster rates of turbulence decay near the wall. This would be in line with other results noticed in grid turbulence of non-Newtonian fluids as well. A study similar to the work of Peixinho et al. 2006 or Hof et al. 2006 would also be intriguing to understand the characteristic lifetimes of turbulence. Additionally, concentrating on how the rate of dissipation and turbulent kinetic energy varies with the Reynolds number and the shear-thinning index, and hence, contrasting it with the Newtonian case is of particular interest. Therefore, it is the intention of this study to undertake Direct Numerical Simulations (DNS) to understand the nature of decay of turbulence in pipe flow of non-Newtonian fluids at low to moderate Reynolds numbers.

Chapter 4

Spectral Element Methods and nek5000

Over the years, the employment of Direct Numerical Simulations has directly been correlated to the availability of computational resources. The necessity to accurately capture the smallest energy contributing scales in a flow has lead to the development of faster and better numerical techniques to solve the Navier-Stokes Equations.

The spectral element method is an advanced implementation of the finite element method, obtained by combining spectral techniques to the same. Here, the solution over each element is defined in terms of *a priori* unknown values at the appropriate spectral nodes (Pozrikidis 2014). This provides an advantage as it maintains the generality of the finite element method, while it improves accuracy by employing spectral techniques. The method is applicable over a wide range of problems, and stable, accurate solution algorithms can be achieved with a lower number of elements. Additionally, while spectral methods require periodicity in the flow direction, due to the decomposition of the solution into Fourier modes, the spectral element method has no such strict requirement (Pozrikidis 2014; Patera 1984).

In the finite element method, the quantity to be solved, which is the velocity for the Navier-Stokes equations, is expressed as

$$\boldsymbol{u_a} = \sum_{i=1}^{N} b_i \phi_i \tag{4-1}$$

where $\boldsymbol{u_a}$ is the approximation of the exact solution, that has been defined in the form of an expansion of N basis functions, with amplitudes b_i (Prasad 2016). The basis functions for the spectral element method are selected from a family of orthogonal polynomials. While finite element methods use local basis functions (non-zero only on small subdomains), spectral methods employs global basis functions (non-zero everywhere), spanning the entire domain of the problem. This polynomial expansion is defined by interpolation nodes within an element, which are distinct from the geometrical nodes. A variational formulation is then set up for the governing differential equation, and the Galerkin's projection is implemented. A system of algebraic differential equations is obtained, which is modified by the boundary conditions, and then solved (Pozrikidis 2014).

4-1 Selection of Basis Functions

The accuracy of a finite element method can be improved in two ways (Pozrikidis 2014):

1. h **refinement**: Reducing the element size, while keeping the polynomial order fixed
2. p **refinement**: Increasing the polynomial order, while maintaining the element size

For h refinement, the error decreases as a power of h, whereas for p refinement, the error decreases faster than any power of $1/p$, which implies exponential convergence. This is termed as spectral convergence (Pozrikidis 2014). Ideally, low-order expansions should be employed where the solution is expected to vary smoothly, while high-order expansions are required where rapid spatial variations exist. Furthermore, it is paramount to achieve the best accuracy for a given system while keeping the computational requirements to a minimum.

The best way to achieve this is by using orthogonal polynomials to define the basis functions. These polynomials are used extensively for the numerical interpolation, integration and solution of differential equations by spectral expansions. The most used interpolation method is the Lagrange interpolation, with the m-th degree Lagrange interpolating polynomial defined as

$$\psi_i(\xi) = \frac{(\xi - \xi_1)\cdots(\xi - \xi_{i-1})(\xi - \xi_{i+1})\cdots(\xi - \xi_{m+1})}{(\xi_i - \xi_1)\cdots(\xi_i - \xi_{i-1})(\xi - \xi_{i+1})\cdots(\xi_i - \xi_{m+1})} \tag{4-2}$$

Eq. 4-2 is used to approximate solutions for a function of interest over an element in the domain. While employing the interpolation, the placement of the nodes plays a key role. Using an even number of nodes gives rise to oscillations near the ends of the interpolation domain, because of the insufficient information provided to the polynomial towards the end of the domain. This is called the Runge effect (Pozrikidis 2014). Therefore, evenly spaced nodes within an element can only be employed if the order of the interpolating polynomial is low. This could however, compromise the accuracy of the solution.

To obtain the highest accuracy for the interpolation, it is required that the intermediate $m-1$ nodes within the domain should be distributed at the zeros of the $(m-1)$ degree interpolating polynomial. This amounts to employing an uneven nodal base for the interior of the domain. Several nodal bases such as the Chebyshev, Jacobi and Legendre nodal bases are available. However, one of the more efficient ones is the Lobatto nodal base. The main advantage of the Lobatto base is that the corresponding node interpolation functions are guaranteed to vary within the range of [-1,1], irrespective of the order of approximation of the interpolating polynomial (Pozrikidis 2014). Lagrange polynomials of different orders are depicted on a Lobatto nodal base in Figure 4.1.

From the discussion above, it becomes clear that using a combined method of refinement, also called as hp refinement, is much more beneficial for the convergence of the solution (Patera 1984). Fischer 1997 recommends a polynomial order in the range of $m = 4 - 15$. When the domain becomes distorted a h refinement is preferred, so as to not drastically increase the computational cost.

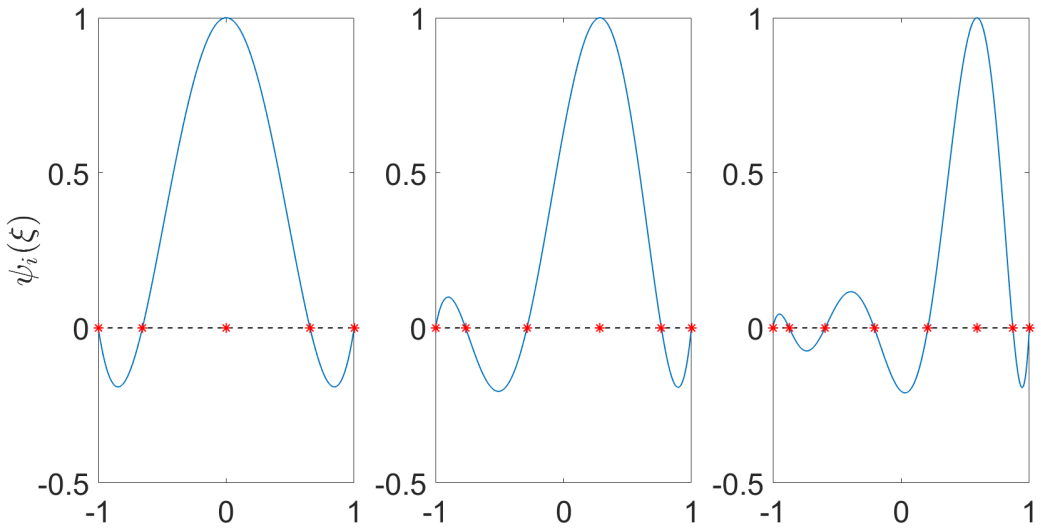

Figure 4.1: Set of Lagrange Polynomials Plotted using Lobatto Interpolation Nodes with Degree: *Left:* $m = 4$; *Center:* $m = 5$; *Right:* $m = 7$

4-2 nek5000

For the present research, higher-order methods are required to accurately predict the nature of decay. To this extent, the stability, accuracy and computational power of spectral element methods has been described, and therefore, this method will be employed in the current study. `nek5000` is a solver that uses the spectral element method to solve the Navier-Stokes equations with good scalability for different models (Paul F. Fischer et al. 2008). It employs a Lagrange interpolation on a Lobatto nodal base, as mentioned above, with a Gaussian integration quadrature to generate the solution (termed the Gauss-Lobatto-Legendre (GLL) distribution). With respect to the formulation of the problem, `nek5000` provides two approaches (Paul F. Fischer et al. 2015; Deville et al. 2002):

1. $\mathbb{P}_N - \mathbb{P}_{N-2}$
    - Algebraic type of solution
    - Discretizes in space using compatible approximation spaces
    - Solves coupled system for pressure and velocity
2. $\mathbb{P}_N - \mathbb{P}_N$
    - Splitting Scheme
    - Discretizes in time first
    - Takes continuous divergence of momentum equation to arrive at a Poisson equation for pressure

Here, $\mathbb{P}_N$ refers to the space of all polynomials of degree less than N. Both these techniques have their advantages and their disadvantages. Khoury et al. 2013 find the $\mathbb{P}_N - \mathbb{P}_{N-2}$ method

to provide some differences in the pressure fluctuations with respect to experiments in their simulation of pipe flows. However, the $\mathbb{P}_N - \mathbb{P}_{N-2}$ method is said to be beneficial as it avoids spurious pressure modes (Fischer 1997). It performs better for low Reynolds number cases than the $\mathbb{P}_N - \mathbb{P}_N$ discretization, while LES performance is better when the $\mathbb{P}_N - \mathbb{P}_N$ discretization is employed. Both the methods are spectrally accurate however, and mostly equivalent.

For the discretised equations, a filtering is required to maintain the numerical stability of the equations. It is essential for high-strain regions and preserves inter-element continuity and spectral accuracy in these cases. The filter attacks only the fine scale modes, which, numerically speaking, should not carry any energy, and suppresses these modes in the spectral element expansion, without compromising the spectral convergence (Deville et al. 2002).

`nek5000` has an efficient strategy for parallel decomposition of the problem. Each element is treated as a virtual processor, so that each element is an independent and indivisible unit (Fischer et al. 1989). Parallel implementation is obtained by mapping groups of elements onto separate processors. Load balance is achieved by making sure that the total number of elements on any given pair of processors does not differ a lot (Fischer et al. 1989). Further discussion on scaling results and solution costs can be found in Appendix A.

Chapter 5

Geometry and Validation

Before attempting to answer questions about the underlying physics, it is necessary to ensure that the results that are generated are trustworthy. Therefore, the first step is to validate the numerical method and check the convergence of the statistics as required. Fully-developed turbulent pipe flow is a well-defined state, and is the starting point for this research as well. Thus, it was decided that the first step should be to set up a simulation for the same. Considering the number of numerical and experimental cases available for fully-developed pipe flow, it would also be easy to verify the results obtained from the current simulations with exising cases. This chapter comments on the set up of pipe flow and the evaluation of the various statistics.

5-1 Grid Generation and Preliminary Setup

To generate the appropriate spectral element grid for `nek5000`, first a mesh appropriate for a finite volume solver is created (see Figure 5.1). With the selection of the order of the interpolating polynomial, a spectral mesh is created in `nek5000`. Following the advice of Fischer 1997 and Khoury et al. 2013, a polynomial order of $N = 7$ is chosen. Provided a suitable finite volume grid, this polynomial order should provide sufficient spectral convergence (Pozrikidis 2014). Therefore, the total number of Gauss-Lobatto-Legendre points per element are 8^3. Filtering of the very fine scales and dealiasing are enabled to ensure the numerical stability of the solution.

To achieve a statistically fully developed pipe flow, a periodic boundary condition in the axial ($z-$) direction is used. The flow rate in this direction is held fixed, and is prescribed by a bulk velocity. Due to the applied periodicity, it is important that the length of the domain is selected in such a way that the periodicity does not unduly affect the results obtained (Eggels et al. 1994). Independence of the results from the domain length is determined by the axial velocity correlations. These correlations are usually expected to decline to zero at half the domain length (Eggels 1994). By this consideration, Eggels et al. 1994 uses a domain length of $L_z = 2\pi D$ for Newtonian pipe flow. Singh et al. 2017 employ a domain length that is twice

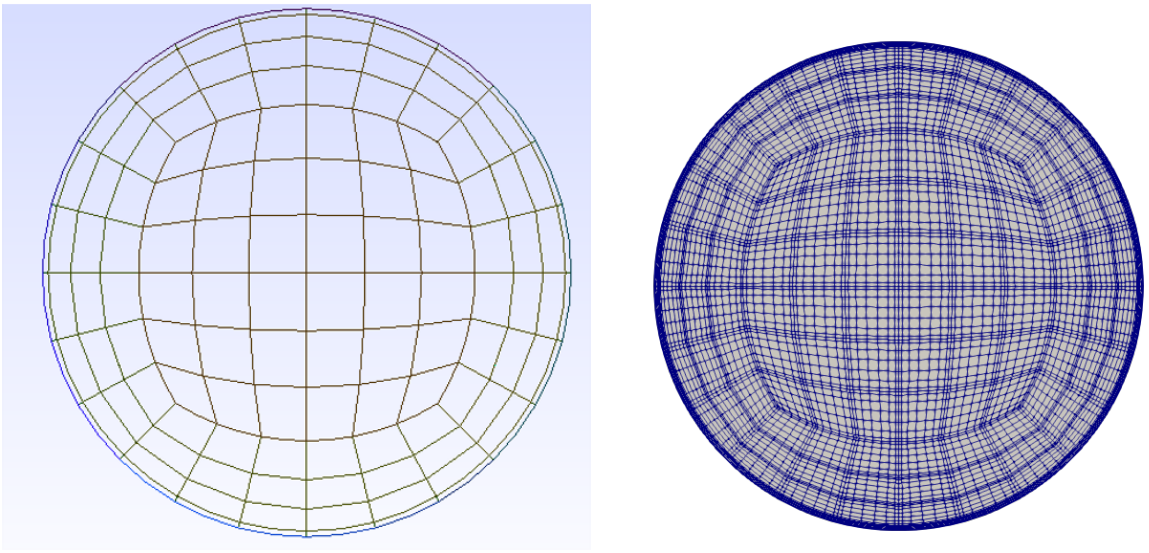

(a) **(b)**

Figure 5.1: (a) Cross-section of the finite Volume Mesh modeled using `gmsh` (b) The corresponding spectral mesh with polynomial order, $N = 7$

this size for their non-Newtonian simulations, although they do this only for better accuracy, and good results are also expected with a length of $L_z = 2\pi D$. Hence, this domain length was chosen as the standard for all simulations, unless stated otherwise.

It has been mentioned before that pipe flows are linearly stable (Drazin et al. 1981), and that an initial perturbation is required to generate turbulence in pipes, with the amplitude being dependent as $\mathcal{O}(\mathrm{Re}^{-1})$ (Hof et al. 2003). Therefore, the initial condition is a fully-developed laminar profile over the pipe cross-section, with random perturbations added to all the velocity components. These perturbations take the form of sinusoidal waves, and have an amplitude that is 2% of the bulk velocity.

To justify a numerical simulation without the use of a turbulence model, it is important that the smallest scales of turbulence are resolved, both spatially and temporally. The smallest scales spatially and temporally are the Kolmogorov length and time scales (Nieuwstadt et al. 2016), $\eta = (\nu^3/\epsilon)^{1/4}$ and $\tau = (\nu/\epsilon)^{1/2}$. For the length scale, a grid resolution that is 2.5-3 times the Kolmogorov length scale is generally sufficient to capture the physics of the flow (Moin et al. 1998). For the time scale, Eggels 1994 provides a more restrictive criterion, called the advective time scale, $\tau_a = \eta/u$. This is the time taken by the small-scale eddies to pass a fixed point when advected by the velocity of the macrostructure. For a wall-bounded, shear driven flow, the scaling for the smallest eddies can also be provided by the viscous length scale, ν/u_*, where u_* is the wall friction velocity. The viscous length scale represents the thickness of the viscous sublayer, and it is required that the grid spacing normal to the wall must be smaller than this length scale (Eggels 1994). This is necessary to resolve the steep gradients arising in the velocity near the wall. A grid independence study was undertaken to notice the influence of the cell size on the results. These results can be seen in Appendix B-1.

For statistics comparison and averaging in time, a non-dimensional time scale, $t_* = R/u_*$, is used. In a similar fashion as the length, using the viscous variables to scale the time, it is seen

Case	No. of Elements	No. of Grid Points	Δr^+	$(r\Delta\theta)^+$	Δz^+
Eggels et al. 1994	$96 \times 128 \times 256$	3.1×10^6	1.88	0.05 - 8.84	7.03
DNS - `nek5000`	9754	4.9×10^6	(0.5,5.95)	(0.98,5.31)	(3.93,10.74)

Table 5-1: Grid spacing comparison for the Newtonian simulation

that the smallest time step required to resolve the flow temporally is $\Delta t = \nu/u_*^2 = 0.0055t_*$. The imposed time step is much smaller than this due to the stability requirements set by the Courant number. In essence, it is required that the Courant number be less than 1, and this condition is met here rigorously. Therefore, the temporal resolution used is adequate to capture all scales of motion (Eggels 1994). The case is homogeneous in the axial direction, and thus, on-the-fly averaging is done in this direction and in time. Averaging is also done in the circumferential direction.

The first validated case is that of Newtonian fully developed pipe flow, compared with the work of Eggels et al. 1994. The second validation is to verify the results for a non-Newtonian simulation, and this is compared with one of the results from the work of Singh et al. 2017.

5-2 Validation - Eggels et al. 1994

In their work, Eggels et al. 1994 simulate a pipe flow at a Reynolds number of $Re_b = 5300$, which provides a friction Reynolds number of $Re_\tau = 180$, defined based on the radius of the pipe. The grid spacing in wall units in the radial (Δr^+), azimuthal ($(r\Delta\theta)^+$) and axial (Δz^+) directions are comparable for the present simulation with that of Eggels et al. 1994 (see Table 5-1). While Eggels et al. 1994 has constant grid spacing in the radial and the axial direction and a linearly expanding grid in the azimuthal direction, simulations employing spectral element methods have a range of values for the grid spacing in all directions (Khoury et al. 2013). This is becuase of the selection of the nodal base in a spectral element solver (Lobatto nodal base for `nek5000`), and the uneven spacing involved in this selection. Lower grid spacing is used near the wall, and higher spacing is employed towards the centre.

Sufficient averaging time is required to obtain converged statistics, especially for the higher-order quantities. Additionally, it is important to gauge the starting time for averaging appropriately, as the initial transients do not reflect the mean flow structure. Including them may require longer averaging times to obtain converged statistics (Vinuesa et al. 2016). The instantaneous wall shear stress is monitored, as seen in Figure 5.2, and the starting time is chosen based on the convergence of this quantity. This indicates the requirement of a linear profile for the time-averaged shear stress (seen in Figure 5.2 on the right). As the Reynolds number simulated is quite low, a lot of time is given before starting the statistics calculation, and several ensembles are collected. A flow development period of $30t_*$ is provided. Statistics are written every t_*, and this time separation between each collected ensemble is large enough to ensure that the collected data fields are uncorrelated. Mason et al. 1986 advise integrating at least 45 time units to ensure sufficient convergence, and therefore, statistics for up to $80t_*$ are used in this simulation.

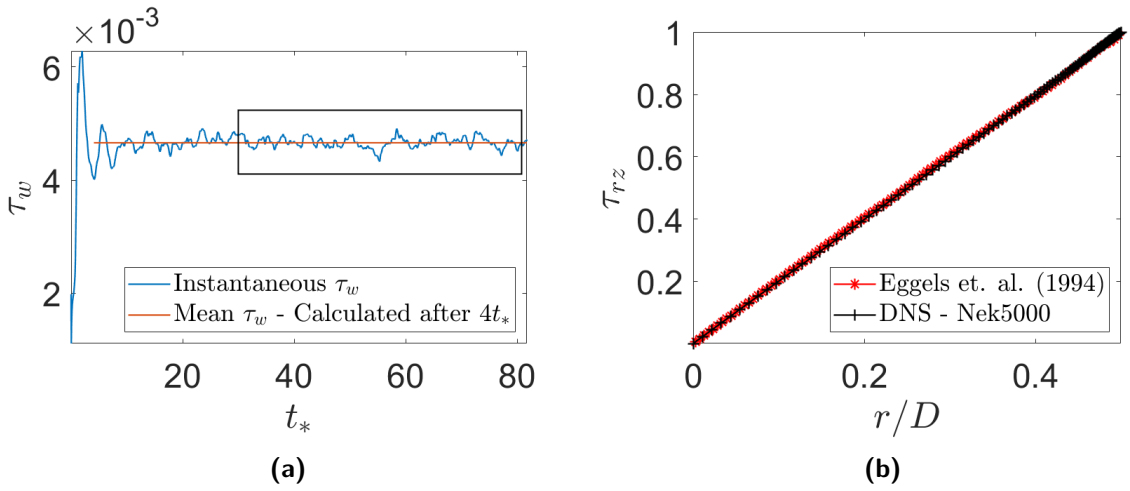

Figure 5.2: (a) Monitoring of Wall Shear Stress: The box represents the time duration that was used for averaging (b) Linear profile of the time-averaged total shear stress

After the simulation is completed, the obtained results are averaged and spectrally interpolated onto a two-dimensional polar mesh, over the cross-section of the pipe. Spectral interpolation maintains the simulation accuracy (Khoury et al. 2013). This is done using the statistical toolbox of Rezaeiravesh et al. 2019. For the polar mesh, equidistant spacing in the circumferential direction is used. A non-uniform grid is employed in the radial direction and finite differences are used for the interpolation (Rezaeiravesh et al. 2019). This makes it easier to post-process the statistics as compared to using a spectral mesh. Some of the statistics are given below. The velocity profile shown in Figure 5.3 is in good agreement with that of Eggels et al. 1994. Higher order statistics are also in good order. The Reynolds stress (5.4a) has a standard deviation of the absolute deviation equal to 0.001%. The RMS values show excellent agreement as well (5.4b), with the maximum standard deviation of the absolute deviation being seen for u_r', and is equal to 0.01%. The TKE budget terms are shown in Figure 5.5 (standard deviation of absolute deviation $\approx$ 0.001% for all the terms).

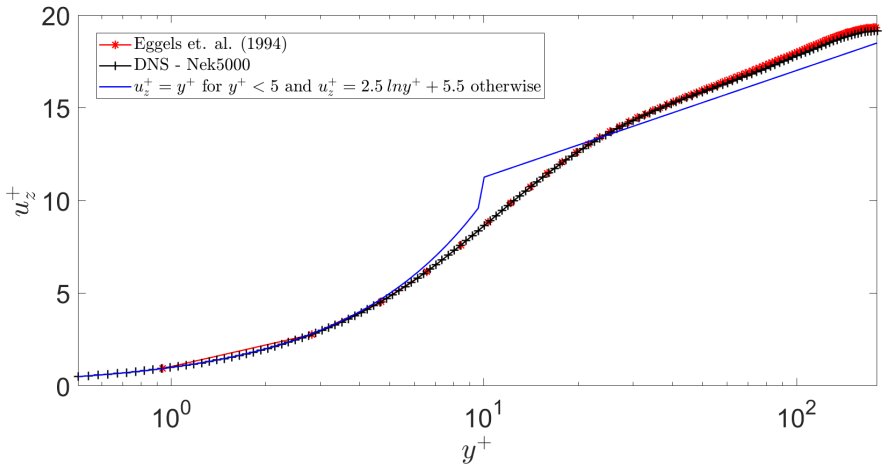

Figure 5.3: Axial Mean Velocity scaled using Inner Variables compared with the values and the empirical relation provided by Eggels et al. 1994

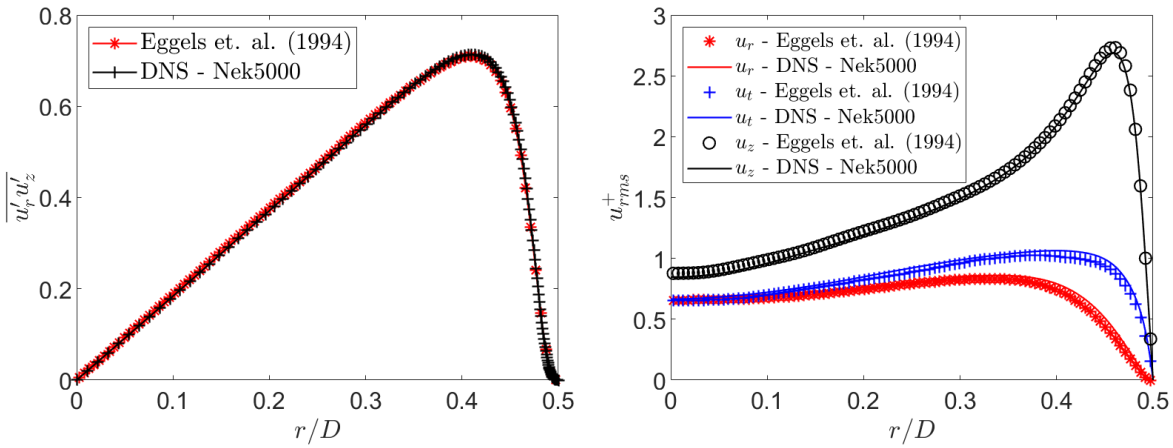

Figure 5.4: (a) Reynolds shear stress comparison (b) Comparison of the RMS values for the velocity components

The budget terms for the individual components of the TKE - $\overline{u_z'^2}$, $\overline{u_r'^2}$ and $\overline{u_\theta'^2}$ - can be seen in Appendix B. The budget for $\overline{u_r' u_z'}$ can also be seen there. There are slight discrepancies in the budgets of $\overline{u_r' u_z'}$ and $\overline{u_r'^2}$ compared to that of Eggels et al. 1994. However, these variations are marginal (maximum absolute deviation less than 3%), and are therefore, considered acceptable.

5-3 Validation - Singh et al. 2017

After obtaining satisfactory results with the statistics of the fully developed pipe flow for a Newtonian fluid, the same is done for non-Newtonian flow as well. To this end, the results

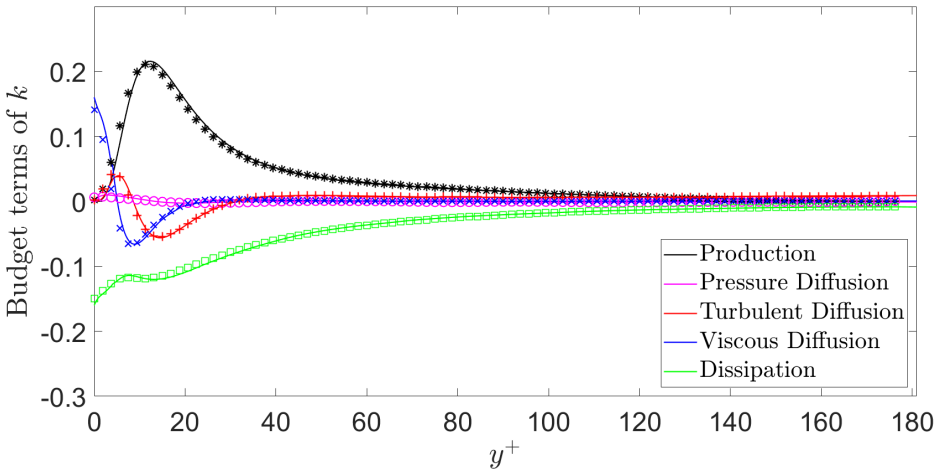

Figure 5.5: Comparison of the budget terms of the TKE: The symbols are the results obtained from Eggels et al. 1994 for the repsective quantities

Case	No. of Elements	No. of Grid Points	Δr^+	$(r\Delta\theta)^+$	Δz^+
Singh et al. 2017	115200	16.6×10^6	0.8	4.5	21
DNS - `nek5000`	12820	6.6×10^6	(0.5,4.97)	(0.98,4.5)	(3.93,10.74)

Table 5-2: Grid spacing comparison for the non-Newtonian simulation

of Singh et al. 2017 are used for validation. They ran DNS for shear-thinning and shear-thickening fluids described using the power-law, with the index varying from $n = 0.4 - 1.2$. A turbulent Reynolds number of $Re_\tau = 323$ was fixed for all the cases in their simulation. They used a two-dimensional spectral element mesh for the pipe cross-section, with a Fourier spectral expansion in the axial ($z-$) direction. The normalization for turbulent non-Newtonian flow is done using the wall viscosity as mentioned in previous sections. Also, as described by Pinho 2003, there are additional terms that arise in the balance of the shear stress and the TKE budget for non-Newtonian fluids (see Section 2-3). It was necessary to accurately evaluate these terms during the post-processing as well.

A power-law model is implemented in `nek5000` in this research. The code is written in such a way that the parallel processing does not require a large amount of computational resource. Mesh resolution plays an important role with decreasing shear thinning. A comparison of the mesh refinement used here along with the one used by Singh et al. 2017 is given in Table 5-2. To validate the statistics, a value of $n = 0.8$ was chosen. This value of n encapsulates the effects of shear-thinning, while also providing accurate results. Additionally, a lower degree of shear-thinning translates to lesser computational time required to achieve convergence of the statistics. The time step and the minimum grid size were well within the requirements mentioned by Eggels et al. 1994. A flow development time is provided and the evolution of the wall shear stress was monitored for this simulation as well. Similar to the case of Eggels et al. 1994, statistics were collected after a linear wall shear stress profile was obtained. Since the Re_τ here is nearly twice that of Eggels et al. 1994, less time is needed for the convergence of statistics, and therefore, fewer ensembles are required to obtain a statistically steady state (Vinuesa et al. 2016). Statistics were written every $0.3t_*$, with this time separation being sufficient for the consecutive collected data fields to be uncorrelated. Averaging was done from a time of $15t_*$ to $30t_*$, which was deemed sufficient for simulations around the same Re_τ (Vinuesa et al. 2016).

To check that the modelling of the viscosity was successful, the normalized mean viscosity, $\nu^+ = \overline{\nu}/\nu_w$, as a function of y^+ is shown in Figure 5.6. Near the wall, the high shear rates ensure that the the flow is similar to a Newtonian fluid (equivalent to using a power-law index of $n = 1$ here). The differences in viscosity become more evident as one moves towards the center of the pipe. A limiter is imposed towards the center of the pipe, where the strain rate goes to zero. A fixed value of viscosity ($\nu = 3.9 \times 10^{-3}$) is set, by using the definition of viscosity for a power-law fluid, and a very low numerical value for the strain rate ($\mathcal{O}(10^{-8})$) at this location. The obtained viscosity profile is in good agreement with the values provided by Singh et al. 2017, as is the normalized axial mean velocity (see Figures 5.6a and 5.6b). For a non-Newtonian fluid, the mean stress tensor contains an additional term due to the fluctuations of the viscosity. This term is called the turbulent viscous stress (Singh et al. 2017), or the "polymer stress" (Ptasinski et al. 2001) (also see Section 2-3). This term adds

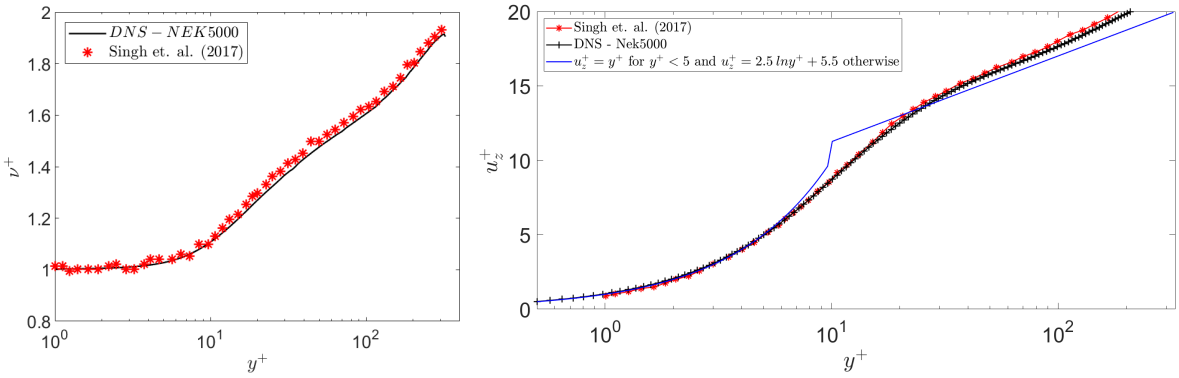

Figure 5.6: (a) Comparison of the normalized mean viscosity (b) Comparison of the normalized axial mean velocity

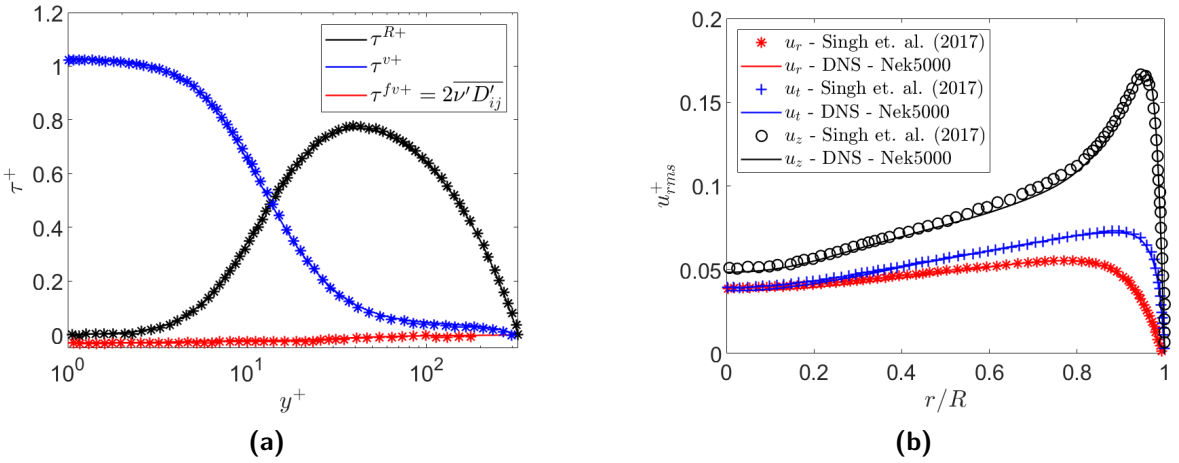

Figure 5.7: (a) Comparison of the Reynolds, viscous and turbulent viscous shear stresses (b) Comparison of the normalized RMS values of the three velocities - The symbols are results obtained from Singh et al. 2017

to the stress balance along with the mean viscous and the Reynolds stress. For $n = 0.8$, this is a very small contribution. It effectively balances out the increase in the viscous stress near the wall, and the decrease in the Reynolds shear stress towards the centre. The stress profiles and the RMS values are shown in Figure 5.7. The statistics show excellent agreement, and thus, the geometry and the convergence criteria used were found to be satisfactory.

The TKE budget is shown in Figure 5.8. The production, the turbulent diffusion and the pressure diffusion are defined similar to a Newtonian flow. The viscous terms in the budget – the dissipation and the viscous diffusion – are now provided using the mean viscosity in their definition. These terms have a kink in their statistics around $y^+ \approx 8$. This is expected to be near the region of maximum shear and the kink is due to a limiter imposed in the solver. The raising of the strain rate to a power could lead to numerical diffusion, and the simulation can indicate a higher diffusivity than expected. This would lead to erroneous calculations and thus, this limiter is introduced to ensure that the viscosity does not explode near the

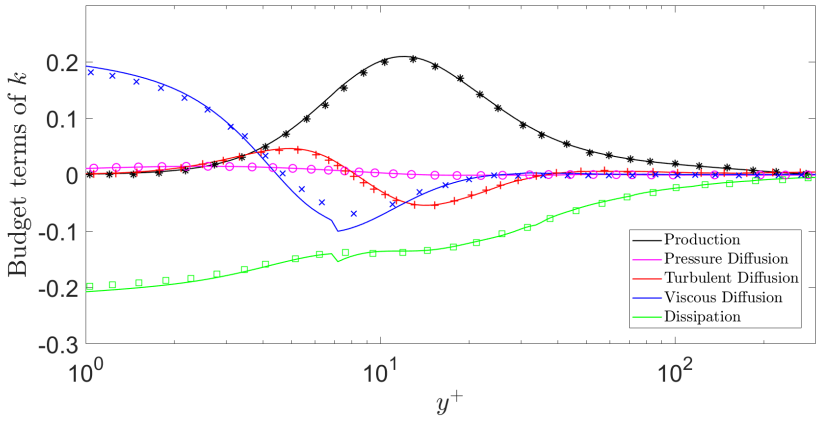

Figure 5.8: Comparison of budget terms of the TKE: The symbols are the results obtained from Singh et al. 2017 for the respective quantities

maximum at the beginning of the simulation. Although, the limiter is not required once the flow is fully-developed, it is difficult to switch it off once active. The effect of the limiter is only apparent for the higher order viscous terms, and does not have any effect on the global flow.

The new terms arising out of the viscous fluctuations in the viscous dissipation – the mean shear turbulent viscous dissipation (5.9a) and the turbulent viscous dissipation (5.9b) – are also shown here in Figure 5.9. It is useful to calculate these terms although they may not contribute much to the study of the decay. Both these terms are positive for $n = 0.8$, and thus, lead to a decrease in the overall dissipation as compared to a Newtonian fluid. The additional terms arising in the viscous transport are also calculated. They have a very minor contribution to the budget (Singh et al. 2017), and can be seen in Appendix B-3. They are an order of magnitude lower than the viscous dissipation terms, and therefore, these terms are also not expected to play a major part in the decay.

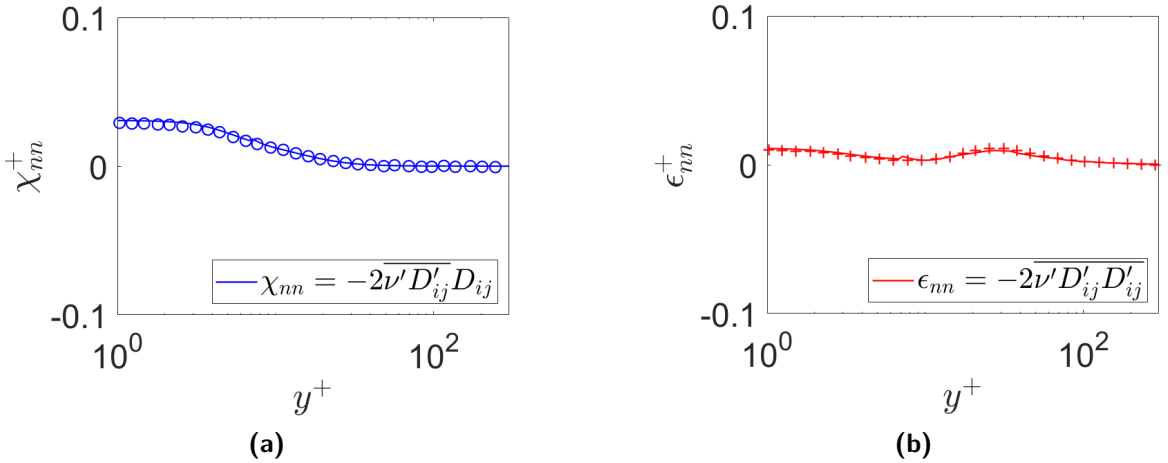

Figure 5.9: (a) Comparison of the normalized mean shear turbulent viscous dissipation (b) Comparison of the normalized turbulent viscous dissipation - The symbols are results obtained from Singh et al. 2017

Chapter 6

The Decay Results

With the confidence in the statistics generated for both the Newtonian and the non-Newtonian flow, it is time to answer some of the questions that have been raised in the earlier sections. This chapter is dedicated to studying the decay of pipe flow turbulence. It starts with an analysis of the deceleration of the fluid from the turbulent to the laminar state. Then, some of the key aspects of the decay are touched upon – first, for Newtonian flow, and then for non-Newtonian flow. Comparisons between different studied variables are also reported in an attempt to further explain the decay. Finally, a discussion is provided with respect to the results generated, and their applicability and limitations within the scope of the research.

6-1 The Deceleration Mechanism

One of the issues in an aneurysm, as shown previously, is the generation of TKE in a cycle and its decay at a later stage. This is believed to lead to a significant variation in the wall shear stress from cycle-to-cycle. In short, it is necessary to characterise transition from a turbulent to a laminar state, and study how the turbulent quantities change. Therefore, it is necessary to discuss how to do this. Narasimha et al. 1979 show several studies including their own, where relaminarizing boundary layers and internal flows were studied using a spatial acceleration or deceleration. This is generally induced in a channel (Narayanan 1968) or in a pipe (Sibulkin 1962) by an expansion in the test section following the fully-developed turbulent flow. The expansion is of a small angle ($1^\circ - 3^\circ$) to ensure as little flow separation as possible, and sufficient length is provided for the flow to eventually develop into a laminar flow.

Imposing a spatial deceleration requires a very large domain length. Typically, these studies have test sections with a streamwise length of $L_z \approx 130 - 150D$. In a DNS, it is very hard to study such long geometries. The simulation time and computational resources required to do so would be extremely large, and thus, it is nearly impossible to apply this method of deceleration. Instead, it was decided to use a periodic domain and use a homogeneous temporal deceleration to modify the flux of the flow. This is the method used by several authors such

as Greenblatt et al. 1999; Greenblatt et al. 2004; He et al. 2000 etc., to study the variation of turbulent quantities under imposed acceleration and deceleration mechanisms. For the use of the deceleration itself, Sreenivasan 1982 states that there should not be much statistical difference in the behaviour of the flow by employing a temporal deceleration, as compared to a spatial decay. This is also accepted for pipe flow transitional studies in general, and many authors employ this method in their research (Kleiser et al. 1991). Cyclic boundaries are used in the streamwise (z) direction. Continuity of the flow is maintained while using periodic boundaries, and thus, the use of a homogeneous temporal acceleration does not promote any unwanted disturbances in the radial or azimuthal directions as the flow traverses the pipe completely and is mapped on to the periodic inlet again. Therefore, a homogeneous temporal deceleration was considered to reduce the velocity and move from a turbulent to a laminar state.

Greenblatt et al. 2004 state that the assumption that inhomogeneous spatial pressure gradients and homogeneous temporal gradients are equivalent, has led to erroneous prediction and correlation of turbulent quantities during the acceleration or deceleration stage itself. However, it must be pointed out that here we are not quite interested in the decelerating section in a detailed manner. It is rather what happens after the deceleration that is of more significant importance. Most of the decay studies using spatial pressure gradients also study the decay quite some distance after the expansion. These studies too do not provide any information on the variation of the quantites during the deceleration itself. Additionally, the flow expansions used negate the effects of flow separation. This is crucial, as flow separation is one of the things that a homogeneous temporal deceleration cannot generate. In fact, it is the major difference in the flow structure of the two deceleration mechanisms. However, the importance of the flow separation on the study of the decay is minimal (Sreenivasan 1982), and thus, a homogeneous temporal deceleration can be used.

6-1-1 Method of Deceleration

A temporal deceleration is used to reduce the bulk velocity of the flow from a turbulent to a laminar state. Some time is provided to ensure that the flow is fully turbulent and then a very rapid deceleration, with ramp times on the scale of the eddy turnover time are used. This is done so as to change the current inertial state as quickly as possible and focus on the effects of the decay, rather than on the deceleration itself. The deceleration is applied to fully-developed pipe flow in the form of a linear ramp as given by (6-1).

$$U_{des} = U_{in} - \left(\frac{U_{end} - U_s}{T_{end} - T_s}\right)(t - T_s) \tag{6-1}$$

where U_{des} is the desired bulk velocity for every time step during the ramp, U_s and U_{end} are the initial and final bulk velocities, and T_s and T_{end} are the beginning and end times for the application of the ramp. The bulk velocity in the domain after every time step is calculated. The difference in flux, as set by the differential in the desired and calculated bulk velocity, is added to the axial velocity. This is effective as the velocity at every stage is known. During the turbulent state, the desired bulk velocity is set to the initial bulk velocity, so that there is no added flux. For the deceleration, the ramp is used to determine the bulk velocity desired, and after the application of the ramp the final velocity is used as the desired bulk velocity. The

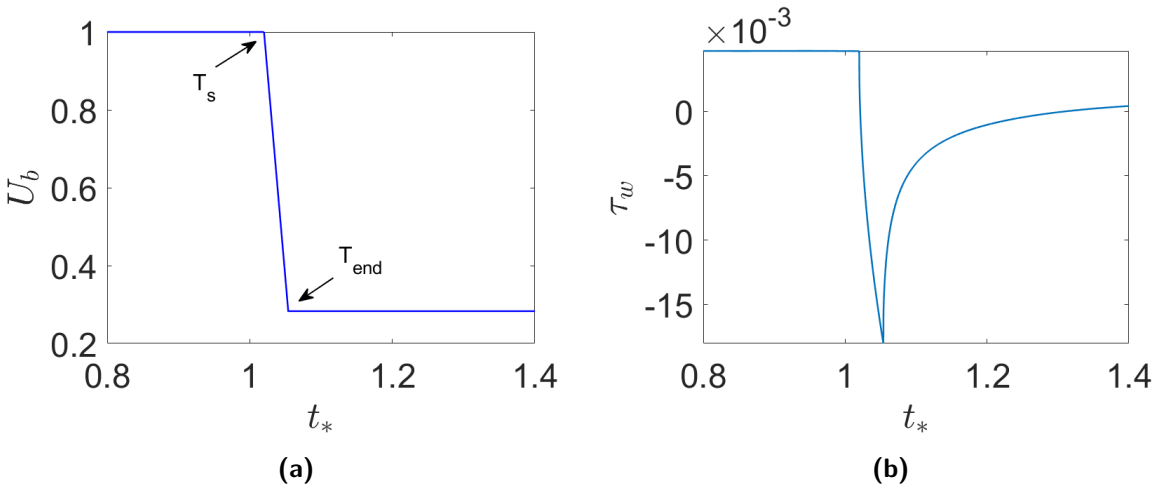

Figure 6.1: (a) The imposed variation of U_b with $U_b = U_{des}$; T_s and T_{end} show the start and finish times of the ramp, with $(T_{end} - T_s)$ being the time duration of application of the ramp. A fully turbulent flow is allowed to continue from $t* = 0 - T_s$, so as to ensure there are no scratch arrays or other discrepancies before the application of the ramp (b) The variation in the time-averaged wall shear stress during the application of the ramp. T_s and T_{end} can be inferred from the graph for the bulk velocity

final velocity is decided based on the Reynolds number. Sreenivasan 1982 provide a critical Reynolds number for channel flows as 1500, below which the flow is undoubtedly laminar. A threshold of $Re_{cr} = 1750 \pm 10$ is proposed by Peixinho et al. 2005 in their transitional study of pipe flows, though this is still a high value for the critical Reynolds number. Although a threshold is difficult to define as such, looking at the literature in this field it was decided that a Reynolds number of $Re = 1500$ is sufficiently low for pipe flows to be fully laminar without any disturbances. Therefore, this is the final fixed Reynolds number for all the flows studied in this research. The Reynolds number helps in determining the final desired bulk velocity for the flow. All results are again characterized by the non-dimensional time t_*, which are based on the quantities defined at the fully-developed turbulent state.

The applied deceleration and the corresponding variation in wall shear stress are plotted in Figure 6.1. Up to $t_* = T_s$, the turbulent flow is active. This is done so as to avoid the presence of any scratch or null arrays in the system due to restarting the fully-developed turbulent state. After which, a linear ramp is applied to decrease the velocity. The velocity after that is determined by the final Reynolds number. The wall shear stress decreases as the deceleration starts and becomes negative. This implies zones of recirculation and local negative velocity near the wall (also see Figure 6.2). This is similar to pulsatile flow, where acceleration and deceleration lead to zones of recirculation within a domain (Ertunc et al. 2010).

The deceleration is rapid but short. He et al. 2000 formulates a non-dimensional ramp rate, defined as $\alpha = D^3/\nu^2(d\overline{U}/dt)$. Compared to the studies of He et al. 2000 and Greenblatt et al. 2004, the ramp rate used here is very high. These authors wanted to study the nature of the acceleration or deceleration and the effects associated with it. However, as mentioned previously, here the main interest is in the decay itself, and therefore, it makes sense to impose decelerations on the turbulent time scale. He et al. 2016 and Guerrero et al. 2021 identify different stages of turbulence with respect to the acceleration. However, using such a large

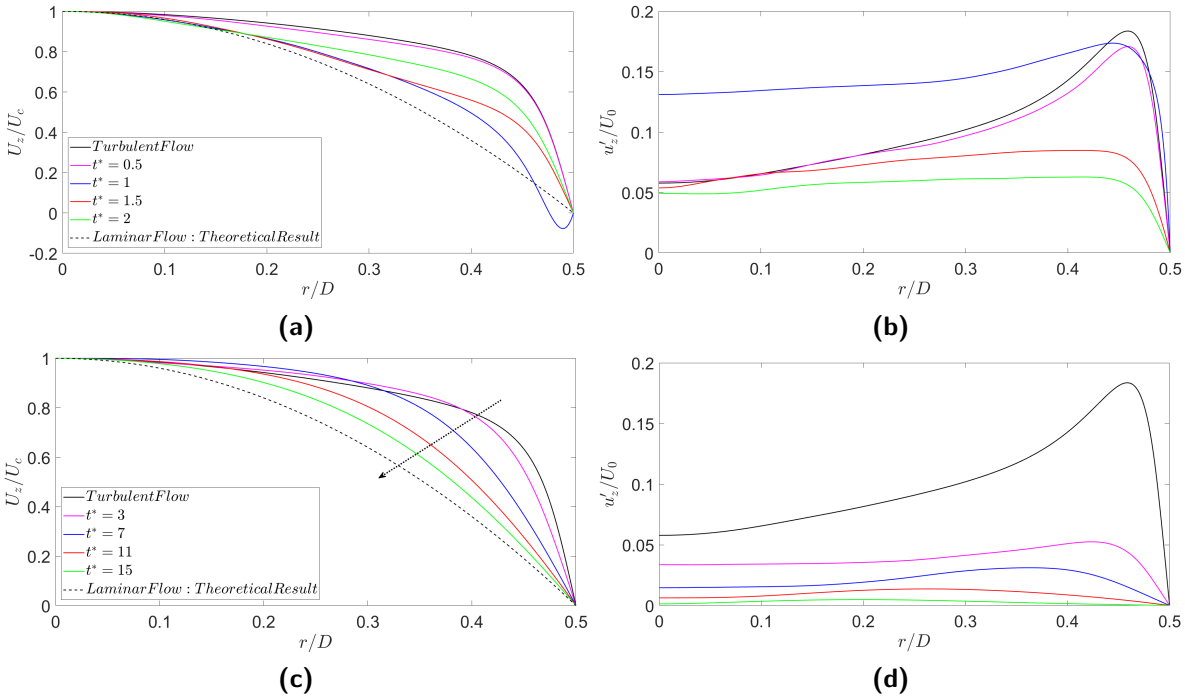

Figure 6.2: *Left*: The instantaneous velocity profiles at different times – (a) For the decelerating section and immediately after (c) For time steps much later than when the applied ramp is active: The arrow indicates the direction of increasing t_* *Right*: Instantaneous normalized RMS values of the axial velocity - The corresponding colours from the velocity profile are used

ramp rate does not allow us to do so.

The instantaneous velocity and axial RMS profiles for a Newtonian flow of $Re_b = 5300$ at different time instants are shown in Figure 6.2. The ramp period is the same as the one used in Figure 6.1. As the deceleration is applied, a point of inflection in the velocity profile is seen near the wall (see Figure 6.2a). This is also the case in accelerating pipe flows, and can be attributed to the velocity correction due to the application of the ramp (Greenblatt et al. 2004). The velocity correction is equivalent at all radii, but since the velocity is lowest near the wall, a point of inflection arises here. As the deceleration is removed, this inflection then propagates towards the center of the pipe. The flow tries to go back to the initial turbulent state as seen in the velocity profile (see Figures 6.2c and 6.2d). But the turbulent intensity has reduced and the flow does not contain sufficient energy to return back to its original state. Instead it continues to decay, and the turbulent quantities reduce. The velocity profile starts losing its' characteristic steep gradient near the wall around $t_* \approx 7 - 9$, and reaches the fully developed laminar state asymptotically. This is also noticeable in the intensities, with them going to zero asymptotically as well. All the results for the decay shown in later sections are with $t_* = 0$ corresponding to the start of the deceleration, i.e., the initial fully-developed flow is now discarded from the results.

Different coherent structures are plotted using the Q criterion in Figure 6.3. Positive Q isosurfaces show areas where the rotation strength is greater than the strain, and these are a great tool for identification of the different mechanisms present in a turbulent flow (Hunt et al. 1988). Just before the deceleration ($t_* = 0$), the structures are identifiable and similar to fully-

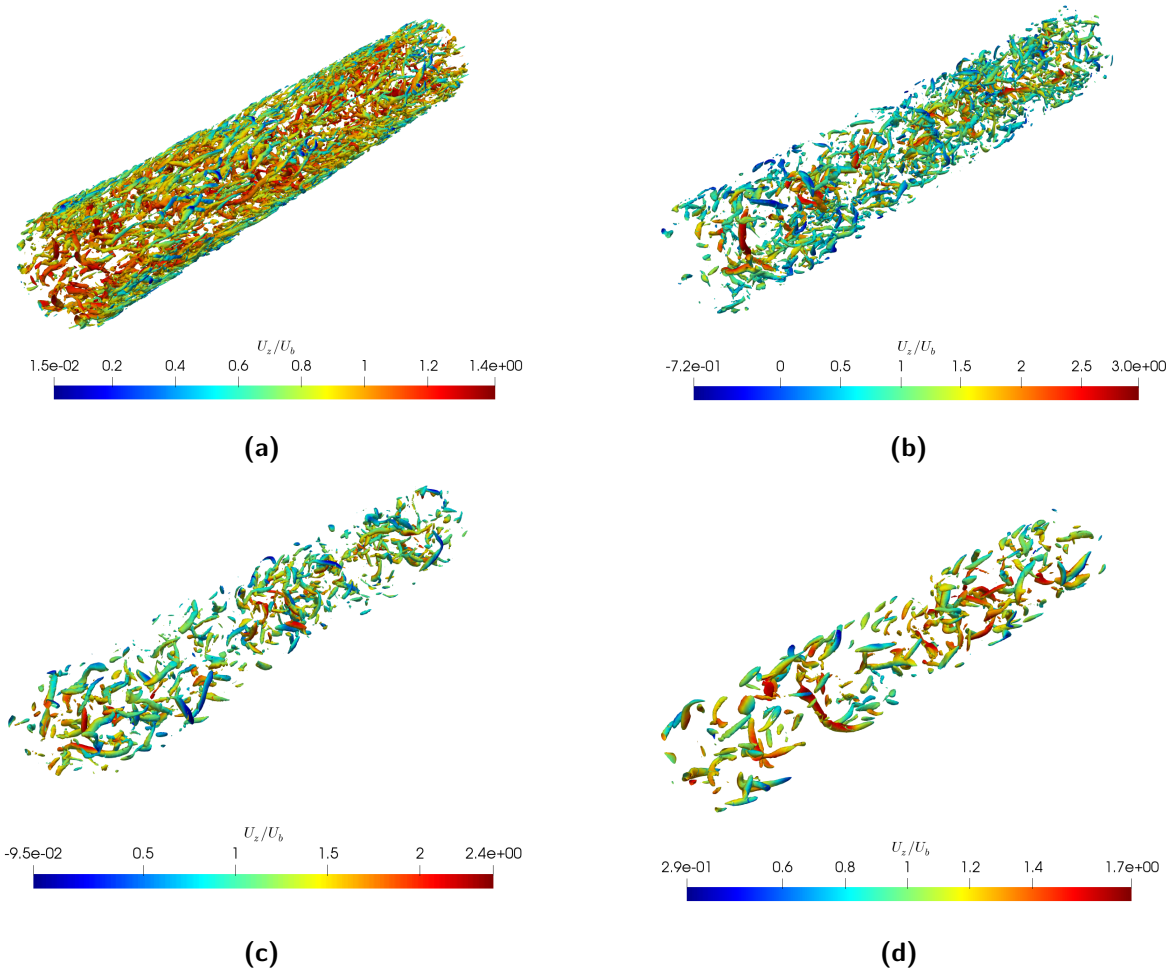

Figure 6.3: The coherent structures present in the pipe at different times during the deceleration determined by the Q criterion. Different threshold values are used for Q at different time steps to emphasize the results. The colouring used is of the instantaneous axial velocity (a) $t_* = 0$ (b) $t_* = 0.65$ (c) $t_* = 1.25$ (d) $t_* = 2.50$

developed pipe flow. A short while after the deceleration has been applied completely, the near-wall structures have decreased in size (see Figure 6.3b). The structures were measured using the ruler option in `Paraview`, and were normalized using the initial friction velocity. They have decreased from a length scale of approximately $100\nu/u_\tau$ to $60\nu/u_\tau$. The organized motions near the wall are the primary turbulence mechanism for the production of TKE and the Reynolds shear stress. Therefore, a decrease in the length of the structures is equivalent to an increase in turbulence, as this implies a higher bursting rate (Nieuwstadt et al. 2016). This is also in accord with the inflection in the velocity profile and the presence of back flow. Sreenivasan 1982 explains the elongation of the structures and the reduction in the bursting rate for accelerating wall-bounded shear flows. The opposite can be expected for an applied deceleration (He et al. 2000). As time goes on, the number of structures has reduced (Figure 6.3c), and the structures increase in length as well (Figure 6.3d). The structures have also moved slightly away from the wall. This indicates the reduction in the turbulent intensities, and therefore, the flow now gradually relaminarizes.

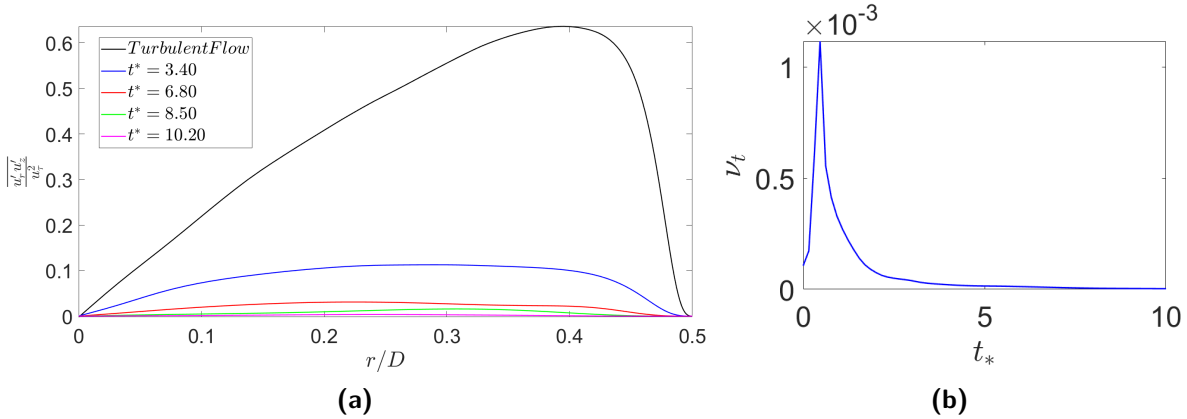

Figure 6.4: (a) Variation of the normalized Reynolds shear stress with respect to t_* for a Newtonian fluid with $Re_b = 10000$ (b) The variation of the average eddy viscosity throughout the pipe cross-section. The eddy viscosity is estimated from the average Reynolds shear stress across the pipe cross-section

6-2 Results - Newtonian Flow

After the rapid deceleration, a study of the decay of turbulence can now be undertaken. First, the results for a single Newtonian fluid with a starting Reynolds number of $Re_b = 10000$ will be discussed. In the previous section, the behaviour of the velocity profile and the axial turbulent intensity after the deceleration was shown. Although the results were for $Re_b = 5300$, similar results are seen for $Re_b = 10000$ as well. The variation of some of the other turbulent quantities are shown here. Figure 6.4 shows the variation of the Reynolds shear stress with non-dimensionalized time. Results are shown after the effects of the deceleration are well over, and the flow is assumed to decay freely. Similar to the turbulent intensitites, the Reynolds stress also decreases along the cross-section of the pipe. This is in accord with the decrease of turbulence throughout the pipe cross-section over time. At $t_* \approx 9$, the Reynolds shear stress has almost reached zero. An estimate for the eddy viscosity can be provided by considering $-\overline{u'_r u'_z} = 2\nu_t D_{rz}$, where ν_t is the eddy viscosity and $\boldsymbol{D}$ is the deformation gradient. Figure 6.4b shows the variation of the eddy viscosity over time. The initial increase in its value is associated with the application of the ramp. After that, the value for the eddy viscosity decreases. During the early stages of decay, the eddy viscosity is an order of magnitude larger than the molecular viscosity. As the Reynolds stress approaches zero, the eddy viscosity behaves in a simialr fashion, and is an order of magnitude lower than the molecular viscosity.

A better understanding of the nature of relaminarization can be gained by analyzing the budget terms – in particular, the production and the dissipation – of the TKE. Figure 6.5a shows the change in the production, while Figure 6.5b shows the variation of the dissipation of TKE. Similar to other turbulent quantities, these also decrease over time. The peak of the production and the dissipation decrease consistently, with the values increasing towards the intermediate radii of the cross-section. This is because of the turbulence diffusing towards the center of the pipe. Another interesting point of note in the figure for the production term is the shifting of the position of maximum production away from the wall. This implies a thickening of the viscous sublayer and the buffer layer, and a shortening of the log-layer in the pipe (Iida et al. 1998). As the flow gradually relaminarizes, it is to be expected that the

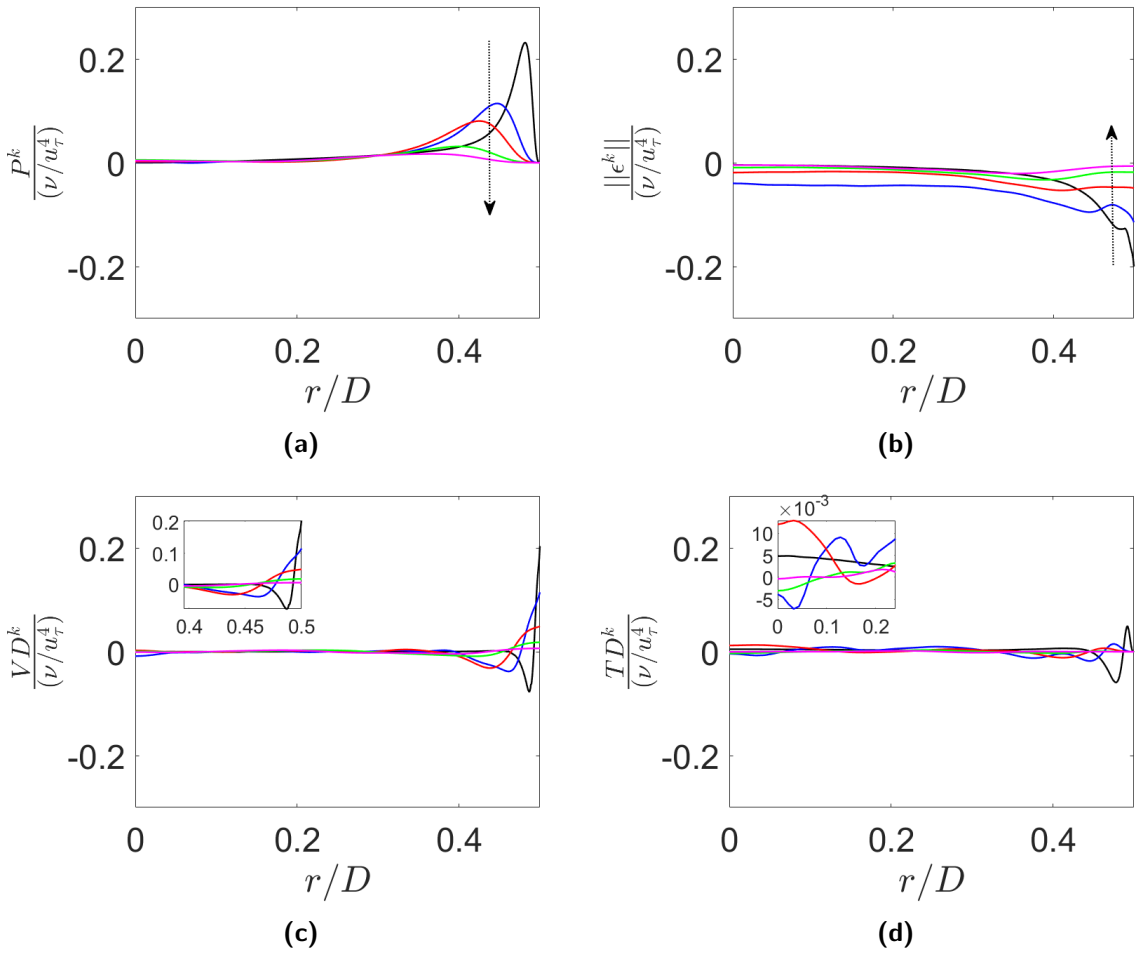

Figure 6.5: The variation of the (a) Production (b) Dissipation - The arrows in (a) and (b) indicate the direction of increasing t_* (c) Viscous diffusion - The box represents a zoom-in from $r/D = 0.4 - 0.5$ to indicate the growth of the viscous sublayer (d) turbulent diffusion - The box represents a zoom-in from $r/D = 0 - 0.2$ to indicate the transfer of energy from the wall to the center - All the budget quantities are normalized by ν/u_τ^4, where u_τ is the friction velocity for the fully-developed turbulent flow. *Legend*: (——) Fully developed turbulent flow (——) $t_* = 3.10$ (——) $t_* = 6.20$ (——) $t_* = 9.30$ (——) $t_* = 12.40$

existing viscous sublayer changes into a laminar boundary layer (Sreenivasan 1982), and this is consistent with the disappearance of the distinct structure of turbulent pipe flow.

Figures 6.5c and 6.5d also shows the viscous and turbulent diffusion terms of the TKE budget. The viscous diffusion balances the dissipation near the wall (Eggels et al. 1994), and it shows similar behaviour to the other budget terms with the maximum value decreasing and the peak moving away from the wall. This further emphasizes the growth of the viscous sublayer. The turbulent diffusion is small as compared to the other budget terms. However, its variation over the pipe cross-section shows that the diffusion terms are responsible for the transfer of energy away from the wall towards the intermediate radii and the pipe center (see zoomed in version of Figure 6.5d).

A key quantity that is used to monitor the decay in pipe flows is the correlation coefficient, as

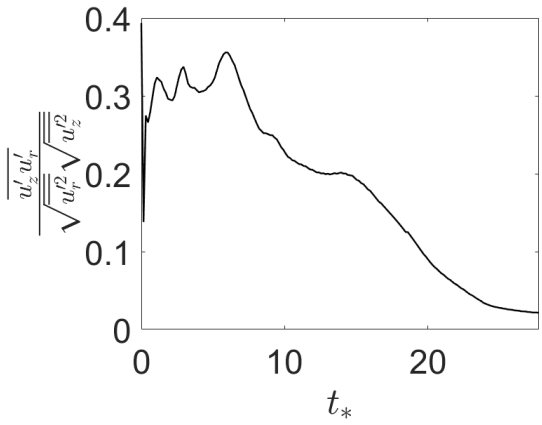

Figure 6.6: The decrease of the volume-averaged correlation coefficient over time

defined by (3-1). It is seen in other relaminarizing flows that the wall-normal and streamwise fluctuations become decorrelated over time (Sreenivasan 1982). This implies a decrease in the correlation coefficient and the process is termed as the "loss of correlation" (Narayanan 1968). From Figure 6.6, it is seen that the volume averaged correlation coefficient tends to zero over time, after an initial increase in the quantity. This initial increase indicates the increased turbulence due to the deceleration. The results seen here are similar to reverse transition studies in channel flows (Narayanan 1968), and also in other wall-bounded flows (Sreenivasan 1982).

The organized motions present in the pipe are depicted in Figure 6.7 using the Q-criterion. This figure now shows the structures for the decaying section of the flow only and not for the deceleration. Due to this being a time-dependent flow, different threshold values for the criterion are used at different time steps. Although this is not ideal for comparison, the presence of the structures can still provide some meaningful information. Quasi-streamwise vortices can be visualized at $t_* = 3.41$, although as compared to a turbulent flow, they are slightly larger in size (average size of $135\nu/u_\tau$ as compared to $100\nu/u_\tau$). There are less structures as well. The decrease of the Reynolds stress and the production of turbulent energy indicates that sweep events are suppressed (Araya et al. 2018). The sweeps are necessary for creation of new streamwise vortices (Nieuwstadt et al. 2016), and a decay process would naturally indicate a reduction in these. As mentioned previously, the turbulent structures are moving away from the wall. The viscous sublayer loses its characteristic streamwise vortices, and the turbulence is now produced by streamwise vortices that are longer and at a region away from the wall (Iida et al. 1998). Over time the length of the structures continues to increase. It is to be expected that the smallest eddies decay faster, leaving the larger eddies in the flow (Batchelor et al. 1948). At $t_* = 8.68$ and $t_* = 10.54$, the threshold values required to notice the structures are extremely low ($Q = 0.006$ and $Q = 0.002$ respectively), meaning that the rate of rotation now present in the flow is nominal. Dubief et al. 2000 state that too small a level of the threshold value would only display structures that play a minimal role on the dynamics of the flow, while increasing the core of the structures seen, and this seems to be the case here as well.

Batchelor et al. 1948 showed in their study of the final regime of decay in homogeneous, isotropic turbulence that the longitudinal integral length scale increases with time. They

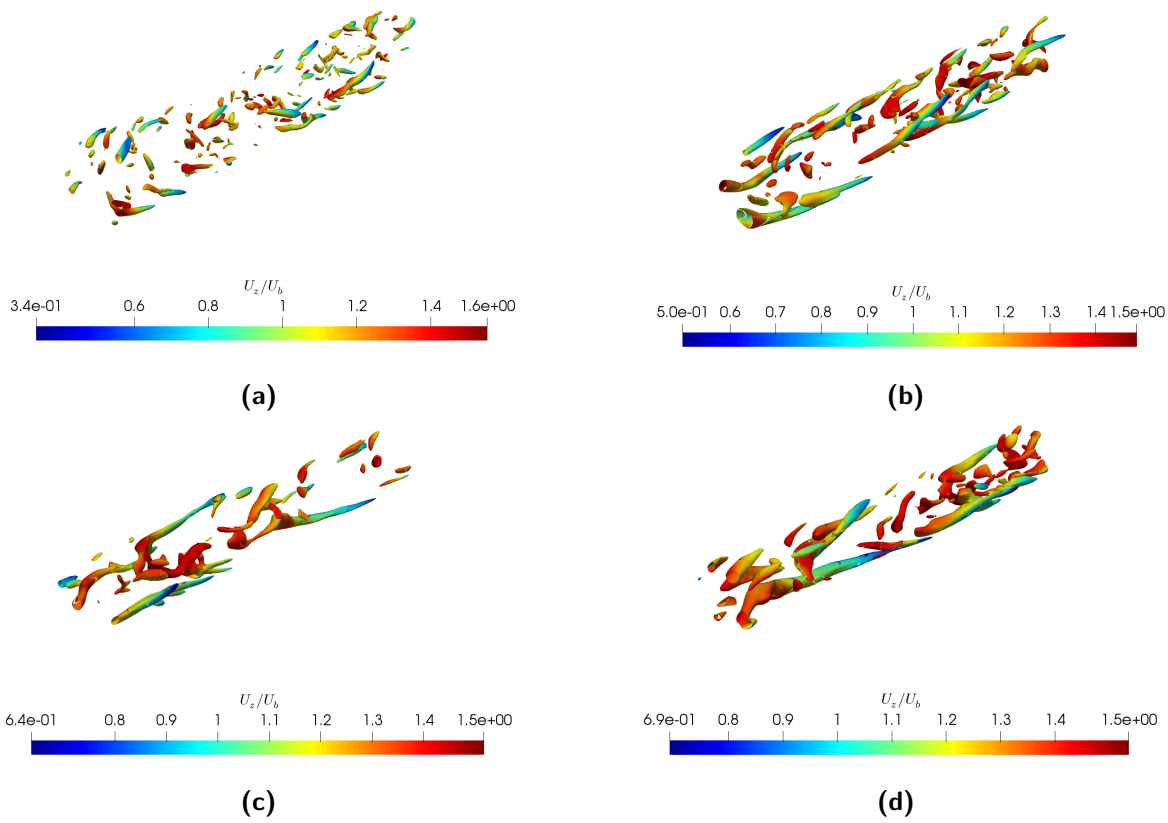

Figure 6.7: The coherent structures present in the pipe at different times during the decay determined by the Q criterion. The structures here are presented after the application of the ramp. Similar to Figure 6.3, different threshold values of Q are employed. The colouring used is of the instantaneous axial velocity (a) $t_* = 3.41$ (b) $t_* = 6.82$ (c) $t_* = 8.68$ (d) $t_* = 10.54$

mention that the eddies face two mechanisms - a stretching that increases their size, and viscous dissipation that allows them to decay. Skrbek et al. 2000 show in their experiments of homogeneous, isotropic turbulence with superfluid He II that while the length scale grows, there is a maximum value it can reach – dictated by the size of the domain – after which the length scale is considered to have saturated. In pipe flows, this is set by the diameter of the pipe. To monitor the growth of the length scale, the two-point spatial longitudinal correlation coefficient, defined by (6-2) (Eggels 1994), is evaluated. Here, z is the axial, homogeneous direction. The correlation is calculated using slab averages. These are averages on a circular cross-section of the pipe at fixed values of z. Averaging is applied in the circumferential direction as well, so as to obtain a velocity distribution per slab dependent on the radial direction only. Due to the uneven distribution of the elements in the spectral element grid, interpolating onto a uniform grid and finding slab averages is not straightforward, and therefore, the correlations are not quite as smooth as they normally would be.

$$\rho_{u_z u_z} = \frac{< u'(r,\theta,z,t)u'(r,\theta,z+\Delta z,t) >}{< u'(r,\theta,z,t)^2 >}$$
$$\Lambda = \int_0^\infty \rho_{u_z u_z} dz \tag{6-2}$$

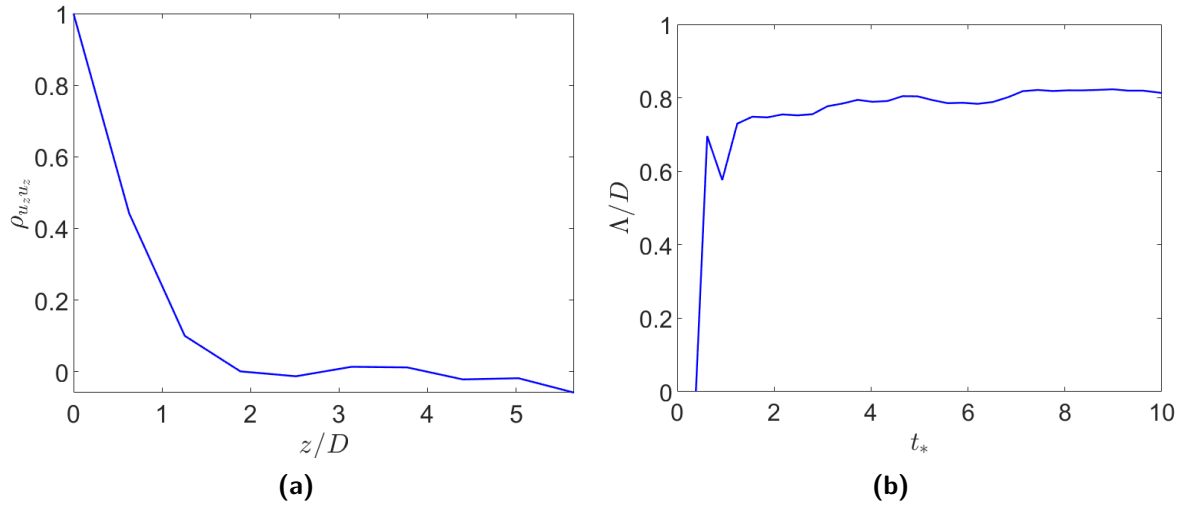

Figure 6.8: (a) The longitudinal correlation coefficient ($\rho_{u_z u_z}$) along the length of the pipe for the decay (b) The growth of the streamwise integral length scale with respect to time. The radial locatio is $r/D = 0.25$ for both (a) and (b)

In essence, it is tough to measure correlations for a decelerating flow without performing some ensemble averaging. However, an effort to do the same has been made here. Figure 6.8 shows the longitudinal correlation coefficient at a location of $r/D = 0.25$, and the variation of the integral length scale with time as well. The length scale is approximately $\mathcal{O}(D)$ at around $t_* = 2.5$. This implies that the saturation of the length scale occurs at a very early stage as compared to the studies of Skrbek et al. 2000 and Touil et al. 2002. The fast growth of the length scale can be attributed to the large applied deceleration and the quick modification of the mean inertial flow to a mean flow with no expected turbulence. From their scaling analysis, Skrbek et al. 2000 also mention including viscosity corrections in the decay leads to an earlier saturation time. Considering that the Reynolds number used here is quite low as compared to Skrbek et al. 2000, it can be hypothesized that the viscosity corrections probably start influencing the decay at an earlier stage, and therefore, an earlier saturation time is noticed here. There are some differences between this research and the study of Skrbek et al. 2000. There is no mean flow present in the study of Skrbek et al. 2000, while there is a mean flow here. The flow studied here is not isotropic, but is highly anisotropic. Additionally, the applied deceleration promotes the degree of anisotropy.

Slab averages are also used to monitor other turbulent quantities. To check the global variation of quantities, averaging in the radial direction (r) is also done. The evolution of the TKE with time is shown in Figure 6.9 - on a logarithmic plot (Figurge 6.9a), and on a semi-logarithmic plot (Figurge 6.9b). A sudden drop-off in the TKE value is seen in the initial stage, where the deceleration is applied in Figure 6.9a. Since we are interested in the region after the deceleration, this section is not used to characterise the decay. After the initial section, two linear profiles are visible in Figure 6.9a. Comparing the time scales in Figure 6.9a and Figure 6.8, it is evident that the first linear section refers to turbulent decay before the saturation of the integral length scale. Using a linear fit, an exponent of -0.9 is seen here. This exponent is lower in absolute value than the exponent provided by the relation of $E \sim t^{-6/5}$ given in Skrbek et al. 2000. The second linear section of the decay begins

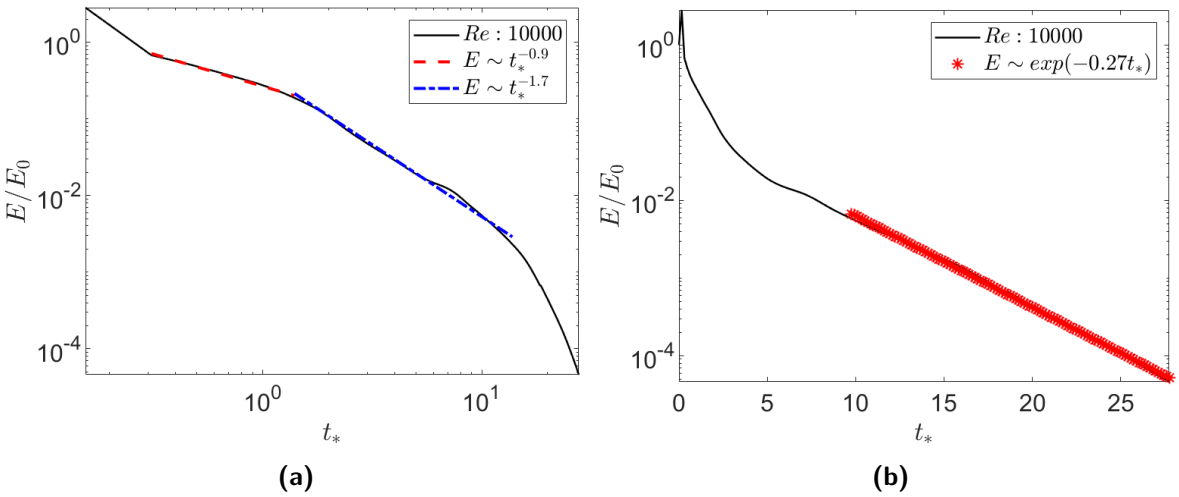

Figure 6.9: The decay of the volume-averaged TKE with respect to time (a) On a logarithmic plot - The two coloured lines are logarithmic fits on the data: (—) Expected decay law before saturation of length scale (—) Expected decay law after saturation of length scale (b) On a semi-logarithmic plot - The symbols here mark an exponential fit for an expected viscosity-dependent flow regime

approximately as the length scale is saturated. Again referring to the work of Skrbek et al. 2000, they show that for homogeneous, isotropic turbulence with a saturated length scale, the TKE decays as $E \sim t^{-2}$. Employing a linear fit once more, the slope for this case is seen to be -1.7, which is again slightly lower in absolute value than the one predicted by Skrbek et al. 2000. The slopes for both the sets could possibly be lower than the work of Skrbek et al. 2000 because of the presence of TKE production in the budget. As mentioned previously, the flow here is not isotropic, and is homogeneous in the axial and circumferential direction only. The anisotropic and inhomogeneous nature of the flow may further promote turbulence, and therefore, a lower decay rate is seen here. After $t_* \approx 12$, there is a clear drop-off of the decay. This qualitatively looks similar to the LES and EDQNM results presented by Touil et al. 2002 for a homogeneous, isotropic flow, with no mean flow, in a bounded domain. These authors hypothesize that the decay, after a long time, is similar to exponential viscous decay. Since the Reynolds number studied here is extremely low ($Re_b = 10000$) as compared to the studies of Touil et al. 2002 ($Re_{l_0} \approx 5000$, where l_0 is the integral length scale), this viscous decay regime is expected to appear at an earlier time in the overall decay process. The exponential decay for the later stages can be noticed in Figure 6.9b

Skrbek 2008 considers the last stage of decay and models it in a similar fashion to the decay of oscillatory motion in viscous fluids. He considers an exponential decay law as $E(t) = E_0 \exp(-\beta t)$. The decay coefficient is given as $\beta = 2\nu\kappa^2$, where ν is the kinematic viscosity and k is the wavenumber. An exponential fit is made for the semi-log plot, and the coefficients are compared. With the non-dimensionalized time scale and using $\kappa = 2\pi/D$ (saturated length scale), the expected value for the damping coefficient is $\beta = 0.29$. The coefficient of the plot is $\beta = 0.27$, which is very close to the expected value of β for $Re = 10000$. This allows us to put into perspective the final stage of decay. In the latter stages, the production and dissipation of TKE are very small. As the flow relaminarizes, the viscosity starts playing a greater role in the decay of turbulence, and the remaining turbulent energy is dissipated by

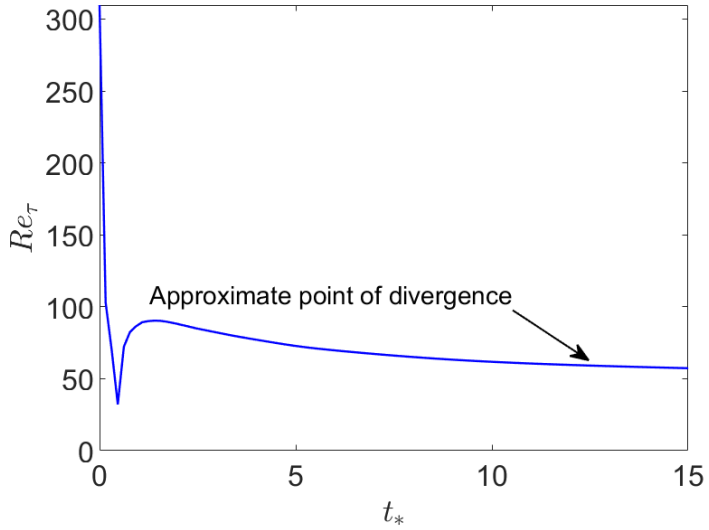

Figure 6.10: The variation of the friction Reynolds number with non-dimensionalized time - The point of divergence from the power-law decay to the exponential decay is marked. This point has a value of $Re_\tau = 62.85$

the action of viscosity only.

It is difficult to predict the switch from the power-law to the exponential decay. As such to pin-point an exact point for relaminarization is not straightforward, but an effort will be made in this study. As mentioned previously, the change in the decay law is seen to occur here for $t_* \approx 12$. Monitoring the change in the friction Reynolds number, it is seen that this value corresponds to $Re_\tau = 62.85$. From Figure 6.10, it is not clear whether any divergence is to be expected. This value could be purely coincidental. However, in their study of relaminarizing channel flows, Iida et al. 1998 find that for $Re_\tau = 60$, the flow is highly intermittent with very low Reynolds shear stress and production of TKE. Furthermore, using small computational boxes, Tsukahara et al. 2014 noticed that the flow is completely laminar at this friction Reynolds number. On increasing the size of the domain, they found that localised turbulent structures, similar to puffs (Wygnanski et al. 1973), exist at the value of $Re_\tau = 60$. This would explain why upto a certain point in the decay, turbulent scaling holds for the nature of the decay. Around $Re_\tau = 60$, scaling on the inner variables might not hold anymore. Localized structures are not noticed in our study, because the friction Reynolds number is not maintained constant like the studies of Iida et al. 1998 and Tsukahara et al. 2014, but is allowed to decrease gradually. Additionally, the computational size of the domain is not large enough to accurately observe puffs, although their existence is highly unlikely due to the gradual nature of relaminarization.

The power spectrum of the axial velocity fluctuations for this case is given in Figure 6.11. The wavenumber is non-dimensionalized using u_*/ν, and the spectrum is non-dimensionalized using u_τ^2 in the footsteps of Perry et al. 1975. The spectrum has been truncated at the smallest and the largest wavenumbers, set by the diameter of the pipe and the Kolmogorov length scale. Qualitatively, the spectrum is similar to the one observed by Sibulkin 1962 for the case of decaying pipe flows. He provides possible scaling laws for the spectrum, which do not seem to hold over here. As expected, the cascade process is visible from the graph. The

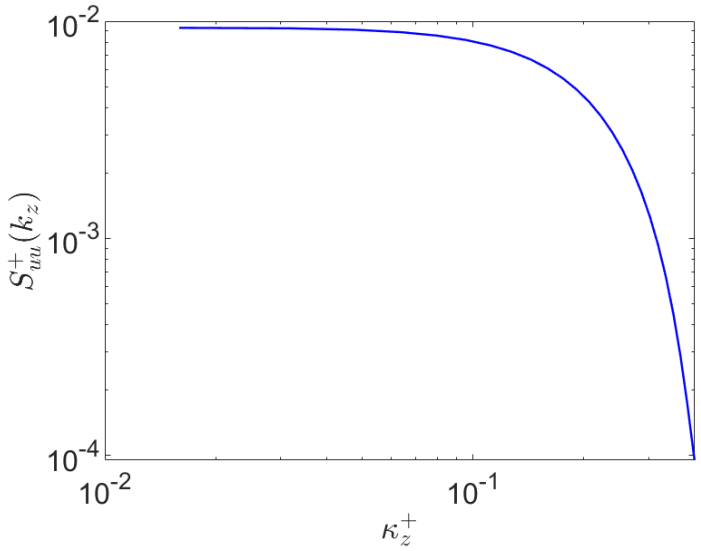

Figure 6.11: The power spectrum of the axial velocity fluctuation for $r/D = 0.25$ and $Re_b = 10000$

Kolmogorov slope of -5/3 is barely evident in this graph indicating that the inertial subrange is very minimal. Pope 2000 gives an analogy where he states that for decaying flows, a fair estimate for the time an eddy spends in the initial subrange is roughly an order of magnitude less than the eddy turnover time. This could probably explain why the inertial subrange is not so evident.

The global decay of the Reynolds shear stress is depicted in Figure 6.12. After the initial deceleration, the nature of the decay for this variable seems to be exponential (from $t_* \approx 3.5$). Looking at Figure 6.4 and Figure 6.5, it is to be expected that the Reynolds stress decays at

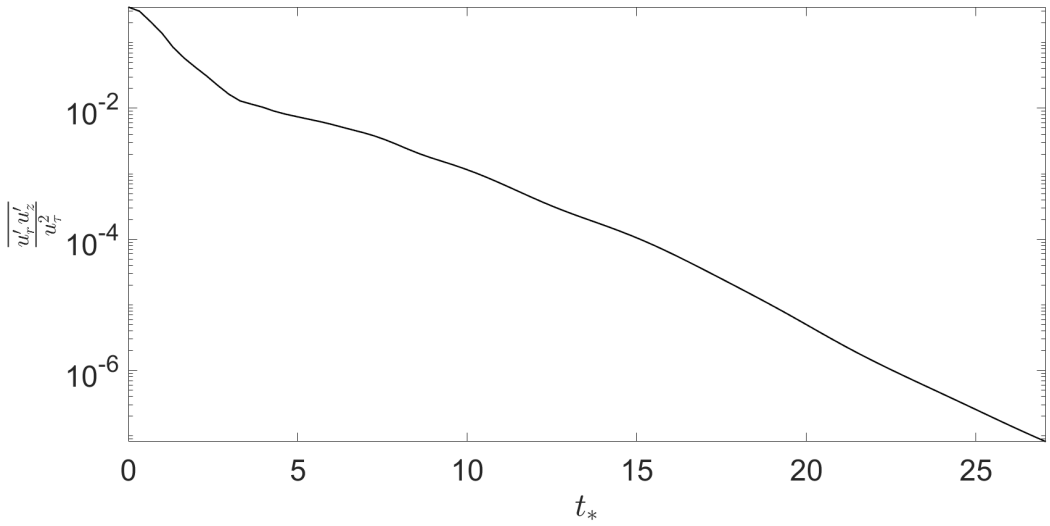

Figure 6.12: The decay of the volume-averaged Reynolds shear stress with non-dimensionalized time

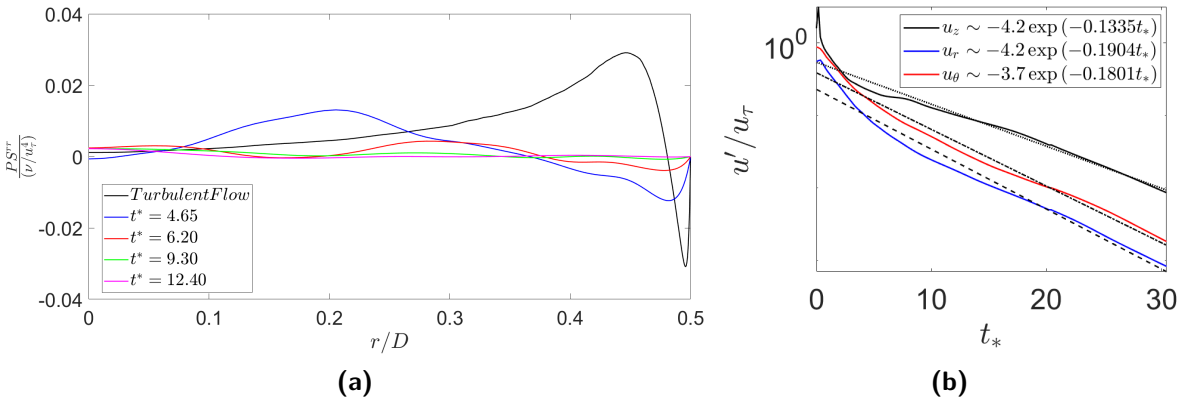

Figure 6.13: (a) The pressure-strain term of the $\overline{u_r'^2}$ budget (b): The volume-averaged RMS velocities on a semi-logarithmic plot: A linear fit is done on the exponential curves to show the overall difference in the decay rate of the three components. This can be seen from the coefficients of t_* within the exponential function

a faster rate than the TKE. It is possible that this is because of the decorrelation mechanisms in the decay of pipe flow (Sreenivasan 1982), although there is no concrete evidence of this.

A few final observations are noted to wrap up this section. The decay of the volume-averaged axial, radial and azimuthal RMS velocities is depicted in Figure 6.13b. Although the nature of decay for these components is similar to the TKE, they are depicted on a semi-logarithmic plot for comparison only. From the figure, it is quite clear that the streamwise turbulent intensity decays much more slowly than the wall-normal and circumferential turbulent intensities. This is similar to results obtained for decaying flows in a channel (Narayanan 1968), and also in other accelerating boundary layer flows (Sreenivasan 1982). These authors found the wall-normal intensities to decay nearly 1.5 times faster than the streamwise intensities, and an equivalent result can be found here. This outcome can be attributed to the anisotropy of wall-bounded flows. In a turbulent flow, the pressure-strain term in the $\overline{u_r'^2}$ budget is responsible for the energy tranfer between components (Eggels et al. 1994). Figure 6.13 also shows this term and its decrease over time. This implies that the energy transfer between the different components is lagging, and thus, it is ineffective to correct anisotropy (Iida et al. 1998). Moreover, the location where the pressure-strain takes a negative value moves towards the center of the pipe, which is an added indicator of the reduction in sweep events, and the conversion of the viscous sublayer into a laminar boundary layer.

Figure 6.14 shows the global decay rate of the TKE at different r/D locations in the pipe. Again, a semi-logarithmic plot is shown for simplicity. It is noticeable that the decay rate in the buffer layer and the viscous sublayer are the fastest as compared to the log-layer and the core region. This is as expected, as the major change in the turbulent quantities is expected to occur near the wall. For the core region, it is seen that just after the deceleration, the energy seems to stabilize at a value for a while (upto $t_* \approx 2$). This is similar to the results seen in accelerated boundary layers where the authors mention "frozen turbulence" in the core, with maximum changes occurring near the wall (Sreenivasan 1982; Guerrero et al. 2021). However, this is not maintained for a long time, and it is hypothesized that this is because of the extremely large deceleration applied here. Sibulkin 1962 and Narayanan 1968 find that the intermediate radii, $r/D = 0.2 - 0.3$, initially shows the slowest decay of

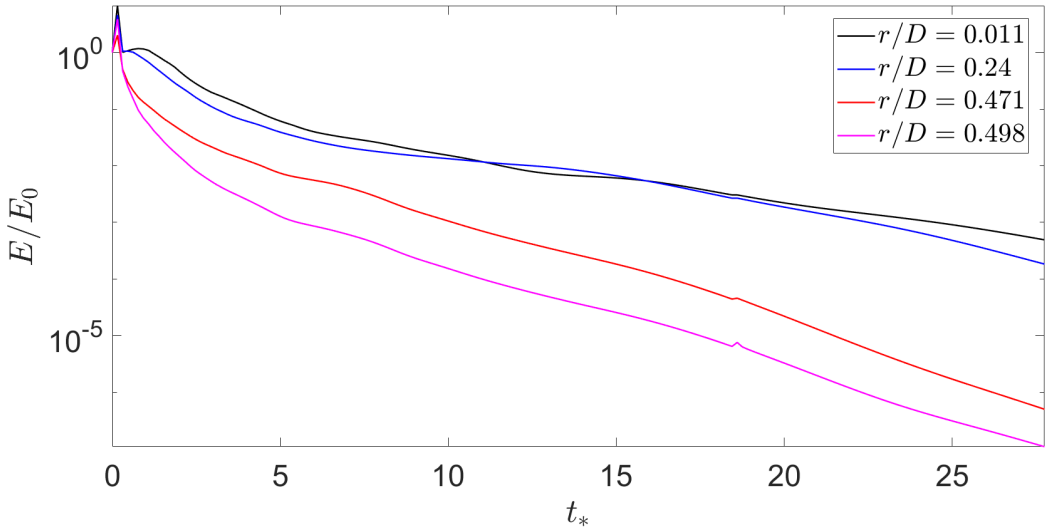

Figure 6.14: The decay of the TKE at different regions of the pipe: $r/D = 0$ is located at the center

all the regions. Sibulkin 1962 hypothesizes that this could be because of the lower rates of dissipation and production in the region, or the diffusion of turbulent energy from the walls to the center. While the hypothesis of Sibulkin 1962 is a valid one, this result is not noticed in these simulations. Here, the core of the pipe and the intermediate region seem to decay at the same rate.

6-2-1 Independence of the Ramp Rate

With an idea on the decay, it is of quite some interest to see what parameters might affect the nature of decay. A study was undertaken to check the effects of the ramp rate on the decay. As mentioned previously, ramps applied over a length of time equivalent to the eddy turnover time ($ETT = \tau_e = \mathcal{L}/u'$, where $\mathcal{L}$ is the length of the eddy) were being used to study the decay. In essence, it is logical to study the behaviour of turbulent flows on a viable time scale, and therefore, the ramp used was ensured to be on scale similar to the one observed in the flow. The dimensionless time scale used in the results, $t_* = R/u_\tau$, is expected to be approximately $10 - 20ETT$. It is now of interest to see what would happen if the ramp were sped up or slowed down.

Figure 6.15 shows the decay of the turbulent kinetic energy for $Re_b = 10000$ using different ramp rates. The time scale denotes the time over which the ramp was applied. The ramp rates that are less than or equal to $\mathcal{O}(1ETT)$ all start at the same time and the applied deceleration is also included in the plot. As expected, the nature of decay is similar irrespective of the ramp rate used. It is also a result that was found by Sibulkin 1962, where he suggested the use of sudden expansions to study the decay. It is true that a majority of the applied decelerations are at times very similar to the eddy turnover time (ETT). However, it is noticeable that the slower ramps used (with applied time of ramp $t_* = 0.75ETT$ and $t_* = 1ETT$) seem to contain slightly less energy than the faster ramps. A study was also undertaken using a ramp rate of $\mathcal{O}(t_*)$. This is a much slower ramp rate as compared to the other scenarios.

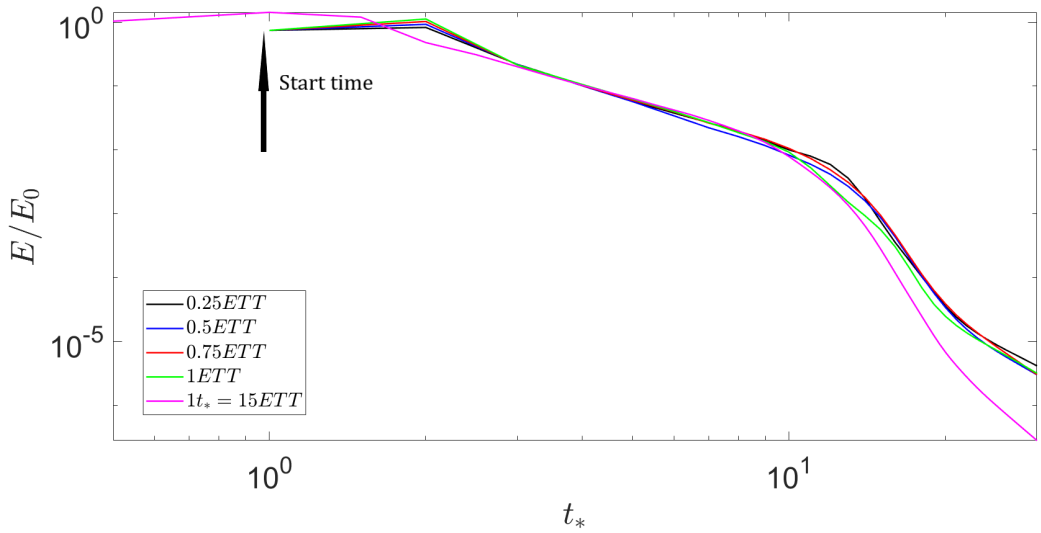

Figure 6.15: The decay of the TKE for different time steps used to generate the linear ramp: The ramps applied for 0.25, 0.5, 0.75 and 1 ETT all start at the same time and is indicated in the figure. For the ramp applied over $1t_*$ only the last quarter of the ramp ($0.75 - 1t_*$ in the figure) is shown

Only the final quarter of the applied deceleration is represented in Figure 6.15. During this stage, it is seen that the TKE increases slowly, as compared to sharp increases noticed for the much higher ramp rates. Additionally, the drop off that was noticed - where the decay is expected to change from a power-law to an exponential decay - occurs at an earlier stage while using slower ramp-rates. While the ramp timings of 0.25, 0.5 and $0.75ETT$ divevrge at approximately the same point, the curve for $1ETT$ diverges at an earlier time from this. The curve for $1t_*$ diverges earlier than $1ETT$ itself. This shows that using slower ramps is not useful, as quite a bit of turbulent information is lost during the deceleration process.

The decay of the Reynolds shear stress is shown in Figure 6.16. Similar to the TKE, the expected decay rates between different ramps are similar here as well. A key result that can be noticed is the saturation of the shear stress into some form of steady state for the higher ramp rates, with the values converging as time passes on in the decay. This is due to the fact that the Reynolds shear stress is expected to go to zero as the flow relaminarizes (Narasimha et al. 1979). For the higher ramp rate though this is not the case, with the shear stress continuously decaying, although the values are too small for the stress to have any effect on the mean flow.

From both Figure 6.15 and Figure 6.16, it is quite obvious that using slower ramps might not be beneficial to study the decay. As mentioned previously, changing the flow state as quickly as possible and allowing the flow to decay naturally thereafter is the best method to study the decay. However, it is still interesting to see that using larger ramp rates (lower time for application of ramp) provides better accuracy of results. A ramp rate on the timing of 0.5 eddy turnover time is used everywhere in this study. The difference between the results obtained for ramp rates less than $1ETT$ is not large enough to cause any underestimation of the decay, and therefore, $0.5ETT$ was chosen arbitrarily.

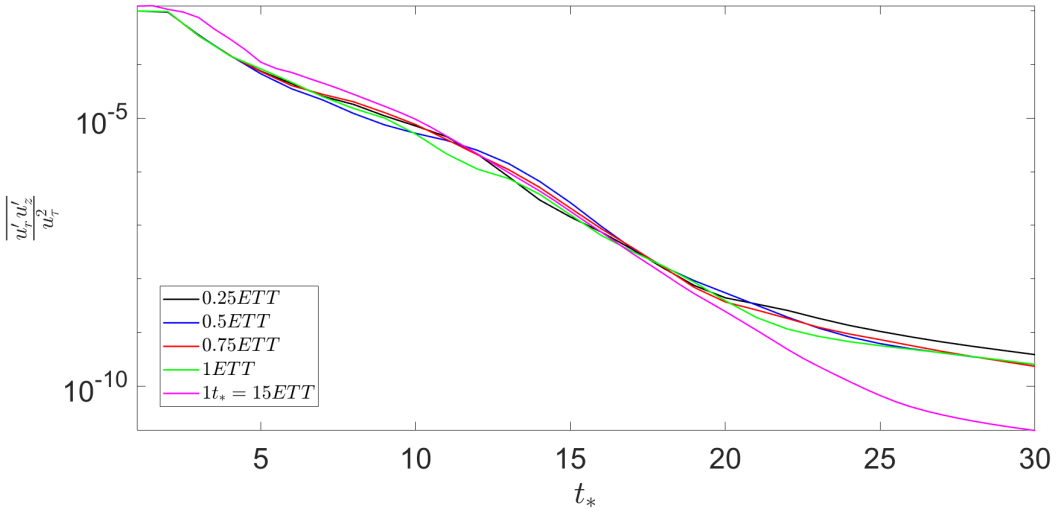

Figure 6.16: The decay of the Reynolds shear stress for the different time steps: The results are shown here from $t_* = 1$, which is after the application of the deceleration

6-2-2 Dependence on the Initial Reynolds Number

Wall-bounded turbulent flows are characteristically scaled on inner and outer variables, and the independence of this scaling with diferent configurations and properties has always been a subject of debate. The Reynolds number of the flow is constantly under scrutiny in this regard. Toonder et al. 1997a find that the turbulence statistics are indeed dependent on the Reynolds number for ranges of 5000 - 25000. This is especially true as the Reynolds number is lower and closer to the laminar state. Therefore, the next parameter that is interesting to study is the initial Reynolds number of the turbulent flow. Most decay studies are carried out at very high Reynolds numbers, to ensure that the flow is sufficiently turbulent for a long period of time. Since it is of interest to study relaminarizing flows here, the range of the starting Reynolds number chosen itself is quite low, and thus, it is quite logical to research the variation in the decay. Three Reynolds numbers are simulated and they are given in Table 6-1.

The decay of the TKE can be noticed in Figure 6.17a, which is a logarithmic plot and Figure 6.18, which is a semi-logarithmic plot. The overall nature of the decay is similar for all three Reynolds numbers, with the curves being qualitatively similar to the results of Touil et al. 2002 for high Reynolds numbers. For $Re_b = 10000$ and $Re_b = 7000$, two regions of power-law decay exist – one before the saturation of the length scale, and one after. For the first stage of power-law decay, the exponent for $Re_b = 7000$ is -1.2. The absolute value of the exponent is larger than the value obtained for $Re_b = 10000$, but it is closer to the value predicted by Skrbek et al. 2000. The demarcation is not clear for the lower Reynolds number case of $Re_b = 5300$, although the length scale saturates at approximately the same time as the other two cases. This is quite a low Reynolds number and therefore, it could be difficult to discern the two regions of power-law decay here. The exponents for both the power-laws are summarized in Table 6-1.

For all three cases, there is a saturation of the length scale, set by the diameter of the pipe. The second stage of power-law decay follows after this. The curves then seem to

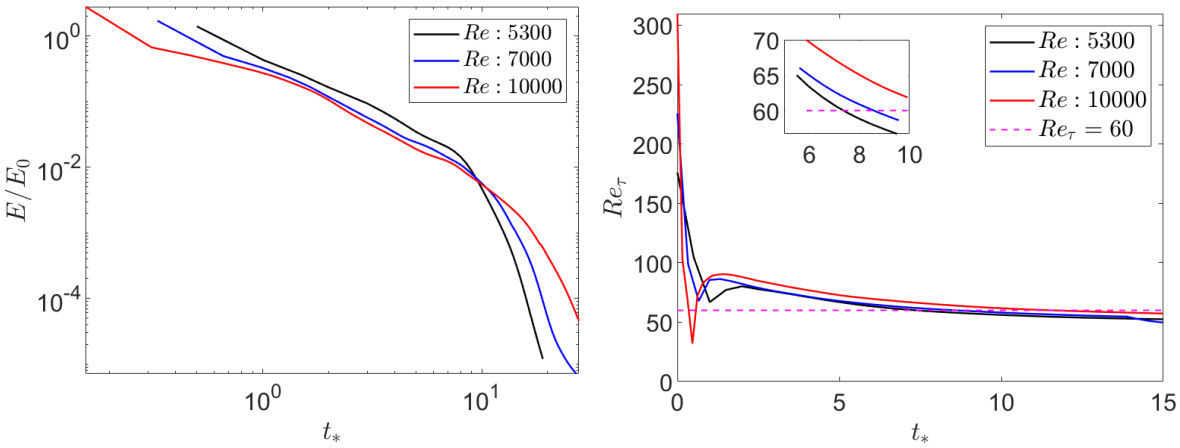

Figure 6.17: (a) The decay of the TKE for different initial Reynolds number depicted on a logarithmic plot (b) The variation of Re_τ over time for the three different Reynolds numbers: The zoomed-in section shows that $Re_b = 5300$ reaches $Re_\tau = 60$ at an earlier time than $Re_b = 7000$ and $Re_b = 10000$, which implies that $Re_b = 5300$ diverges first

diverge and follow the exponential viscous regime, with $Re_b = 5300$ diverging first, followed by $Re_b = 7000$ and $Re_b = 10000$ curves. This implies that the virtual origin in time to describe the exponential decay changes with the initial Reynolds number. The variation in virtual origin could possibly be because of the increasing intermittency of the flow with decreasing Reynolds number. Skrbek et al. 2000 make a similar observation in their study of homogeneous, isotropic turbulence. They state that the effects of the intermittency on the decay law is to change the virtual origin prescribing the law, rather than change the nature of decay itself. It was also mentioned previously that the point of divergence could possibly be predicted by the reducing friction Reynolds number. For $Re_b = 10000$, this point coincided with $Re_\tau \approx 60$, and this is also true for the other two Reynolds numbers. Faster divergence from the power-law decay to the exponential decay is evident from Figure 6.17b, where the zoomed-in section of the graph shows that $Re_\tau = 60$ is reached faster as the initial Reynolds number decreases. As mentioned previously, various authors find localised turbulent structures in their studies at this value of Re_τ (Iida et al. 1998; Tsukahara et al. 2014). Therefore, around $Re_\tau = 60$, scaling on the inner variables might not hold anymore and the differences in the decay for the three cases is now expected to arise due to the difference in their viscosities. This could possibly be used as an indicator for when the decay law changes from a power-law to an exponential behaviour, as it is one of the few points of quantitative similarity noticed between the three different cases for the point of divergence. However, it is difficult to comment why this happens, and further discussion is provided in Section 6-4.

Fitting linear curves on the logarithmic plots to estimate the power-law decay (not shown in figure), it is seen that the decay exponent after the saturation of the length scale, is approximately $m = 1.7$ for all three cases. This is close to the value of $m = 2$ expected by Skrbek et al. 2000. The difference in the power-law index, as opposed to that noticed by Skrbek et al. 2000, is attributed to the presence of production and the anisotropy of the flow, as mentioned before. Skrbek et al. 2000 also predict that the rate of decay increases as one studies lower Reynolds numbers. However, the range of Reynolds numbers studied

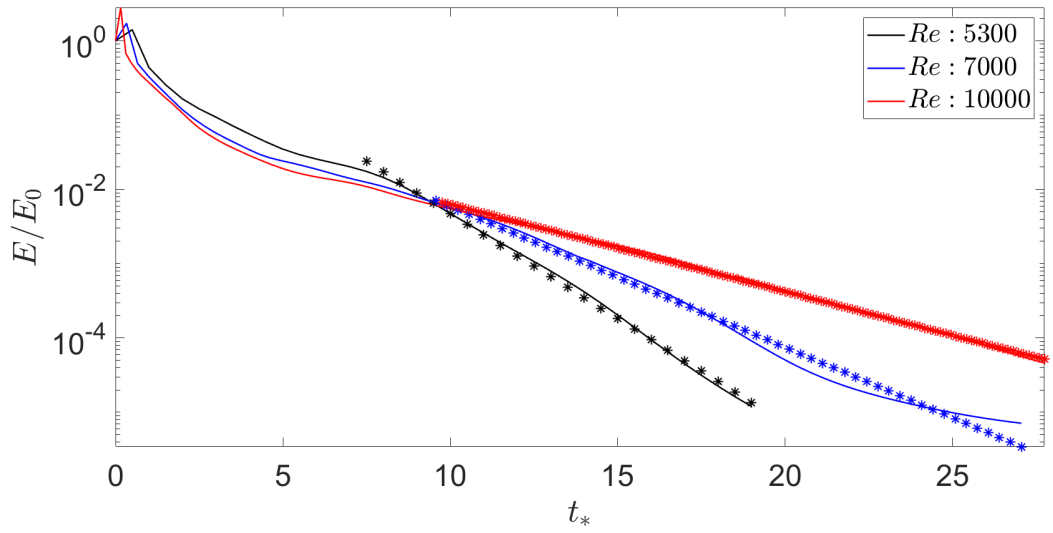

Figure 6.18: The decay of the TKE for different initial Reynolds number depicted on a semi-logarithmic plot: The curves represent the obtained result, while the symbols are linear fits for the data to show the exponential viscous decay for the different Reynolds numbers

Re_b	R/u_τ $[s]$	s for $E \sim t^{-s}$	m for $E \sim t^{-m}$	β for $E \sim \exp(-\beta(t_* - t_{vo}))$	β_{th}
5300	14.71	-	1.73	0.5	0.37
7000	15.15	1.2	1.65	0.33	0.31
10000	16.13	0.9	1.67	0.27	0.29

Table 6-1: Parameter space and results obtained to study the influence of the initial Reynolds number: s is the power-law index before saturation; $Re_b = 5300$ does not have a value for this section as described in the text. m is the power-law index after saturation is reached. β_{th} is the expected theoretical value of the damping coefficient assuming a constant length scale of $\kappa = 2\pi/D$

here might not be sufficient to notice this behaviour. For the viscous exponential decay, fits of the nature $E \sim E_0 \exp(-\beta(t_* - t_{vo}))$ are attempted, where t_{vo} represents the non-dimensionalized time from where the exponential decay is active. The estimated values of $\beta = 2\nu\kappa^2$, with $\kappa = 2\pi/D$, are in good agreement with the fits for the cases of $Re_b = 7000$ and $Re_b = 10000$, while there is some discrepancy between the values for $Re_b = 5300$. The values of all the coefficients are summarized in Table 6-1.

6-2-3 Modelling using RANS

It is difficult to model decaying flows. This is one of the fundamental issues that most laminarizing flows have faced over the years (Sreenivasan 1982). With this in mind, an attempt was made to study the decay of the flow with a RANS model. The study was conducted in `OpenFOAM` with a low Reynolds number $k - \epsilon$ model. The three Reynolds numbers studied in the previous section were also evaluated here. A fully-developed turbulent pipe flow was set

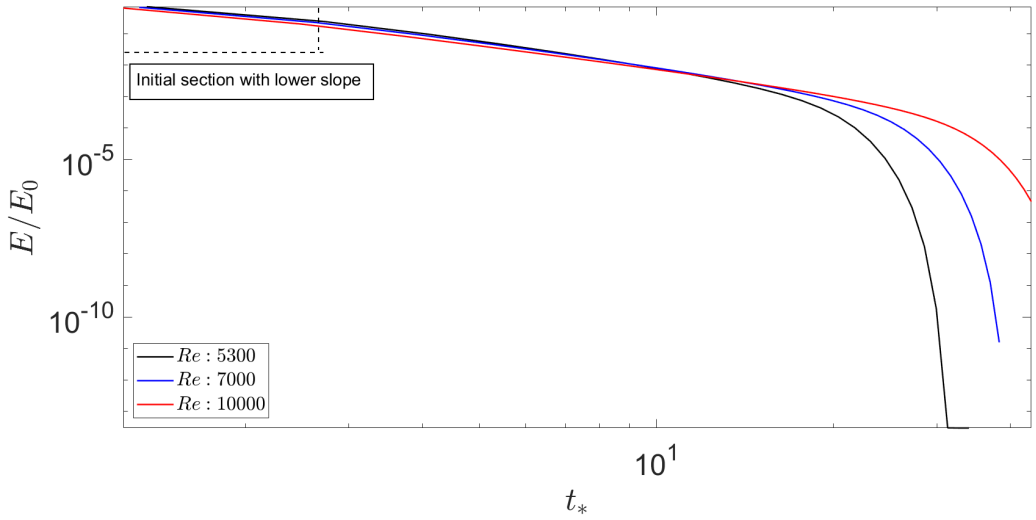

Figure 6.19: The decay of the TKE as modelled by RANS: The initial section (marked in the figure) has a lower slope than the rest of the decay. The drop-off in the TKE also seems to appear at a much later stage for all the three Reynolds numbers as compared to the DNS results

up for each case, and an equivalent deceleration as the DNS study was applied here as well.

The plots for the TKE, k, and the dissipation rate, ϵ, are shown in Figure 6.19 and Figure 6.20. The qualitative nature of the decay is simlar to the DNS results. The initial section of the power-law decay is very small now, and is not quite clear from the graph. The power-law decay region itself is extended. Fitting the data, it is seen that the power-law exponent is now closer to -2.5 for all the cases. This is similar to the case of the final period of decay of isotropic turbulence as predicted by Batchelor et al. 1948. The points of divergence from the power-law to the exponential decay now occur at much later times – $t_* = 9, 14, 17$ instead of

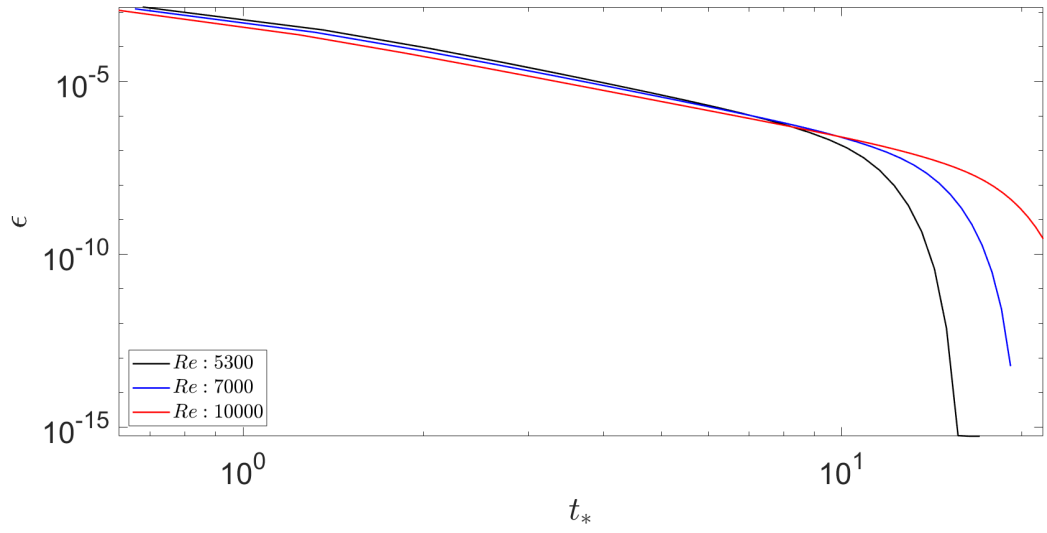

Figure 6.20: Decay of the dissipation rate with respect to non-dimnsionalized time: The nature of the graph is similar to Figure 6.19

$t_* = 7, 9, 12$ with increasing values of Re_b. The divergence shown as occuring near $Re_\tau \approx 60$ for all the cases is now not seen at all. Furthermore, the RANS model does not seem to predict the change in the length scale and its saturation. This is because of the inability of the RANS model to exactly understand the presence of the geometry.

The inability of the RANS model to accurately predict the decay was not unexpected. The fixing of the length scale by the RANS model is ineffective for this study, and therefore, it is quite understandable why several authors in the past have not been able to appropriately address this issue. This also shows the necessity of using DNS and resolving as many of the energy-containing length scales as possible. Using a higher-order method such as `nek5000`, only enhances the accuracy of the obtained results.

6-3 Results - Non-Newtonian Flow

With a grasp on the decay of Newtonian flows, it is time now to study the effects of introducing a varying viscosity to the flow. As mentioned previously, blood can be treated as a shear-thinning fluid (Macosko 1994). To this end, the decay of power-law fluids has been studied. It is also of some interst to study the variation of the decay with shear-thinning itself. Therefore, it is easier to study power-law fluids, since the only parameter to vary is the shear-thinning index.

As mentioned previously, pipe flows for non-Newtonian fluids are more stable than for Newtonian fluids (López-Carranza et al. 2012), and thus, transition is delayed. Therefore, the largest initial Reynolds number ($Re_\tau = 315$ for Newtonian, $Re_\tau = 323$ for non-Newtonian fluids) is used to compare the decay. To study the decay, a linear ramp on the scale of the

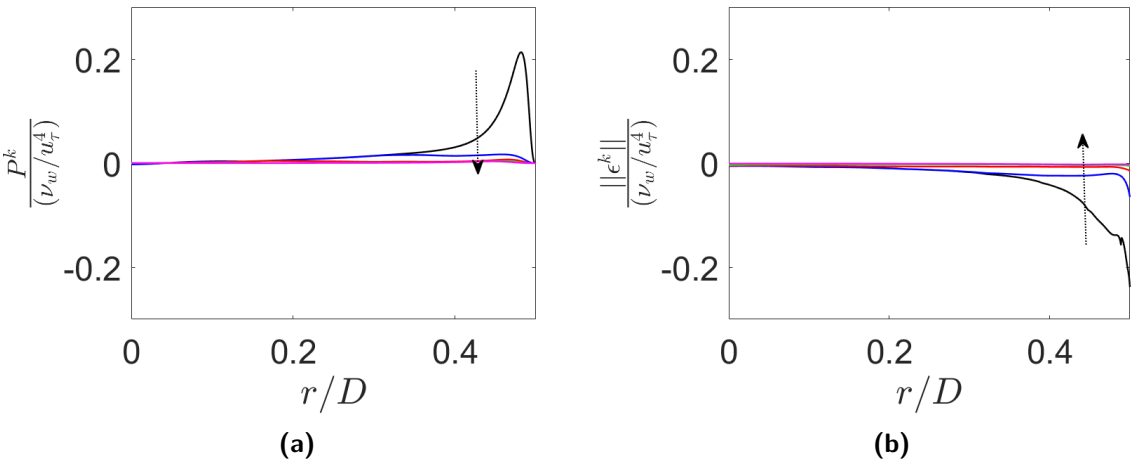

Figure 6.21: The variation of the (a) Production (b) Dissipation - The arrows in (a) and (b) indicate the direction of increasing t_* - All the budget quantities are normalized by ν_w/u_τ^4, where u_τ is the friction velocity, and ν_w is the wall viscosity for the fully-developed turbulent flow. The quantities here ($n = 0.8$) decrease at a faster rate than the Newtonian flow ($n = 1$) (see Figure Figure 6.5). The final two time stamps are very tough to discern because of their values beeing extremely close to zero. *Legend*: (——) Fully developed turbulent flow (——) $t_* = 3.10$ (——) $t_* = 6.20$ (——) $t_* = 9.30$ (——) $t_* = 12.40$

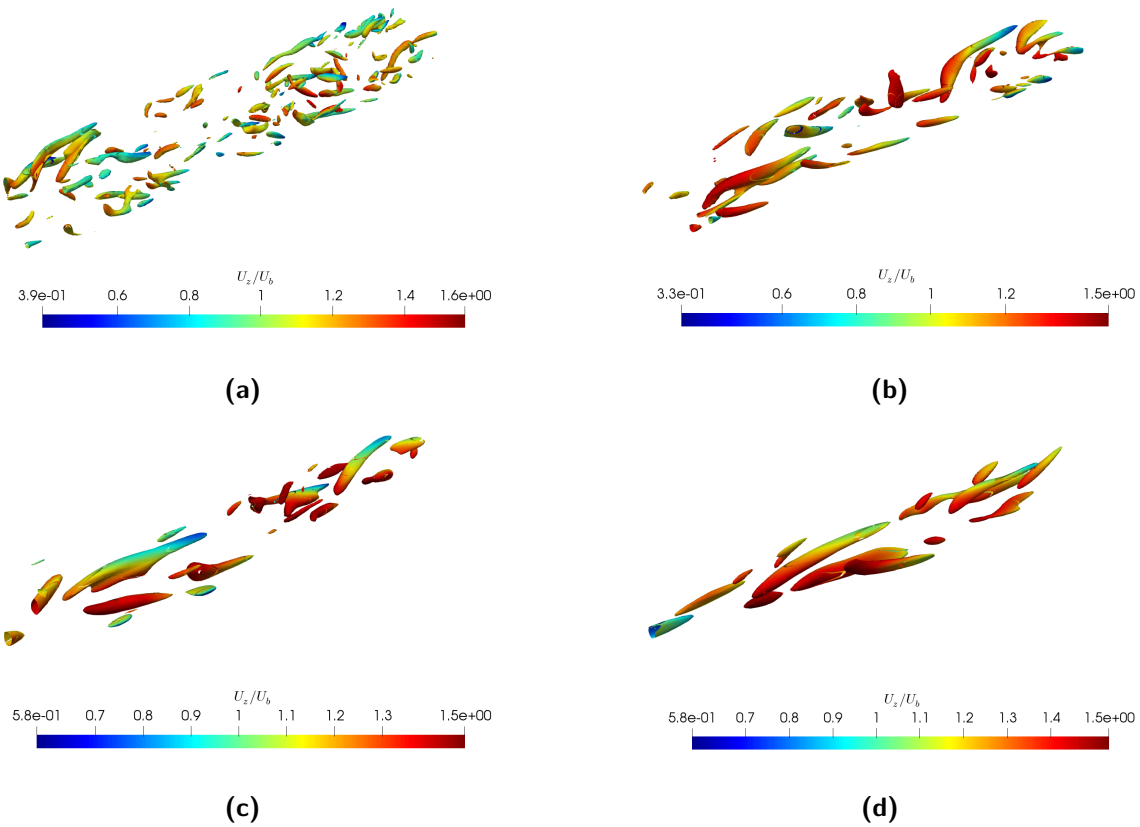

Figure 6.22: The coherent structures present in the pipe at different times during the decay determined by the Q criterion. The structures here are presented after the application of the ramp. The values of t_* here, again indicate that the flow laminarizes at a faster rate for a non-Newtonian fluid ($n = 0.8$) than a Newtonian fluid ($n = 1$). Similar to Figure 6.7, different threshold values of Q are employed. The colouring used is of the instantaneous axial velocity (a) $t_* = 2.12$ (b) $t_* = 4.55$ (c) $t_* = 6.36$ (d) $t_* = 8.18$

eddy turnover time is used here as well. The deceleration mechanisms are similar to those employed for the Newtonian flow. As the flow decelerates, the velocity reverses at the wall for non-Newtonian flows as well. The turbulent intensities increase as the deceleration is applied, after which the fluid does not have enough energy to reach the turbulent state. Instead the remaining turbulence decays, and the flow reaches a laminar state.

The decay of turbulence is qualitatively similar for non-Newtonian and Newtonian flows. This view seems to hold with the analysis of Chow et al. 1967, where a decay independent of the nature of the fluid was shown for non-Newtonian fluids as well. After the applied deceleration, there is a decrease in the turbulent quantities, such as the Reynolds shear stress and the TKE budget terms. These quantities decrease over time and asymptotically reach zero. Figure 6.21 show the decrease in the production and the dissipation of the TKE budget over time for $n = 0.8$. The same time stamps as Figure 6.5 are used to compare the values. It is evident that the decay is qualitatively faster in a generalized Newtonian fluid than a Newtonian fluid. The last two time stamps are barely visible in Figure 6.21, indicating that the flow has probably already decayed and reached a laminar state.

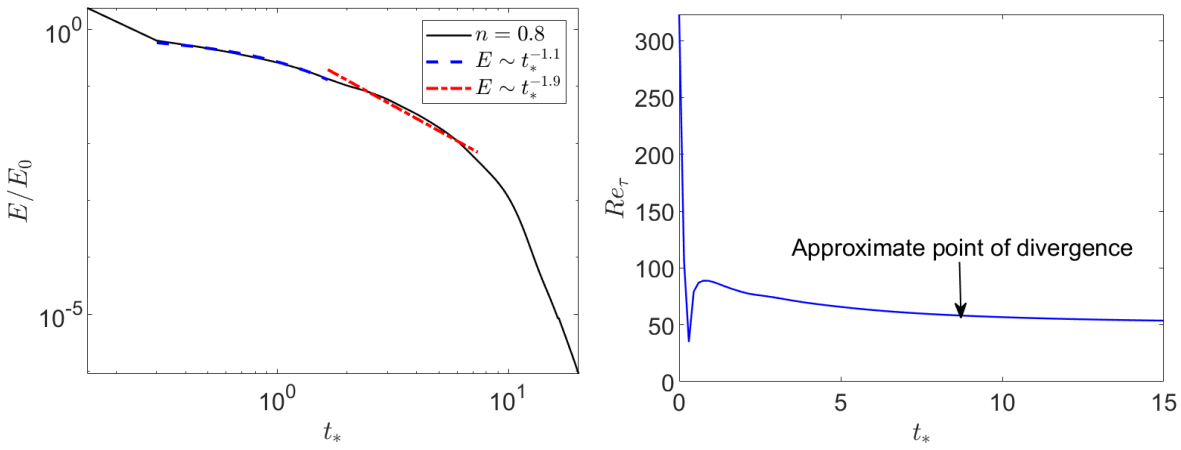

Figure 6.23: (a) The decay of the volume-averaged TKE over time for $n = 0.8$ depicted on a logarithmic point: The blue line represents a liner fit to indicate the power-law decay before the saturation of the length scale occurs, while the red line indicates the power-law decay after the saturation of the length scale (b) The variation in Re_τ over time: The point of divergence indicates the approximate time when the decay diverges from a power-law to an exponential decay. The value is $Re_\tau = 61.5$

The organized motions in the pipe for the decaying flow are shown in Figure 6.22. These results are again for $n = 0.8$ and are qualitatively similar to the Newtonian flow. The structures increase in length over time and their number decreases, indicating that the bursting rate is reducing. The thickness of the viscous sublayer increases and eventually, a laminar boundary layer is formed. This is clear from the structures moving away from the wall and towards the centre. The time stamps used here again reinforce that the decay is faster here than for the Newtonian flow.

The decay of the volume-averaged TKE for $n = 0.8$ is shown in Figure 6.23a on a logarithmic plot. Similar to Newtonian flows, there are two regions of power-law decay – one before saturation of the length scale, and one after saturation. This is followed by an exponential viscous decay. The value of the exponent for the first stage of decay is -1.1, and for the second stage it is -1.9. For both the power-law decays, the exponents are comparable to the values provided by Skrbek et al. 2000 for homogeneous, isotropic, Newtonian flows. However, comparing these values with the results obtained here for the Newtonian case of $Re_b = 10000$ ($Re_\tau = 323$), the absolute values obtained for $n = 0.8$ are slightly higher. During the turbulent regime, the scaling between a non-Newtonian and Newtonian fluid is not expected to vary by much, and thus, the difference in the exponents could simply be becuase of the error arising out of these estimated fits. Figure 6.23b shows the variation of Re_τ with non-dimensionalized time for $n = 0.8$. The point of divergence from the power-law decay to the exponential decay is marked on the graph. Similar to the Newtonian fluids the value is $Re_\tau \approx 60$ here as well, but the point now occurs at an earlier time than for the Newtonian flow ($t_* = 8.5$ here as compared to $t_* = 12.5$ for $n = 1$ and $Re_b = 10000$).

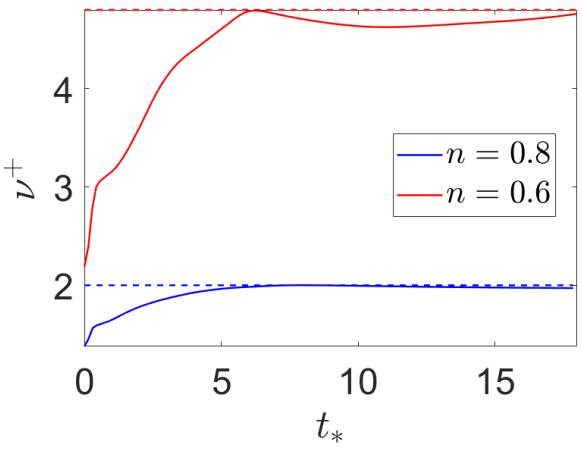

Figure 6.24: Normalized average viscosity with time: The dotted lines show the average viscosity for the fully-developed laminar flow, normalized using the wall viscosity of the fully-developed turbulent pipe flow. The average viscosities approach the laminar value asymptotically

6-3-1 Influence of Shear-thinning

It is also beneficial to study the effects of shear-thinning on the decay. The power-law value for blood is $n = 0.67$, and therefore, two values of the power-law index, $n = 0.6$ and $n = 0.8$, will be studied here. The parameters necessary to define the flow are provided by Singh et al. 2017, and therefore, a fully-developed turbulent state can be set up and verified. These results should also enable suitable discussion on how the results obtained here can be applied to an aneurysm.

Unlike Newtonian flows, there is also a change in viscosity here over time. Using Reynolds averaging for the non-Newtonian viscosity (Pinho 2003), the slab-averaged viscosity can be monitored with time. The average viscosity is normalized using the wall viscosity, and this is depicted in Figure 6.24. The viscosity increases with time until it reaches a steady-state solution. It is expected that the shear rate will decrease over time as the flow starts to relaminarize. The existing gradients in the flow are expected to reduce and become less steep over time. This explains why the viscosity increases. The increase in viscosity is also consistent with the fact that the decay law diverges from the power-law to an exponential decay at an earlier stage (see Figures 6.23a and 6.26a). As the turbulence decays, the flow becomes more viscosity dependent at a faster rate as the degree of shear-thinning increases. This could explain why turbulent scaling for the power-law decay holds equivalently for both non-Newtonian and Newtonian fluids, where the flow is almost independent of the viscosity, but the point of divergence occurs earlier in non-Newtonian fluids. For laminar flow of power-law fluids, the analytical result for the velocity profile is given by (6-3) (Metzner et al. 1955).

$$w(r) = \left(\frac{\tau_w}{KR}\right)^{1/n} \left(\frac{R^{1/n+1} - r^{1/n+1}}{\frac{1}{n}+1}\right) \tag{6-3}$$

Differentiating with respect to r, and substituting it in the constitutive equation for the viscosity, a radial distribution for the laminar viscosity can be found. The average viscosity

for laminar flow can be calculated for both the fluids, and compared with the viscosity obtained here for relaminarizing flows. Doing so, it is seen that for both flows, the viscosity obtained here is slightly lower than the expected value for a fully-developed laminar state. This strengthens the impression that the flows are asymptotically reaching a laminar state. Figure 6.24 plots the average viscosity for both the cases. The result matches excellently for the case of $n = 0.8$, while the result for $n = 0.6$ shows some variance. This could possibly be because of the increase in intermittency of the flow with increasing shear-thinning (Singh et al. 2017).

Figure 6.25a plots the development of the integral length scale for the three fluids at a radial location of $r/D = 0.25$. This indicates that the length scale is of $\mathcal{O}(D)$ for all three fluids fairly early. The rate of growth of the integral length scale is not very different for the Newtonian fluid and $n = 0.8$. This could be because the value of $n = 0.8$ is quite large to fully indicate the effects of shear-thinning. The results of $n = 0.6$ seems to suggest that the saturation length is reached quicker with increasing shear-thinning, although this is not quite evident from the decay of the TKE. The higher dissipation of TKE implies that the energy-containing eddies decay faster with increasing shear-thinning, and have shorter lifetimes (Rahgozar et al. 2017). From the growth of the length scale, it is even more clear that the qualitative nature of decay is similar for Newtonian and generalized Newtonian fluids. The power spectrum for the axial velocity fluctuations is plotted in Figure 6.25b. Again, the spectrum is truncated at the smallest and the largest wavenumber, similar to Figure 6.11. The graphs are qualitatively similar. Similar to the results of Toonder et al. 1997a, the energy has shifted to the smaller wavenumbers for the non-Newtonian fluids. Indeed, the amount of energy shifted seems to increase with shear-thinning. Since, the spectrum is truncated the energy being lesser at the smaller scales (like the results of Toonder et al. 1997a) is not quite certain. However, the cascade seems to become faster with the increase in shear-thinning and therefore, it can be expected that there is less energy contained at the small scales with increasing shear-thinning.

Figure 6.26 shows the decay of the TKE for the three different fluids. For the power-law

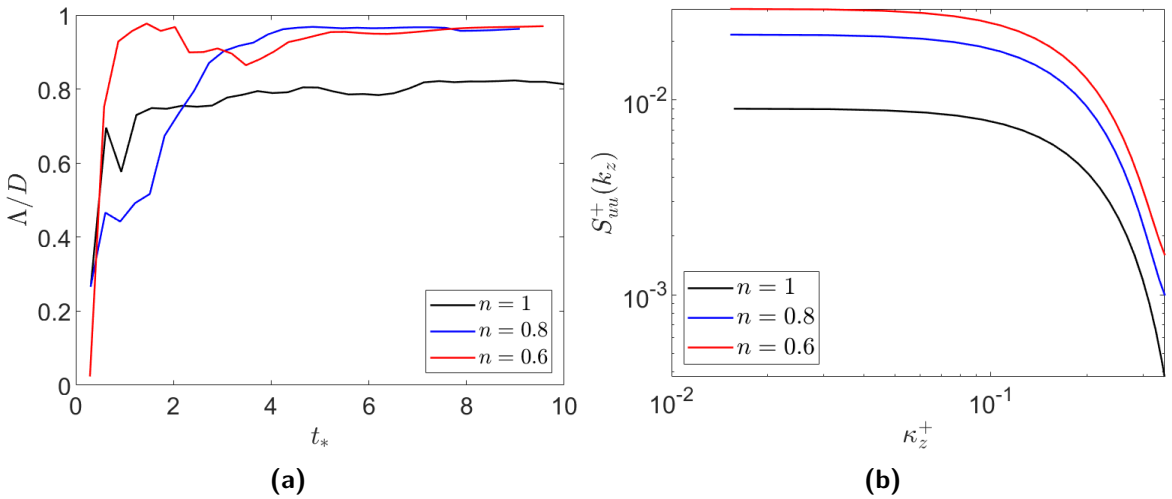

Figure 6.25: (a) Variation of the streamwise integral length scale over time (b) The power spectrum of the axial velocity fluctuations for the three cases - Both plots are given at a radial position of $r/D = 0.25$

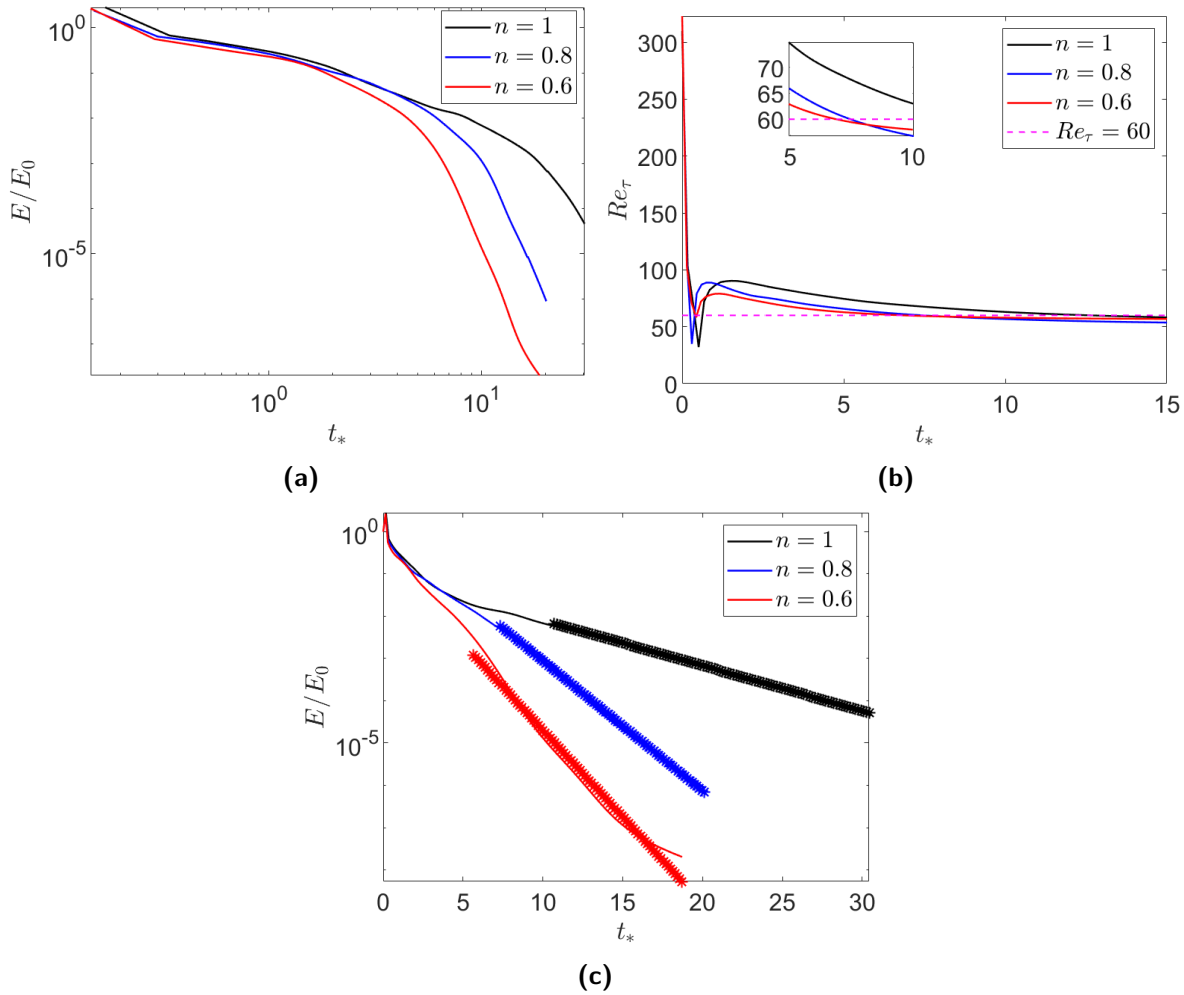

Figure 6.26: The decay of the volume-averaged TKE for different values of n - (a) On a logarithmic plot (b) The variation of Re_τ over time: The zoomed-in section shows that $n = 0.6$ reaches $Re_\tau = 60$ the fastest, followed by $n = 0.8$ and $n = 1$ (c) On a semi-logarithmic plot: The symbols represent linear fits on an exponential curve to show the difference in the decay rate of the three fluids

decay stages, the flow does not seem to distinguish between the non-Newtonian and the Newtonian fluid, indicating that the flow is sufficiently turbulent for the solutions obtained to be independent of viscosity. Soon after, the flow starts to settle into an exponential decay, expressed in the form of $E \sim E_0 \exp(-\beta(t_* - t_{vo}))$. It was mentioned previously that the flow diverges from a power-law decay to an exponential decay at approximately $Re_\tau = 60$, and this seems to also be true for both the power-law fluids. From the decay plots and the development of the average viscosity it is clear however, that the flow diverges at an earlier time as the degree of shear-thinning increases.

The parameter space studied and the values of the constants for the decay fits are summarized in Table 6-2. As mentioned previously, it must be noted here that the poewr-law decay holds for smaller times as the shear-thinning increases, and the viscous, exponential decay is reached at a faster rate. For the exponential fits, the damping constant, β, is defined here as $\beta = 2\overline{\nu}\kappa^2$,

n	s for $E \sim t^{-s}$	m for $E \sim t^{-m}$	Re_τ	β for $E \sim \exp(-\beta(t_* - t_{vo}))$	β_{th}
1	0.9	1.67	62.85	0.27	0.29
0.8	1.1	1.88	61.50	0.71	0.74
0.6	1.15	1.93	63.31	0.94	1.08

Table 6-2: Parameter space and results obtained to study the influence of shear-thinning - (i) Re_τ indicates the point where divergence is expected to occur (ii) The expected theoretical values for β are calculated using the theoretical average viscosity and are given as β_{th}

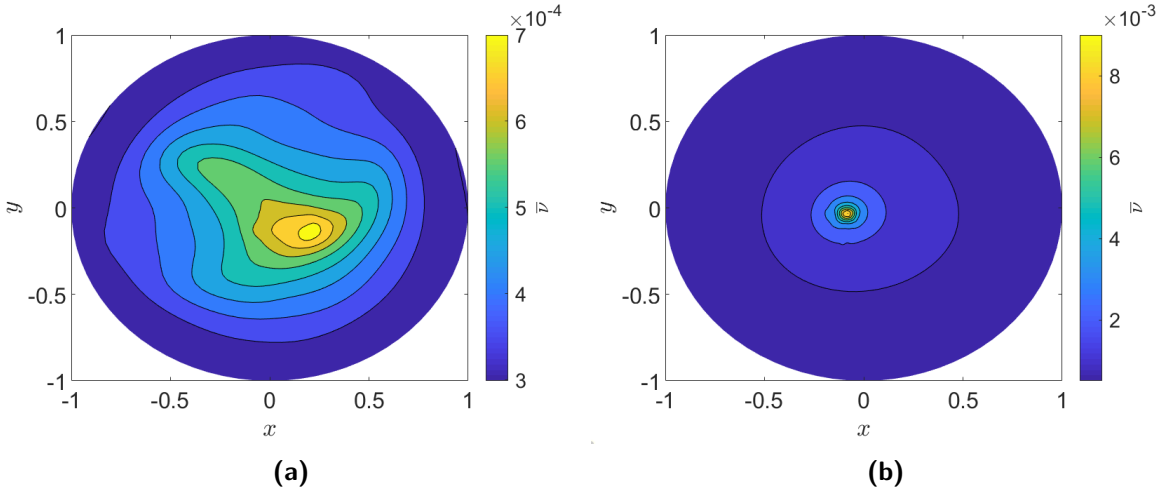

Figure 6.27: The viscosity contours for the two power-law fluids at $t_* = 8$. The distribution is more uniform for $n = 0.6$ than $n = 0.8$, further proving that the turbulence decays faster for $n = 0.6$ (a) $n = 0.8$ (b) $n = 0.6$

with $\kappa = 2\pi/D$, and $\overline{\nu}$ taken to be constant in time during the exponential decay. Using the average viscosity values for $n = 0.8$ and $n = 0.6$, the theoretical estimated values and the obtained values are in decent agreement, with the error expected to arise from the selection of the virtual origin. From the decay curves and their points of divergence, it is a fair estimation that the overall decay increases with shear-thinning. The value of β increases with shear-thinning, indicating that the decay is more exponential as the power-law index decreases in value. Figure 6.27 shows the contours for the instantaneous velocity and the viscosity for $n = 0.8$ and $n = 0.6$ at $t_* = 8$. It can be seen that the viscosity distribution is more uniform for $n = 0.6$ as compared to $n = 0.8$ at the same time, which implies that the gradients in the flow are less steep, and thus, the flow for $n = 0.6$ is more laminar than for $n = 0.8$.

To close this section, it is again of interest to see the pace of decay for the three RMS velocities. Figure 6.28a plots the decay of the volume-averaged turbulent intensities with time for $n = 0.8$. Similar to the Newtonian decay, the axial intensity decays at a slower rate than the wall-normal and circumferential intensities. This shows the highly anisotropic nature of the flow. With the nature of decay being similar between the non-Newtonian and Newtonian flows, this result is as expected. The rate of decay at different regions of the pipe for $n = 0.8$ are presented in Figure 6.28b. The fastest decay occurs near the wall, with the

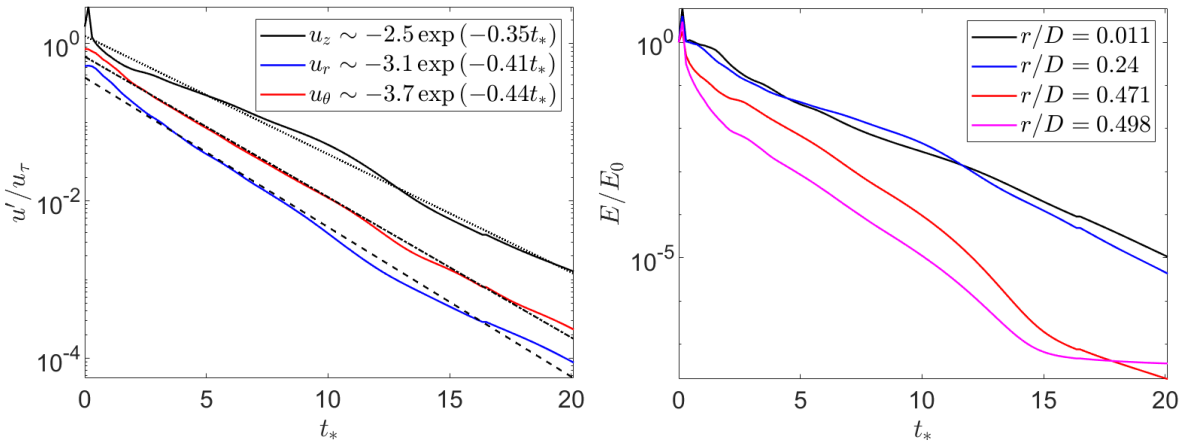

(a) (b)

Figure 6.28: *Left*: Global decay of the RMS velocities for $n = 0.8$ *Right*: The decay of the TKE for different regions of the pipe for $n = 0.8$

viscous sublayer and the buffer layer showing the fastest decay. The core region also shows similar behaviour to the Newtonian flow. The energy does not seem to decay upto $t_* \approx 3$, indicating some form of "frozen turbulence" at the centre. But the applied deceleration is too large to maintain this state for long time periods, and the flow slowly reaches the laminar state asymptotically. A point of difference between Figure 6.28b and Figure 6.14 is that for the non-Newtonian flow the laminarity of the sublayer is quite evident, with the TKE converging to a constant value ($\mathcal{O}(10^{-7})$) over time. This behaviour is not quite discernible for Newtonian flows. This only gives more credence to the fact that shear-thinning increases the pace of the decay. Given that the nature of decay is similar, the results presented above (Figure 6.28) also hold for $n = 0.6$.

6-4 Discussion

In the past few pages, results from the study of the decay of turbulence have been reported. This section is to summarize the key results and comment on the quality of the research undertaken. It is of interest for aneurysms to study decaying tubrulence. As mentioned previously, aneurysms are subject to the formation of vortex rings (Rawat et al. 2019), which are unstable and break down in subsequent cardiac cycles. It was also seen that the TKE of the flow in an aneurysm does not decay with the mean flow kinetic energy and periodic kinetic energy, but rather, much later in the cycle (Poelma et al. 2015). To this end, it is of interest to study decaying flows in a confined geometry. The geometry of a pipe was chosen as it satisfies this minimum requirement for the study. The presence of a well-defined statistically steady state that could be used as a baseline to start researching the decay was an added bonus.

The decay was studied by applying a deceleration to a fully-developed turbulent flow and bringing the flow to a laminar state. It was seen in Section 6-2-1 that it is more appropriate to study the decay by using ramps on the time scale of a turbulent eddy. Doing so, three regions of decay are discerned after the deceleration process is complete – an initial power-law decay,

a power-law decay beset by the saturation of the energy-containing length scale, followed by the stage of viscous, exponential decay. There are some discrepancies in the results. For the Newtonian case of $Re_b = 5300$, the two power-law regimes are not clearly visible. Additionally, the value of β obtained for the exponential decay of this case, shows an error of approximately 30%. But the consistency of this modelling with the other results obtained here, indicates that this discrepancy could arise becuase of the initial Reynolds number being very close to the transition regime. Toonder et al. 1997b show that the statistics for fully-developed pipe flow are dependent on the Reynolds number, and therefore, this could possibly be the case here as well.

The results obtained are qualitatively similar to the results described by Skrbek et al. 2000; Skrbek 2008; Touil et al. 2002 and others, although there are some differences between these studies and the one carried out here. Most of these authors study homogeneous, isotropic turbulence. The case studied here is anisotropic and inhomogeneous in one direction. Additionally, its homogeneity in the axial direction immediately after the application of the deceleration is questionable, although it is quite sure that the flow during the decay is homogeneous in the streamwise direction. The presence of the production of TKE here also makes it difficult to exactly characterize the similarity between the flows of Skrbek et al. 2000 and Touil et al. 2002, and the one studied here. Touil et al. 2002 also show results for an inhomogeneous flow between two plates with no base mean flow and find similar results as the homogeneous, isotropic flow. Therefore, the results here are completely viable.

The essence of this study is to characterize the relaminarization of the flow. With the turbulent quantities asymptotically reducing to zero, it is evident that relamiarization is underway. Since, a transition from turbulent to laminar state is present, it becomes interesting to point out where exactly the switching between the states occur. Relaminarization is a gradual process and therefore, the point of switching between the two states is difficult to pinpoint exactly. However, it is interesting to note that the divergence from the power-law to the exponential decay occurs at $Re_\tau \approx 60$ for all the cases studied. As mentioned previously, several authors have noticed that this friction Reynolds number is critical in terms of understanding relaminarization in channel flows (Iida et al. 1998; Tsukahara et al. 2014). For fully-developed flows at this Reynolds number, these authors notice the flow to be intermittent with patches of localized turbulence when using large computational domains, and the flow to be completely laminar when smaller computational boxes are used. Noticing intermittency is quite difficult here, because of the continuous decrease of the friction Reynolds number in the flow. However, what is clear from the literature and this study is that around $Re_\tau = 60$ and after, the viscosity plays a much bigger role in the decay of turbulence than other turbulent mechanisms. The flows diverge from a turbulent scaling and a scaling based on viscosity is provided for this section. This exponential estimation for the viscous decay was borrowed from the hypothesis of Skrbek 2008, and it is good to see that the scaling holds for both Newtonian and non-Newtonian flows.

With the presence of three regions of decay, it becomes a question of judging when exactly one region ends, and the other begins. This raises the question of the selection of a virtual origin. As these flows relaminarize, they are subject to intermittency and to an extent this should affect the selection of the virtual origin. Skrbek et al. 2000 hypothesize that the decay law is not expected to change because of the presence of intermittency. It is expected however, that a new virtual origin is defined to account for this. The study here does not include any intermittency effects, but as mentioned, the only change expected is in the precise definition

of the starting points of the different stages of decay.

A study was undertaken to understand the changes in the decay with varying initial Reynolds number. It is expected that if the flow is sufficiently turbulent, the nature of decay should be independent of the Reynolds number. This seems to hold for a while, before the flows start deviating from one another. This deviation occurs at approximately $Re_\tau = 60$, where the change over from the power-law to the exponential viscous decay is expected. The difference in flows for the exponential regime is expected to arise out of the differences in viscosity of the different flows.

The difficulties of turbulence modelling for decaying flows is another topic that was briefly addressed. A low Reynolds number $k - \epsilon$ model was used to simulate decaying, Newtonian flows for the same three Reynolds numbers as the DNS. Unlike the DNS, the different power-law regions are not clearly visible. Moreover, the power-law decay holds for a very long time, and it is tough to characterize the point of divergence at $Re_\tau \approx 60$. The inability of the RANS model to understand the growth of the length scale and the presence of the bounded geometry is a serious disadvantage to study this type of flow. Thus, it is essential to resolve much smaller scales and therefore, an LES or DNS study is more beneficial to accurately determine the differnt facets of this study.

To put the results obtained in the context of an aneurysm requires some thought. Using a deceleration is qualitatively equivalent to studying one half of a cardiac cycle, and therefore, the results can be transferred to an aneurysm to some extent. Large expansion angles in aneurysms also cause flow separation, which has not been studied here. It has been noticed in other studies that to describe the decay of turbulent quantities, the nature of the flow separation is not quite important (Sreenivasan 1982). Hence, several authors propose the use of sudden expansions to study the decay of the flow on the scale of an eddy turnover time (Sreenivasan 1982; Sibulkin 1962), and this is what is done here.

Consider that the diameter, length, expansion angle and flow rate are known for a given aneurysm. From the flow rate and the expansion angle, an estimate on the deceleration of the blood flow as it approaches the aneurysm can be provided. Supposing that the combination of expansion angle and flow rate is such that the friction Reynolds number of the flow is never greater than $Re_\tau = 60$ in the aneurysm, then the exponential viscous decay is the only expected decay regime to be present in the aneurysm. If the combination is sufficient for the turbulent scaling to hold ($Re_\tau > 60$), then the power-law decay can be expected.

Differentiating between the two stages of power-law decay is dependent on the length and the diameter of the aneurysm. The energy containing length scale for the flow in an aneurysm can be estimated and it can be compared with the diameter to see if saturation of the length scale has occurred. The study here shows that some time passes between the applied deceleration and the saturation of the length scale. Therefore, the length of the aneurysm also has a major role to play. The length of the aneurysm raises the question of how much time the flow has within an aneurysm to actually go through the two stages of power-law decay mentioned here. Additionally, added recirculation, as blood from a new cycle enters the aneurysm while some amount of the blood from the previous cardiac cycle still remains (Rawat et al. 2019), could play a major role in accumulating turbulence over time and preventing the saturation of the length scale. Considering how long the turbulent scaling actually holds, it is not reasonable that all the stages of decay will be seen together in a single aneurysm for a single cardiac cycle. Such a long aneurysm would not be safe and would require treatment immeidately.

An important question that this research set out to answer is the usage of non-Newtonian modelling for blood flows. This is a large area of debate (Steinman 2012), and it is very tough to answer that question convincingly, although an attempt is made here. The results here show the dependence on the viscosity for the decay, and clearly indicate that the rate of decay increases with shear-thinning. As mentioned previously, blood has a power-law index of $n = 0.67$, and can therefore be considered to be sufficiently shear-thinning to require this modelling. For the turbulent scaling, the nature of the fluid is not discernible, simply because the viscosity does not affect the flow at the largest scales. However, including the shear-thinning definitely incresaes the rate of decay qualitatively. The decay changes between its different stages earlier than for Newtonian flows. Modelling blood as a shear-thinning fluid in an aneurysm then implies that even a turbulent decay could possibly revert to the exponential viscous decay very quickly. The dependence of the viscosity on the decay for the exponential regime shows that if only the viscous decay is present in an aneurysm, then including the effects of shear-thinning makes a larger difference than if the power-law decay holds.

Chapter 7

Conclusion

This document details the applications of turbulent non-Newtonian flow and its importance. In essence, this research is carried out to understand the underlying physics of interaction between the varying viscosity and the phenomenological nature of turbulence (Pinho 2003). With regards to this a description has been provided about fully developed turbulent pipe flows, both qualitatively and quantitatively. The discussion has then been extended to non-Newtonian fluids. The differences in non-Newtonian and Newtonian flows, both in terms of application and phenomenology, have been emphasized. Major differences have been found in modelling blood as a non-Newtonian fluid as compared to a Newtonian fluid in some researches (Rodkiewics et al. 1990), while other studies do not show the need to model the non-Newtonian nature of blood flow for all flow rates (Steinman 2012). There is no conclusive evidence to push the debate either way, and therefore, including the non-Newtonian nature of the fluid in this study made the discussion more intriguing.

The number of variable parameters in an actual aneurysm are too high. Thus, it is easier to quantify certain parameters by looking at a simplified case. Studying the decay has great practical value and could be useful to characterize aneurysms as well. The idea of this research study is to characterize the decay of turbulence from a well-defined state. Fully developed pipe flow fits this description, in particular when considering the fact that the geometry of an aneurysm is similar to that of a pipe. To this extent, a DNS study using `nek5000` has been carried out. Using a higher-order method has been beneficial and has improved the accuracy of the results. The applied methods have been validated for Newtonian and non-Newtonian flows by the comparison of fully-developed flow statistics.

A deceleration is applied to reduce the flow from a turbulent to a laminar state. It is shown that three regions of decay exist, and possible scaling for the same is also provided. The major effort in this thesis is dedicated to verifying if the different stages of decay can be clearly identified for all the cases simulated. The difference between the first two stages can be identified by the saturation of the energy containing length scale. Both these stages follow a power-law decay. This was explained to be qualitatively similar to the results of Skrbek et al. 2000. After a while, there is a change over in the decay law, and the decay is now seen to be exponential. The scaling hypothesized by Skrbek 2008 is used for this region, and it is

shown here that this is a valid hypothesis. The point of divergence between the power-law and exponential decay regimes has been debated. It is shown that this divergence occurs at $Re_\tau \approx 60$ for all cases. This is an intriguing result and can be used as a future stepping stone to understand and characterize transition and relaminarization in pipe flows. Including the effects of intermittency to study this would also further the discussion. The influence of the ramp rate applied for the deceleration and the initial Reynolds number is studied as well. A RANS modelling approach is also attempted to check if a turbulence model can be used to explain the decay. However, it is clear that DNS provides better results for decaying flows.

The differences in the decay of Newtonian and non-Newtonian fluids have been emphasized, with shear-thinning increasing the rate of the overall decay. The results are then put into context for an aneurysm. It is hypothesized that the shear-thinning of blood needs to be modelled depending on the regime of decay seen in an aneurysm. With the clear difference in results for the differnt shear-thinning fluids during the exponential decay, it is evident that for the exponential regime, modelling the shear-thinning provides more accurate reuslts. Although modelling the shear-thinning might not be necessary for the turbulent decay quantiatively, the shift in the point of divergence with increasing shear-thinning indicates that it might be useful to model the turbulent flow as a generlaized Newtonian fluid as well.

The overall outlook of the research is positive. It has been able to address most of the questions it set out to answer. However, there are some shortcomings that need to be looked at in the future. The modelling of the non-Newtonian flows in `nek5000` was a success for the most part, apart from the requirement of a limiter at the location of maximum shear. This led to some disparities of the maxima for the higher-order viscous quantities. Although there was no considerable effect of this on the global flow, a smoother limiter could be used to avoid this. The use of limiters itself can be made null and void by studying viscosity models other than the power-law model. Model such as the Carreau-Yasuda or Casson model are better suited to model blood as well, and therefore, the result obtained using these models could be quite intriguing.

The majority of the decay studies available are carried out for homogeneous, isotropic turbulence. It is tough to characterize and compare the results available for these studies with those of pipe flows. The highly anisotropic nature of this flow is shown in the research. Additionally, the homogeneity of the flow in the axial direction just after the deceleration is applied is also questionable. To appropriately study the correlations and the development of the length scale for decelerating flows, performing an ensemble averaging would be more helpful. The results here for the same are lacking convergence. It would also be ideal to study a pipe of length $\mathcal{O}(100D)$. This requires a high computational load and therefore, this is difficult to do.

For an aneurysm, the results are presented in this research with quite some ambiguity. Therefore, performing a simulation of an aneurysm will shed light on the decay processes present in it. Some of the variables not considered here, such as the effects of the pulsatile nature of blood flow on the decay should also be studied. Although it was shown that flow separation does not have a major role to play in the decay, it would be beneficial to validate this. The topic of decay is a difficult one to characterize, especially in the context of an aneurysm. However, an effort has been made here to answer some of the questions raised, while avenues to explore other research interests have also been created.

Appendix A

Parallel scaling of `nek5000`

Fig. A.1 depicts the variation of the solution time with respect to the number of processors. τ_{comp} corresponds to the total computing effort required. The direct stiffness summation is represented by τ_{ds}, while the inner-product communication time is represented by τ_{ip}. τ_{sol} is the summation of the three aforementioned terms. It can be noticed that the total computing cost decreases with an increase in the number of processors, while the parallel overhead costs increases, as there is more mapping and communication required between elements. τ_{ip} can become the dominant factor as the total number of processors increases, and thus, there is a minimum attainable solution time at a finite number of processors (Fischer et al. 1989).

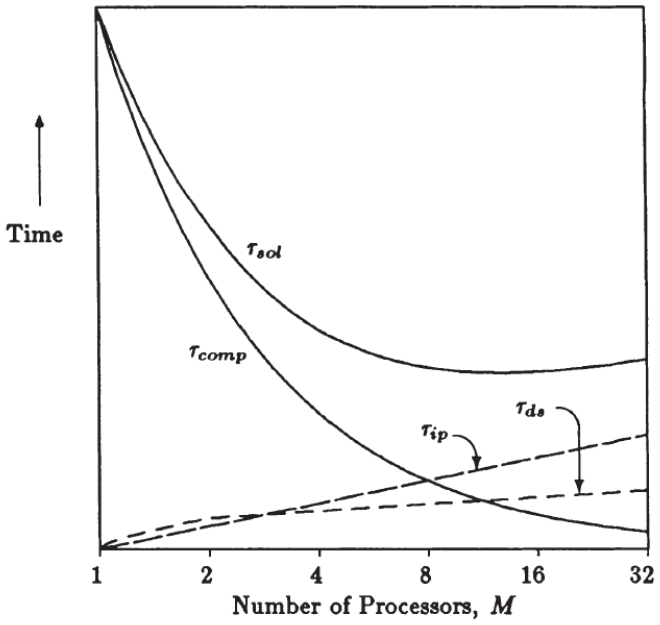

Figure A.1: Computing Costs Associated with Parallel Decomposition, Measured in Wall Clock Time (Fischer et al. 1989)

Parallel costs were also evaluated for the local cluster. A cylindrical pipe geometry with 1875 global elements, employing a polynomial degree of order 7 (N = 7, lx1 = 8). This gives the total degrees of freedom as $1875 \times 8^3 = 960000$. The case was parallelized and tested, starting from 8 cores until 56 cores. Fig. A.2 shows the logarithmic variation of the time required per time step with the total number of cores. This reinforces the fact that the computational cost decreases with the increase in the total number of processors, and the scalability in `nek5000` is quite efficient.

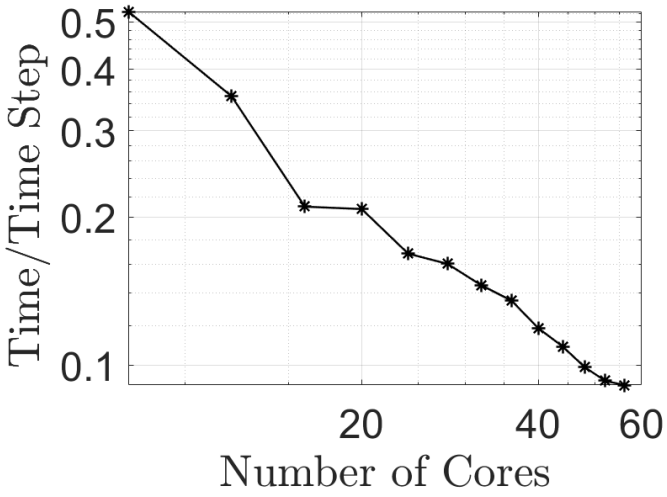

Figure A.2: Efficiency of Parallel Scaling in `nek5000`

Appendix B

Additional Validation Results

B-1 Grid Independence Study

A grid independence study was done to check the influence of the grid on the results. Some of the results are shown below. Five cases were studied, and the results were validated with those of Eggels et al. 1994. The number of elements for these were 1875, 3900, 7840, 9764 and 12820. The interpolating polynomial used for the GLL distribution is of order $N = 7$, and thus, the total degrees of freedom for each case is $8^3 \times$ Number of Elements. Figure B.1a shows the average wall shear stress for each case and the expected value. For the first two element sizes, the value is quite erratic. Therafter, the values are close to the expected value, and thus, one of the sizes from these must be selected.

Figure B.1b shows the Reynolds shear stress for the different cases. As the number of elements increases, the results are closer to the expected value. For 9764 and 12820 elements, the results match exactly with those of Eggels et al. 1994, and therefore, one of these values will be selected for the rest of the simulations. To finalise the selection, the computational time required for each element size is plotted in Figure B.2. The time required increases with the number of cells in the simulation. Considering that both 9764 and 12820 elements provide the same results that are in good agreement with those of Eggels et al. 1994, the case which required lesser computational time was chosen. This leads to the selection of the case with 9764 elements. The total degrees of freedom are 4.9×10^6.

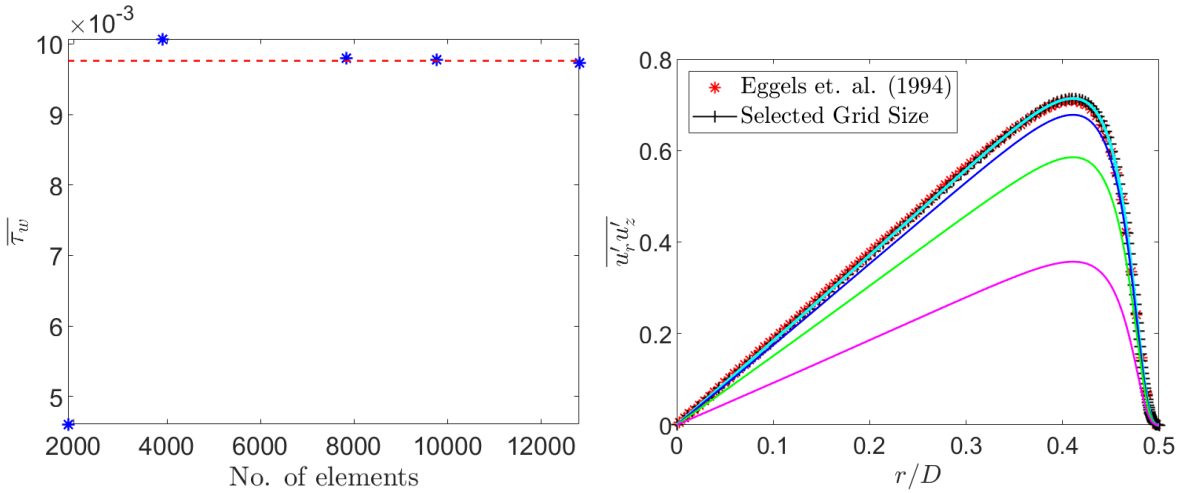

Figure B.1: (a) The obtained value of the time-averaged wall shear stress for different element sizes: The red line indicates the expected value for the case (b) The Reynolds shear stress plotted for different grid sizes, The selected value (Grid Size = 9764) and the results from Eggels et al. 1994 is given in the figure. Each grid size has $[(N+1)^3 \times \text{Grid Size}]$ degrees of freedom with $N = 7$ *Legend*: (——) Grid size = 12820 (——) Grid size = 7840 (——) Grid size = 3900 (——) Grid size = 1875

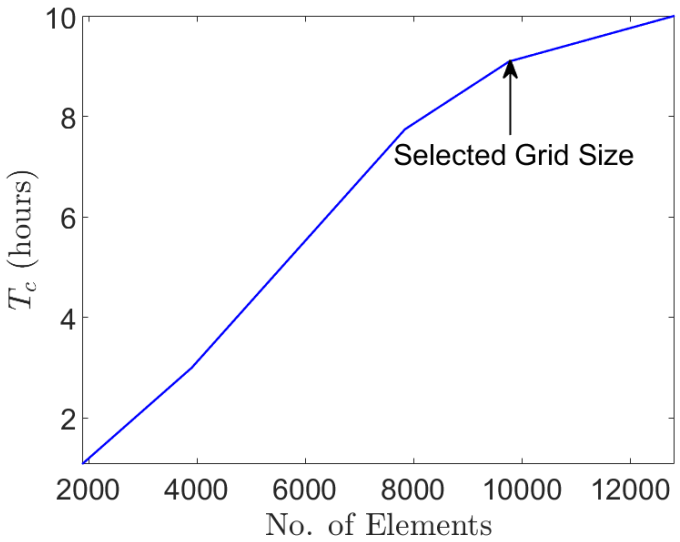

Figure B.2: Required computational time for different grid sizes. The selected grid size (9764 elements) is marked in the figure

B-2 Additional Budget Terms - Eggels et al. 1994

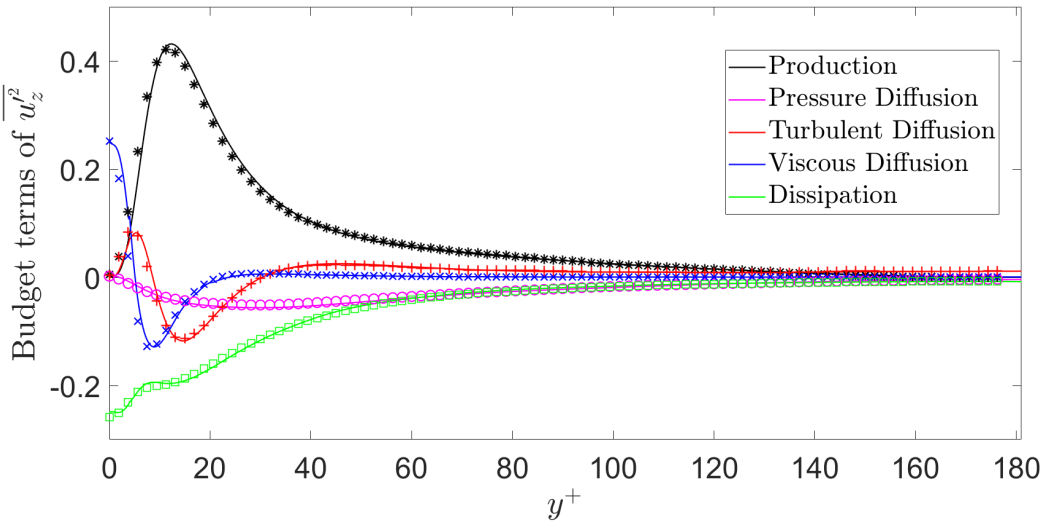

Figure B.3: Budget terms of $\overline{u_z'^2}$: The symbols are the results obtained from Eggels et al. 1994 for the respective quantities

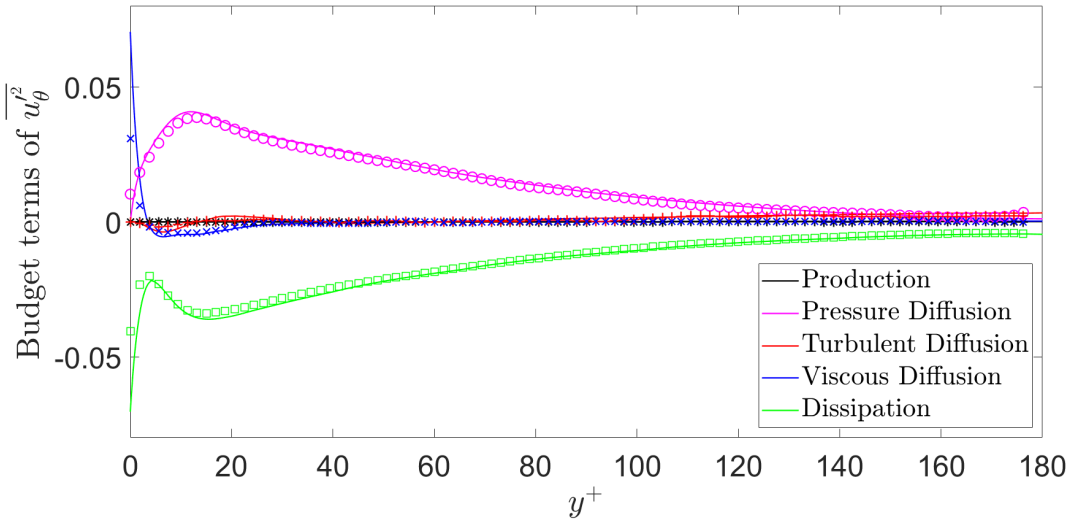

Figure B.4: Budget terms of $\overline{u_\theta'^2}$: The symbols are the results obtained from Eggels et al. 1994 for the respective quantities

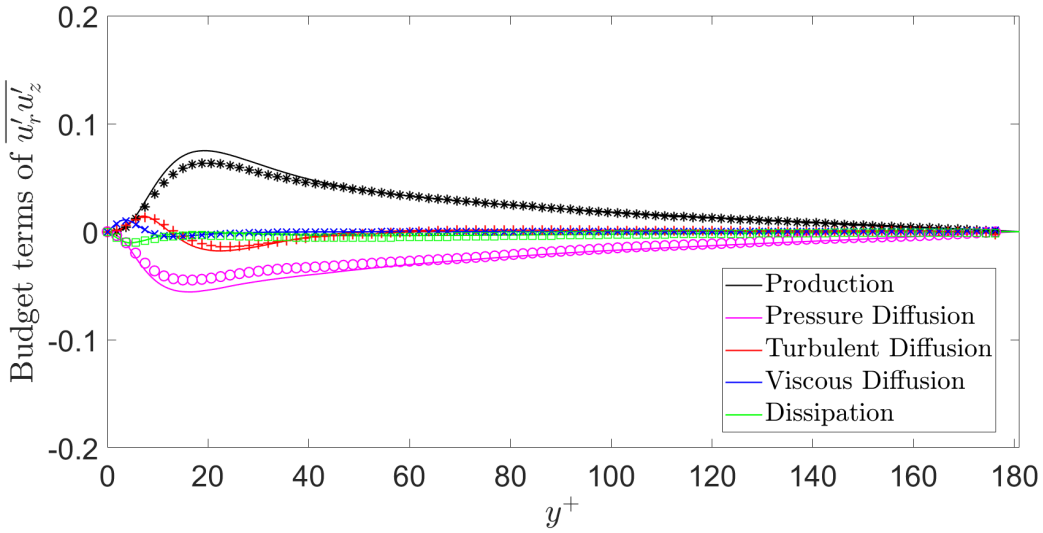

Figure B.5: Budget terms of $\overline{u_r' u_z'}$: The symbols are the results obtained from Eggels et al. 1994 for the respective quantities

B-3 Additional Results - Singh et al. 2017

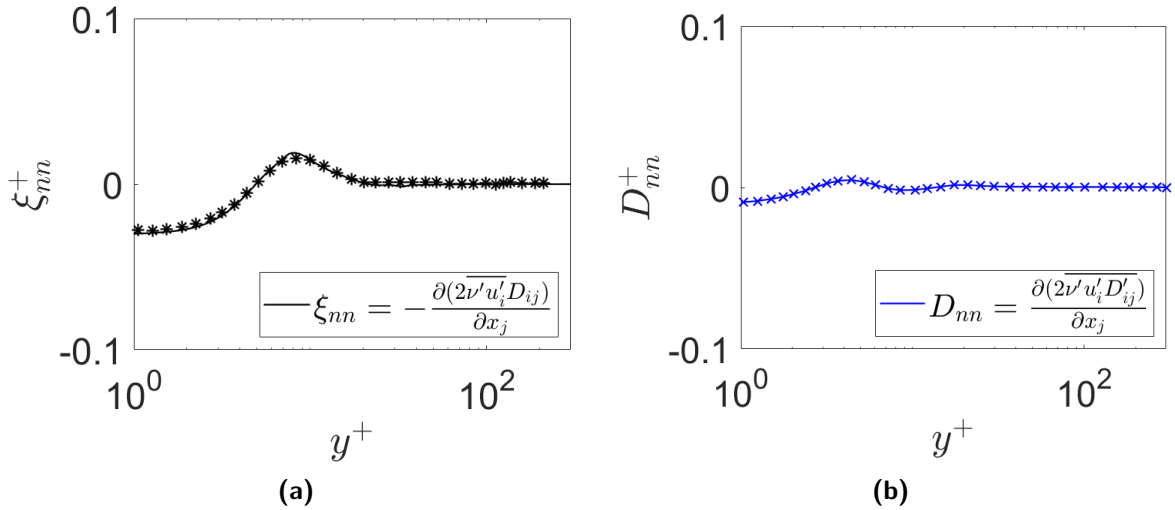

(a) **(b)**

Figure B.6: (a) Comparison of the normalized mean shear turbulent viscous transport (b): Comparison of the normalized turbulent viscous transport - The symbols are results obtained from Singh et al. 2017

Bibliography

Araya, G. and D. Rodriguez (2018). "Visualization and Assessment of Turbulent Coherent Structures in Laminarescent Boundary Layers". In: *J. Vis.* 21, pp. 191–202. DOI: 10.1007/s12650-017-0460-4.

Archer, P.J., T.G. Thomas, and G.N. Coleman (2008). "Direct Numerical Simulation of Vortex Ring Evolution from the Laminar to the Early Turbulent Regime". In: *Journal of Fluid Mechanics* 598, pp. 201–226. DOI: 10.1017/S0022112007009883.

Arzani, Amirhossein (2018). "Accounting for Residence Time in Blood Rheology Models: Do we really need non-Newtonian Blood Flow Modelling in Large Arteries?" In: *J. R. Soc. Interface* 15: 20180486. DOI: http://dx.doi.org/10.1098/rsif.2018.0486.

Batchelor, G.K. and A.A. Townsend (1948). "Decay of Turbulence in The Final Period". In: *Proc. R. Soc. London Ser. A.* 194, pp. 527–543. DOI: 10.1098/rspa.1948.0095.

Bessonov, Nikolay et al. (2016). "Methods of Blood Flow Modelling". In: *Mathematical Modelling of Natural Phenomena, EDP Sciences* 11, pp. 1–25. DOI: http://dx.doi.org/10.1051/mmnp201611101.

Bewersdorff, H.W. and H. Thiel (1993). "Turbulence Structure of Dilute Polymer and Surfactant Solutions in Artificially Roughened Pipes". In: *Applied Scientific Research* 50, pp. 347–368.

Biasetti, J., F. Hussain, and T.C. Gasser (2011). "Blood Flow and Coherent Vortices in the Normal and Aneurysmatic Aortas: A Fluid Dynamical Approach to Intraluminal Thrombus Formation". In: *J. R. Soc. Interface* 8, pp. 1449–1461. DOI: http://dx.doi.org/10.1098/rsif.2011.0041.

Biferale, L. et al. (2003). "The Decay of Homogeneous Anisotropic Turbulence". In: *Physics of Fluids* 15.8, pp. 2105–2112. DOI: https://doi.org/10.1063/1.1582859.

Chow, P.L. and E. Saibel (1967). "Some Non-Newtonian Effects in the Decay of Isotropic Turbulence". In: *Int. J. Engng. Sci.* 5, pp. 723–739.

Darbyshire, A.G. and T. Mullin (1995). "Transition to Turbulence in a Constant Mass-Flux Pipe Flow". In: *Journal of Fluid Mechanics* 289, pp. 83–114.

Deville, M.O., P.F. Fischer, and E.H. Mund (2002). *High-Order Methods for Incompressible Fluid Flow*. Cambridge University Press.

Doorn, Eric van, C.M.White, and K.R. Sreenivasan (1999). "The Decay of Grid TUrbulence in Polymer and Surfactant Solutions". In: *Physics of Fluids* 11.8, pp. 2387–2393. DOI: https://doi.org/10.1063/1.870100.

Draad, A.A., G.D.C. Kuiken, and F.T.M. Nieuwstadt (1998). "Laminar-turbulent Transition in Pipe Flow of Newtonian and Non-Newtonian Fluids". In: *Journal of Fluid Mechanics* 377, pp. 267–312. DOI: 10.1017/S0022112098003139.

Drazin, P.G. and W.H. Reid (1981). *Introduction to Hydrodynamic Stability*. Cambridge University Press.

Dubief, Y. and F. Delcayre (2000). "On coherent-vortex identification in Turbulence". In: *Journal of Turbulence* 1.011.

Eckhardt, B. et al. (2007). "Turbulence Transition in Pipe Flow". In: *Annu. Rev. Fluid. Mech.* 39, pp. 447–468.

Eggels, J.G.M. (1994). "Direct and Large Eddy Simulation of Turbulent Flow in a Cylindrical Pipe Geometry". PhD thesis. Delft University of Technology.

Eggels, J.G.M. et al. (1994). "Fully Developed Turbulent Pipe Flow: A Comparison between Direct Numerical Simulation and Experiment". In: *Journal of Fluid Mechanics* 268, pp. 175–209. DOI: 10.1017/S002211209400131X.

Ertunc, K. Haddad O., M. Mishra, and A. Delgado (2010). "Pulsating Laminar Fully Developed Channel and Pipe Flows". In: *Physical Review Letters, American Physical Society* 81 (016303). DOI: 10.1103/PhysRevE.81.016303.

Faisst, H. and B. Eckhardt (2003). "Traveling Waves in Pipe Flow". In: *Physical Review Letters, American Physical Society* 91 (224502).22. DOI: 10.1103/PhysRevLett.91.224502.

Fischer, Paul F. and Anthony T. Patera (1989). "Parallel Spectral Element Methods for the Incompressible Navier-Stokes Equations". In: *Solution of Superlarge Problems in Computational Mechanics*, pp. 49–65.

Fischer, P.F. (1997). "An Overlapping Schwarz Method for Spectral Element Solution of the Incompressible Navier-Stokes Equations". In: *Journal of Computational Physics* 133, pp. 84–101.

G. Tripathi, P. Mishra dn (1971). "Transition from Laminar to Turbulent Flow of Purely Viscous non-Newtonian Fluids in Tubes". In: *Chemical Engineering Science* 26, pp. 915–921.

Greenblatt, D. and A. Moss (1999). "Pipe-Flow Relaminarization by Temporal Acceleration". In: *Physics of Fluids* 11.11, pp. 3478–3481. DOI: https://doi.org/10.1063/1.870205.

Greenblatt, D. and E.A. Moss (2004). "Rapid Temporal Acceleration of a Turbulent Pipe Flow". In: *Journal of Fluid Mechanics* 514, pp. 65–75. DOI: 10.1017/S0022112004000114.

Guerrero, B., M. F. Lambert, and R.C. Chin (2021). "Transient Dynamics of Accelerating Turbulent Pipe Flow". In: *Journal of Fluid Mechanics* 917, A43. DOI: 10.1017/jfm.2021.303.

He, S., K. He, and M. Seddighi (2016). "Laminarisation of Flow at Low Reynolds Number due to Streamwise Body Force". In: *Journal of Fluid Mechanics* 809, pp. 31–71. DOI: 10.1017/jfm.2016.653.

He, S. and J.D. Jackson (2000). "A Study of Turbulence Under Conditions of Transient Flow in a Pipe". In: *Journal of Fluid Mechanics* 408, pp. 1–38. DOI: 10.1017/S0022112099007016.

Hof, B., A. Juel, and T. Mullin (2003). "Scaling of Turbulence Transition Threshold in a Pipe". In: *Physical Review Letters, American Physical Society* 91 (244502).24. DOI: 10.1103/PhysRevLett.91.244502.

Hof, B. et al. (2006). "Finite Lifetime of Turbulence in Shear Flows". In: *Nature* 443, pp. 59–62. DOI: 10.1038/nature05089.

Hunt, J.C.R., A.A. Wray, and P. Moin (1988). "Eddies, Streams and Convergence Zones in Turbulent Flows". In: *Center for Turbulence Research, Proceedings of the Summer Program 1988*.

Iida, O. and Y. Nagano (1998). "The Relaminarization Mechanisms of Turbulent Channel Flow at Low Reynolds Numbers". In: *Flow, Turbulence and Comustion* 60, pp. 193–213.

Kármán, T. von and L. Howarth (1938). "On the Statistical Theory of Isotropic Turbulence". In: *Proc. R. Soc. London Ser. A.* 164, pp. 192–215. DOI: 10.1098/rspa.1938.0013.

Khoury, G.K. El et al. (2013). "Direct Numerical Simulations of Turbulent Pipe Flow at Moderately High Reynolds Numbers". In: *Flow Turbulence Combust* 91, pp. 475–495. DOI: 10.1007/s10494-013-9482-8.

Kleiser, L. and T.A.Zang (1991). "Numerical Simulation of Transition in Wall-Bounded Shear Flows". In: *Annu. Rev. Fluid. Mech.* 23, pp. 495–537.

Kolmogorov, A.N. (1941). "The Local Structure of Turbulence in Incompressible Viscous Fluid for very Large Reynolds Numbers". In: *C.R. Akad. Sci. SSR* 30, p. 310.

Ku, D.N. (1997). "Blood Flow in Arteries". In: *Annu. Rev. Fluid. Mech.* 29(1), pp. 399–434.

Laufer, John (1954). "The Structure of Turbulence in Fully Developed Pipe Flow". In: *NACA Report, 1174*, pp. 417–434.

Lawn, C.J. (1971). "The Determination of the Rate of Dissipation in Turbulent Pipe Flow". In: *Journal of Fluid Mechanics* 48, pp. 477–505. DOI: 10.1017/S002211207100171X.

Lee, M. J., J. Kim, and P. Moin (1990). "Structure of Turbulence at High Shear Rate". In: *Journal of Fluid Mechanics* 216, pp. 561–583.

Liberzon, A. et al. (2006). "On Turbulent Kinetic Energy Production and Dissipation in Dilute Polymer Solutions". In: *Physics of Fluids* 18 (125101). DOI: https://doi.org/10.1063/1.2397536.

López-Carranza, S.N., M. Jenny, and Nouar C (2012). "Pipe-Flow of Shear-Thinning Fluids". In: *C.R. Mecanique* 340, pp. 33–48. DOI: http://dx.doi.org/10.1016/j.crme.2012.05.002.

Macosko, Christopher W. (1994). *Rheology Principles, Measurements and Applications*. VCH Publishers Inc. Chap. 1,2,3.

Mason, P.J. and N.S. Callen (1986). "On the Magnitude of the Subgrid-scale Eddy Coefficient in Large-Eddy Simulations of Turbulent Channel Flow". In: *Journal of Fluid Mechanics* 162, pp. 439–462. DOI: 10.1017/S0022112086002112.

McComb, W.D., J. Allan, and C.A. Greated (1977). "Effect of Polymer Additives on the Small-Scale Structure of Grid Generated Turbulence". In: *Physics of Fluids* 20.6, pp. 873–879. DOI: https://doi.org/10.1063/1.861977.

Metzner, A.B. and J.C. Reed (1955). "Flow of non-Newtonian Fluids-correlation of the laminar, transition and turbulent flow regions". In: *AIChE Journal* 1(4), pp. 434–440. DOI: https://doi.org/10.1002/(ISSN)1547-5905.

Moin, P. and K.Mahesh (1998). "Direct Numerical Simulation: A Tool in Turbulence Research". In: *Annu. Rev. Fluid. Mech.* 30.1, pp. 539–578.

Narasimha, R. and K.R. Sreenivasan (1979). "Relaminarization of Fluid Flows". In: *Acta Mechanica* 19, pp. 221–309.

Narayanan, M. A. Badri (1968). "An Experimental Study of Reverse Transition in Two-Dimensional Channel Flow". In: *Journal of Fluid Mechanics* 31, pp. 609–623.

Nieuwstadt, F.T.M., B.J. Boersma, and J. Westerweel (2016). *Turbulence: Introduction to Theory and Applications of Turbulent Flows*. Springer International Publishing Switzerland. DOI: 10.1007/978-3-319-31599-7_5.

Owen, P.R. (1969). "Turbulent Flow and Particle Deposition in the Trachea". In: *Circulatory and Respiratory Mass Transport*, pp. 236–255.

Patel, V.C. and M.R. Head (1968). "Reversion of Turbulent to Laminar Flow". In: *Journal of Fluid Mechanics* 34, pp. 371–392.

Patera, Anthony T. (1984). "A Spectral Element Method for Fluid Dynamics: Laminar Flow in a Channel Expansion". In: *Journal of Computational Physics* 54, pp. 468–488.

Paul F. Fischer, James W. Lottes and Stefan G. Kerkemeier (2008). *nek5000 Web page*. URL: http://nek5000.mcs.anl.gov.

– (2015). *nek5000 Documentation*. URL: http://nek5000.mcs.anl.gov.

Peixinho, J. and T. Mullin (2006). "Decay of Turbulence in Pipe Flow". In: *Physical Review Letters, American Physical Society* 96 (94501). DOI: 10.1103/PhysRevLett.96.094501.

Peixinho, J. et al. (2005). "Laminar Transitional and Turbulent Flow of Yield Stress Fluid in a Pipe". In: *Journal of Non-Newtonian Fluid Mechanics* 128, pp. 172–184. DOI: http://dx.doi.org/10.1016/j.jnnfm.2005.03.008.

Perry, A.E. and C.J. Abell (1975). "Scaling Laws for Pipe-Flow Turbulence". In: *Journal of Fluid Mechanics* 67, pp. 257–271. DOI: 10.1017/S0022112075000298.

Perry, A.E., S. Henbest, and M.S. Chong (1986). "A Theoretical and Experimental Study of Wall Turbulence". In: *Journal of Fluid Mechanics* 165, pp. 163–199.

Pinho, F.T. (2003). "A GNF Framework for Turbulent Flow Models of Drag Reducing Fluids and proposal for a $k - \epsilon$ Type Closure". In: *Journal of Non-Newtonian Fluid Mechanics* 114, pp. 149–184.

Pinho, F.T. and J.H. Whitelaw (1990). "Flow of non-Newtonian Fluids in a Pipe". In: *Journal of Non-Newtonian Fluid Mechanics* 34, pp. 129–144.

Poelma, Christian, P.N. Watton, and Y. Ventikos (2015). "Transitional Flow in Aneurysms and the Computation of Haemodynamic Parameters". In: *J. R. Soc. Interface* 12: 20141394. DOI: http://dx.doi.org/10.1098/rsif.2014.1394.

Pope, Stephen B. (2000). *Turbulent Flows*. Cambridge University Press.

Pozrikidis, C. (2014). *Introduction to Finite and Spectral Element Methods Using MATLAB, 2nd Ed.* Taylor & Francis Group, LLC.

Prasad, Pradyumna M.K. (2016). "Comprehensive Assessment of NEK5000 DNS Capabilities: Turbulent Channel Flow and Conjugate Heat Transfer". MA thesis. Delft University of Technology.

Ptasinski, P.K. et al. (2001). "Experiments in Turbulent Pipe Flow with Polymer Additives at Maximum Drag Reduction". In: *Flow Turbulence and Combustion* 66, pp. 159–182.

Radhakrishnan, Adithya Krishnan Thota et al. (2020). "Laminar-Turbulent Transition of a non-Newtonian Fluid Flow". In: *Journal of Hydraulic Research*. DOI: https://doi.org/10.1080/00221686.2020.1770876.

Rahgozar, S. and D.E. Rival (2017). "On Turbulence Decay of a Shear-Thinning Fluid". In: *Physics of Fluids* 29, 123101. DOI: https://doi.org/10.1063/1.5012900.

Rawat, Digvijay, Mathieu Pourquie, and Christian Poelma (2019). "Numerical Investigation of Turbulence in Abdominal Aortic Aneurysms". In: *Journal of Biomechanical Engineering* 141(6), [061001]. DOI: https://doi.org/10.1115/1.4043289.

Rezaeiravesh, S., R. Vinuesa, and P. Schlatter (2019). "A Statistics Toolbox for Turbulent Pipe Flow in `Nek5000`". In: *Technical Report, TRITA–SCI–RAP 2019:008*.

Rodkiewics, C.M., Prawal Sinha, and J.S. Kennedy (1990). "On the Application of a Constitutive Equation for Whole Human Blood". In: *Journal of Biomechanical Engineering* 112, pp. 198–206.

Rudman, M. and H.M. Blackburn (2006). "Direct Numerical Simulation of Turbulent non-Newtonian Flow using a Spectral Element Method". In: *Applied Mathematical Modelling* 30, pp. 1229–1248. DOI: http://dx.doi.org/10.1016/j.apm.2006.03.005.

Rudman, M. et al. (2004). "Turbulent Pipe-Flow of Shear-Thinning Fluids". In: *Journal of Non-Newtonian Fluid Mechanics* 118, pp. 33–48. DOI: http://dx.doi.org/10.1016/j.jnnfm.2004.02.006.

Saffman, P.G. (1967). "The Large-Scale Structure of Homogeneous Turbulence". In: *Journal of Fluid Mechanics* 27, pp. 581–593.

Sekimoto, A., S. Dong, and J. Jiménez (2016). "Direct Numerical Simulation of Statistically Stationary and Homogeneous Shear Turbulence and its' Relation to Other Shear Flows". In: *Physics of Fluids* 28 (035101). DOI: https://doi.org/10.1063/1.4942496.

Sibulkin, M. (1962). "Transition from Turbulent to Laminar Pipe Flow". In: *Physics of Fluids* 5.1, pp. 280–284. DOI: https://doi.org/10.1063/1.1706612.

Singh, J., M. Rudman, and H.M. Blackburn (2017). "The Influence of Shear-Dependent Rheology on Turbulent Pipe Flow". In: *Journal of Fluid Mechanics* 822, pp. 848–879. DOI: 10.1017/jfm.2017.296.

Skrbek, L. (2008). "Counterflow Turbulence in He II and Its Decay". In: pp. 91–139.

Skrbek, L. and S.R. Stalp (2000). "On The Decay of Homogeneous Isotropic Turbulence". In: *Physics of Fluids* 12.8, pp. 1997–2019. DOI: https://doi.org/10.1063/1.870447.

Sreenivasan, K.R. (1982). "Laminarescent, Relaminarizing and Retransitional Flows". In: *Acta Mechanica* 44, pp. 1–48.

Steinman, David A. (2012). "Assumptions in Modelling of Large Artery Hemodynamics". In: 5, pp. 1–18.

Toonder, J.M.J. den and F.T.M. Nieuwstadt (1997a). "Reynolds Number Effects in a Turbulent Pipe Flow for Low to Moderate Re". In: *Physics of Fluids* 9.11, pp. 3398–3409. DOI: https://doi.org/10.1063/1.868193.

Toonder, J.M.J. Den, M.A. Hulsen, and F.T.M. Nieuwstadt (1997b). "Drag Reduction by Polymer Additives in a Turbulent Pipe Flow: Numerical and Laboratory Experiments". In: *Journal of Fluid Mechanics* 377, pp. 198–231. DOI: 10.1017/S0022112097004850.

Touil, Hatem, Jean-Pierre Bertoglio, and Liang Shao (2002). "The Decay of Turbulence in a Bounded Domain". In: *Journal of Turbulence* 3.49. DOI: 10.1088/1468-5248/3/1/049.

Tsukahara, T. et al. (2014). "DNS of Turbulent Channel Flow at Very Low Reynolds Numbers - Expanded Version". In: *4th Int. Symp. on Turbulence and Shear Flow Phenomena*.

Varghese, Sonu S., Steven H. Frankel, and Paul F. Fischer (2007). "Direct Numerical Simulation of Stenotic Flows, Part 2. Pulsatile Flow". In: *Journal of Fluid Mechanics* 582, pp. 281–318. DOI: 10.1017/S0022112007005836.

Vinuesa, R. et al. (2016). "Convergence of Numerical Simulations of Turbulent Wall-Bounded Flows and Mean Cross-Flow Structure of Rectangular Ducts". In: *Flow Turbulence Combust* 51, pp. 3025–3042. DOI: 10.1007/s11012-016-0558-0.

Virk, P.S., H.S. Mickley, and K.A. Smith (1970). "The Ultimate Asymptote and Mean Flow in Structure in Toms' Phenomenon". In: *Journal of Applied Mechanics*, pp. 488–493.

Vonlathen, R. and P.A. Monkewitz (2013). "Grid Turbulence in Dilute Polymer Solutions: PEO in Water". In: *Journal of Fluid Mechanics* 730, pp. 76–98. DOI: 10.1017/jfm.2013.316.

Wygnanski, I.J. and F.H. Champagne (1973). "On Transition in a Pipe. Part 1. The Origin of Puffs and Slugs and the Flow in a Turbulent Slug". In: *Journal of Fluid Mechanics* 59, pp. 281–335.

Yip, T.H. and S.C.M. Yu (2001). "Cyclic Transition to Turbulence in Rigid Abdominal Aortic Aneurysm Models". In: *Fluid Dyn. Res.* 29, pp. 81–113.